学位論文

Quantum entanglement and holography

(量子エンタングルメントとホログラフィー)

平成２８年１２月博士（理学）申請

東京大学大学院理学系研究科

物理学専攻

中口 悠輝

Abstract

In this thesis, aiming to understand better how quantum gravity theory encodes spacetime structure as physical degrees of freedom or equivalently quantum information, I have studied various aspects of quantum entanglement from the viewpoint of holographic principle, which I believe is the most fundamental principle of quantum gravity theory. Quantum entanglement and the role it plays in holographic principle are reviewed. My research on this topic is divided into four parts.

In the first part, we propose [1] a new universal behaviour of quantum entanglement with respect to a mass gap in field theories based on a study on mutual information, a measure of quantum entanglement shared by separate regions. This proposal is checked for some explicit examples, a free field theory and the holographic dual of a strongly coupled field theory, for an annular region whose shape is complicated enough to construct meaningful mutual information. This observation thus gives not only a consistency check of the holographic principle, but also gives us a new insight into quantum entanglement in field theories.

In the second part, with a concrete holographic setup of a thermalizing state represented by a growing black hole geometry, we demonstrate [2] that entanglement entropy can grow linearly with time even without growth of time slice or wormhole in gravity side, while a famous literature attributes the linear growth of a holographic entanglement entropy of a thermalizing state to the growth of the volume of time slice or wormhole through a black hole. This study thus improves our understanding of how the time dependence of entanglement entropies is represented in gravity side of holography, especially for thermalization processes.

In the third part, we examine [3] how we can extend the notion of renormalized entanglement entropy from a flat space to curved spaces, where renormalized entanglement entropy is known to be a measure of degrees of freedom in the sense that it monotonically decreases along renormalization group flows. There are two ways to extend it according to whether we interpret the derivative with respect to the size of the spacial region in the definition of the renormalized entanglement entropy as enlarging the spacial region or as scaling the space, and our example shows that the former successfully decreases along the renormalization group flow while the latter does not. This result serves a concretized realization of our intuition that physical degrees of freedom are encoded in quantum entanglement of spacial regions.

In the fourth part, we show [4] that the recent proposal for the holographic formula of Rényi entropy, which contains more detailed information about quantum entanglement than entanglement entropy, expectedly satisfies inequalities that Rényi entropies should obey, given that bulk geometries are stable. This study thus gives a nontrivial consistency check of the formula and of the holographic principle itself. Moreover, we reformulate quantities representing quantum entanglement in analogy with statistical mechanics, which provides us a concise interpretation of the Rényi entropic inequalities as the positivities of entropy, energy and heat capacity and makes clear a thermodynamic structure in the derivation of the holographic formula for quantum entanglements.

Contents

1 Introduction **5**

2 Quantum Entanglements in Field Theories and Holographic Theories **10**
2.1 Techniques to calculate entanglements 10
2.1.1 Replica trick 10
2.1.2 Lattice discretization 14
2.2 Entanglements in field theories 17
2.2.1 General forms 17
2.2.2 CFT_2 18
2.2.3 Ball shaped regions in CFT_d 20
2.2.4 Gapped theories 22
2.3 More on entanglements 22
2.3.1 UV cutoff independent measures of entanglements 22
2.3.2 Mathematical inequalities for entanglements 23
2.4 Entanglements in holographic theories 24
2.4.1 AdS space 24
2.4.2 Holographic formulae for entanglements 27
2.4.3 Derivation of the holographic formula 29
2.4.4 Area law in holographic theories 31
2.4.5 AdS_3/CFT_2 32
2.4.6 Ball shaped regions in AdS_{d+1}/CFT_d 33

3 A New Universality of Entanglement in Gapped Theories and Holography **34**
3.1 Mutual information across an annulus 35
3.1.1 Mutual information in CFT's 35
3.1.2 Mutual information in gapped theories 36
3.2 Mutual information for a free massive scalar 37
3.2.1 Numerical results for the mutual information 38
3.2.2 Small and large width limits in CFT 39
3.3 Holographic mutual information 42
3.3.1 In CFT_3 dual to AdS_4 background 42
3.3.2 In a gapped system dual to the CGLP background 45
3.4 Universal behaviors of quantum entanglements 50

4 Time-dependent Entanglement and Holography **53**
4.1 The time-dependent Janus black hole . . . 53
4.1.1 The metric . . . 54
4.1.2 The CFT interpretation . . . 56
4.2 The holographic EE of an interval . . . 57
4.2.1 Area of the extremal surface . . . 57
4.2.2 Some special limits . . . 60
4.2.3 Time dependence . . . 62
4.3 HEE of two intervals and the phase transition . . . 63
4.3.1 Two phases . . . 63
4.3.2 Phase transition . . . 65
4.4 Discussions . . . 68

5 Renormalized Entanglement Entropy on a Curved Space **70**
5.1 Renormalized entanglement entropy . . . 70
5.1.1 Two REE's on cylinder . . . 70
5.2 Free massive scalar field . . . 72
5.2.1 Conformal transformation to a non-singular space . . . 72
5.2.2 Small mass expansion of cap entropies . . . 73
5.2.3 Large mass expansion of cap entropies . . . 75
5.2.4 The two REE's and numerical results . . . 77

6 Rényi Entropic Inequalities and Holography **82**
6.1 Rényi entropic inequalities . . . 82
6.2 Analogy to statistical mechanics . . . 83
6.2.1 Partition function Z and the escort density matrix ρ_n . . . 84
6.2.2 Modular entropy $\tilde{S}_n$ . . . 85
6.2.3 Capacity of entanglement $C(n)$ . . . 85
6.2.4 Rényi entropic inequalities from the viewpoint of the analogy . . . 86
6.2.5 Holographic formula from the view point of the analogy . . . 86
6.3 Proof of the Rényi entropic inequalities . . . 87
6.3.1 A holographic proof . . . 87
6.3.2 Legendre transformed expression for capacity of entanglement . . . 89
6.4 Calculations of the capacity of entanglement . . . 91
6.4.1 Conformal field theory . . . 91
6.4.2 Free fields . . . 92
6.4.3 Gravity duals . . . 94
6.4.4 Large and small n limits . . . 96
6.5 Discussion . . . 97

7 Conclusions **100**

Acknowledgements **104**

A Details of numerical calculations **105**
A.1 Calculating annulus entropies 105
A.1.1 Radial lattice discretization 105
A.1.2 Finite lattice size effect 106
A.1.3 Large angular momentum 106
A.2 Calculating cap entropies on cylinder 107
A.2.1 Angular decomposition 107
A.2.2 Lattice discretization 108
A.2.3 Large angular momentum 109

B Details on holographic calculations **111**
B.1 γ-expansion in the Janus black hole 111
B.2 On holographic calculation of $C(1)$ using graviton propagator 112

C Details on field theory calculations **115**
C.1 Integration of the conformal factor 115
C.2 Possible extension of SSA to Rényi entropies 115

Chapter 1

Introduction

A key concept in modern quantum gravity theory is holography or holographic principle [5, 6, 7], which opened the door to a non-perturbative definition of quantum gravity as an equivalent non-gravity quantum theory in one lower dimensions. The equivalent non-gravity theory usually can be regarded as a theory located on the boundary of the gravity theory at infinity, in some sense. This equivalence between a $(d+1)$-dimensional gravitational theory (usually called "bulk theory") and a d-dimensional non-gravitational theory (usually called "boundary theory") is sometimes called holographic duality. This duality allows us to interpret a gravitational world as a holographic image constructed from the data on its boundary at infinity, because all the information of the world is already encoded somehow on its boundary. This is why this principle is named "holography"; the world emerges from its boundary.

In quantum gravity theory, the notion of spacetime becomes vague because general states are quantum superpositions of possible spacetime geometries, but in the classical limit, classical on-shell spacetime geometries dominate and we can say more surely that there is a spacetime in the world, which satisfies classical equations of motions like Einstein equations. Since we already know classical gravity theories, this classical limit in the bulk theory is one of the fundamental tools to study holographic duality. Typically, the classical limit in the bulk side corresponds to the large degrees of freedom limit in the boundary side, such as the large N limit in gauge theories [8] or the large central charge limit in two dimensional conformal field theories [9] . This is because the coefficient of the bulk classical gravity actions, namely, the gravitational coupling constant $1/G_N$, where G_N is the bulk Newton constant, is typically holographically proportional to the numbers of degrees of freedom in the boundary side, such as the number of gluons N^2 or the central charge c. The spacetime thus emerges as a macroscopic or collective notion, similarly to the emergence of thermodynamics or fluid dynamics in coarse-graining microscopic details. We can also obtain a different geometry in this classical limit by taking a different quantum state from the start; as we will see later in this thesis, a thermal state gives a black hole geometry [10, 11, 12, 13, 14] and a time-dependent state gives a time-dependent geometry [15, 16, 17, 18]. It follows that holography also provides a useful toolkit to study black hole physics within unitary quantum theory, with an advantage over stringy constructions of black holes with branes [19, 20], in the ability to describe non-perturbative processes such

as black hole formations represented by (Anti de-Sitter) Vaidya metrics, for example. These unitary descriptions of black hole dynamics reinforce the belief that there is no information loss even in black holes.

The most successful example of the holography is so-called AdS/CFT correspondence [8, 21, 22, 23, 24], which says that a quantum gravity theory on $(d+1)$-dimensional Anti de-Sitter space, AdS_{d+1}, is equivalent to a d-dimensional conformal field theory, CFT_d. This holographic duality is originally derived from considerations of D branes, which are non-perturbative extended objects on which strings can end in string theory, a successful theory of quantum gravity particulary suitable for perturbative calculations. In the classical limit in the bulk, we usually take another limit as well that the string length l_s is much shorter than the typical length scale L of the geometry so that we can suppress higher derivative corrections of gravity actions in string theory and can get Einstein gravity. For AdS_{d+1} spaces, the typical length scale is its AdS radius $L = \sqrt{-d(d-1)/(2\Lambda)}$, where $\Lambda(< 0)$ is its cosmological constant. This point particle limit $l_s \ll L$ typically makes the dual boundary theory strongly coupled. In these limits, the vacuum state gives the pure AdS space, and thermal states give AdS Schwarzschild black holes. We can also get a different bulk by modifying the theory itself, and so there are a variety of directions to extend AdS/CFT correspondence, whose examples include a capped off geometry given by the vacuum state of a gapped theory [25, 26, 27], as we will see later. Now holography is widely studied in more general situations than AdS/CFT correspondence, no matter whether they have stringy constructions with branes or not, such as many kinds of holographic models of condensed matters [28, 29, 30, 31], generalizations to non-relativistic theories [32, 33, 34] or to higher spin theories [35, 36, 37], and dS/CFT correspondence [38] or flat space holography [39, 40].

Mainly based on the study of AdS/CFT correspondence, a considerable number of dictionaries have been composed to translate physical quantities or concepts in one theory to the other via the holographic duality, such as global symmetries, correlation functions, responses to external sources, partition functions, thermodynamics, phase transitions, and spectrum of operators. The holographic duality remains mysterious, though, especially on how the information or structure of the bulk spacetime is encoded in the boundary quantum theory in one lower dimensions. This mystery would be very fundamental to holography in the sense that quantum gravity theory is a quantum theory for spacetimes. Understanding this mystery probably also helps us to study physics inside black hole horizons in a unitary way, particulary on how quantum information fallen into black holes and constituting the black holes is stored and can be recovered.

There have been a huge amount of attempts to probe the bulk structure via holography, of which one of the most important breakthroughs is the holographic formula of entanglement entropy [41, 42] assigning a surface area in the bulk side to quantum entanglement in the boundary side, at the rate of one (qu-)bit per four Planck areas. This relation is so important because area is one of the most elemental quantities for spacetime geometries, and in fact, the formula is a realization of the original idea of the holographic principle [6, 5] that asserts in quantum gravity theory, the degrees of freedom live not in volumes but in areas. This formula includes the famous Bekenstein-Hawking formula [43, 44] for black hole entropy as a special case when we consider the entanglement of the

whole spacial region for a thermal state. Overviews on the recent developments of the holographic entanglement entropy are available in reviews e.g. [45, 46].

Before seeing the holographic entanglement entropy formula, let us review the definition of entanglement entropy, the most fundamental quantity to study quantum entanglement. In quantum theories, entanglement entropy S_A of a state subspace $\mathcal{H}_A$ is defined as the von Neumann entropy $S_{\rm vN}[\rho] \equiv -{\rm Tr}[\rho \log \rho]$ of the reduced matrix $\rho_A = {\rm Tr}_{\bar{A}}[\rho_{\rm total}]$ as[1]

$$S_A \equiv -{\rm Tr}[\rho_A \log \rho_A] \,. \tag{1.1}$$

It measures how much quantum information of the degrees of freedom in $\mathcal{H}_A$ is entangled with the outer degrees of freedom, namely, how much quantum information will be lost for the subspace $\mathcal{H}_A$ if the outer subspace is ignored. In quantum field theories, entanglement entropy is defined for a space region A on a time slice, assuming that we can construct a state space $\mathcal{H}_A$ representing degrees of freedom on the region A by some appropriate procedures. The boundary of the region $\Sigma = \partial A$ is often called entangling surface. The total state is often taken as the vacuum $\rho_{\rm total} = |0\rangle \langle 0|$ for simplicity.

For static systems holographically described by Einstein gravity in the asymptotically AdS space, the holographic formula or so-called Ryu-Takayanagi (RT) formula [41, 42]

$$S_A = \min_{\partial \gamma_A = \partial A} \frac{{\rm Area}[\gamma_A]}{4G_N} \,, \tag{1.2}$$

associates the entanglement entropy of a given region A in the boundary side with the area of the codimension-two minimal bulk surface γ_A that is anchored at the entangling surface $\Sigma = \partial A$ on the boundary and is homologous to the region A (see Fig. 1.1).

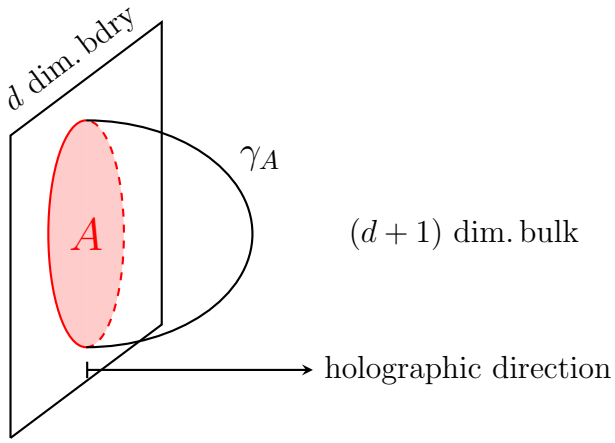

Figure 1.1: The configuration of the bulk minimal surface γ_A, whose area holographically gives the entanglement entropy of the red region A on the boundary. The titled rectangle represents the boundary on which the dual non-gravity field theory lives. The time direction is suppressed in this picture.

[1] Throughout this thesis, we always normalize a density matrix as ${\rm Tr}[\rho] = 1$.

Taking the whole spacial region as the region A for a thermal state described by a black hole geometry, the entanglement entropy becomes just the thermal entropy and the homology condition says that the corresponding minimal surface γ is just the surface of the black holes, and so this formula reduces to Bekenstein-Hawking formula,

$$S_{\text{black hole}} = \frac{\text{Area[black hole surface]}}{4G_N} \,. \tag{1.3}$$

In this sense, this holographic formula is a generalization of Bekentein-Hawking formula from thermal entropies to more general quantum information or entanglements, or from black hole horizons to more general bulk surfaces, and can be a lot of help to study how the information or structure of the bulk spacetime is encoded in the boundary quantum theory in one lower dimensions.

In fact, to bulk spacetimes, this formula is so fundamental that we can derive linearized Einstein equations from mathematical properties of entanglements via this formula for ball shaped regions [47], though it is shown only for small perturbations around the CFT vacuum, holographically dual to small perturbations around the pure AdS space. This novel derivation of equation of motion for spacetime geometries suggests a possibility that all the structure or dynamics of spacetimes may be governed by mathematical properties of quantum entanglements, via this simple holographic formula.

To generalize this derivation of gravitational equations of motion to more general states other than the CFT vacuum, dual to more general bulk spacetime geometries other than pure AdS space, however, we have to understand better about entanglements and holographic entanglements of such more general states and more general geometries. In this thesis, I have then studied entanglements in two such more general cases, the vacuum of a gapped theory dual to a capped-off geometry (chapter 3), and a time-dependent state of CFT (chapter 4) dual to a time-dependent geometry.

As a result, while a known formula proposed for entanglement entropy in gapped theories says that entropies are additive with regions, we discovered that there are non-additive corrections to the formula and entanglement entropy is not additive even in gapped theories. This non-additivity of entanglement entropy indicates that by taking multiple regions instead of a single region, we obtain much more information about the spacetime geometry via the holographic entanglement entropy formula, even in gapped theories. This suggests that studies of entanglements for multiple regions may help one generalize the limited works on deriving gravitational equations of motion from the holographic formula. Other new insights we have obtained into entanglements or holographic entanglements with a gap or time dependence will be helpful information in future to study any relation between equation of motions for spacetimes and quantum entanglements, for capped-off geometries and time-dependent geometries.

While it is not known whether we can derive full non-linear equation of motions for spacetimes only from the mathematical properties of entanglements, if so, probably we have to know more about entanglements or holographic entanglements. So it is natural to study a holographic formula for (entanglement) Rényi entropy, defined as

$$S_{n,A} \equiv -\frac{1}{n-1} \log \text{Tr}[\rho_A^n] \,, \tag{1.4}$$

since it contains much more information about quantum entanglement than entanglement entropy, in that it knows more about the whole spectrum of density matrices, sometimes called entanglement spectrum. In condensed matter physics, for example, entanglement spectrum is used as a more powerful tool to identify topological orders than entanglement entropy [48], while entanglement entropy is just one value uniquely determined by the whole entanglement spectrum and can be obtained by the $n = 1$ limit of the Rényi entropy, $S_A = \lim_{n\to 1} S_{n,A}$. In this thesis, I have studied how mathematical properties of Rényi entropies are translated into the bulk language via its holographic formula proposed recently, giving a nontrivial consistency check for the formula (chapter 6). Other measures of quantum entanglements may also be of help, and I have studied one such quantity called renormalized entanglement entropy (chapter 5), which has a characteristic mathematical property that they monotonically decrease along renormalization group (RG) flows.

Chapter 2

Quantum Entanglements in Field Theories and Holographic Theories

In this chapter, we review fundamental concepts and techniques that will appear in the following chapters on my research.

2.1 Techniques to calculate entanglements

2.1.1 Replica trick

In this subsection, we review a technique called *replica trick* [49, 50], which allows one to calculate entropies in field theories as some partition functions. It would be hard to study general density matrices in field theories, and so let us focus only on density matrices that admit a path integral representation.

The simplest example for such a density matrix is the vacuum density matrix,[1] $\rho_0 \equiv |0\rangle\langle 0|$. The explicit expression can be obtained by rewriting both the vacuum state $|0\rangle$ and its conjugate $\langle 0|$ in a path integral form. Let x denote the space directions, and let $\phi(x)$ denote collectively the fields we consider. Since only the vacuum state survives in an infinite Euclidean time evolution, the vacuum wave functional, $\Psi_0[\phi(x)] \equiv \langle\phi(x)|0\rangle$,

[1] In this thesis, we assume that the vacuum does not degenerate.

can be expressed as a past semi-infinite Euclidean time path integral,[2]

$$\Psi_0[\phi(x)] = \frac{1}{\sqrt{Z}} \int_{M,\, t_E<0}^{\varphi(0,x)=\phi(x)} \mathcal{D}\varphi(t_E,x)\, e^{-I_E[\varphi(t_E,x)]}, \tag{2.4}$$

over the fields in all the past region $t_E < 0$ of the Euclidean spacetime M. The pathes $\varphi(t_E, x)$ are summed over under the boundary condition $\varphi(0, x) = \phi(x)$, namely, we only take paths that match the argument of the wave functional, $\phi(x)$, on the boundary $t_E = 0$. In the same way, its conjugate state, $\Psi_0^*[\phi(x)] = \langle 0|\phi(x)\rangle$, is expressed as a future semi-infinite Euclidean time path integral,

$$\Psi_0^*[\phi(x)] = \frac{1}{\sqrt{Z}} \int_{M,\, t_E>0}^{\varphi(0,x)=\phi(x)} \mathcal{D}\varphi(t_E,x)\, e^{-I_E[\varphi(t_E,x)]}, \tag{2.5}$$

over the fields in all the future region $t_E > 0$. Their inner product,

$$\langle 0|0\rangle = \int \mathcal{D}\phi(x)\, \langle 0|\phi(x)\rangle\, \langle \phi(x)|0\rangle \tag{2.6}$$

$$= \int \mathcal{D}\phi(x)\, \Psi_0[\phi(x)]\Psi_0^*[\phi(x)]\,, \tag{2.7}$$

then gives the Euclidean path integral over the whole Euclidean time,

$$\langle 0|0\rangle = \frac{1}{Z} \int \mathcal{D}\phi(x) \int_{M,\, t_E\neq 0}^{\varphi(0,x)=\phi(x)} \mathcal{D}\varphi(t_E,x)\, e^{-I_E[\varphi(t_E,x)]} \tag{2.8}$$

$$= \frac{1}{Z} \int_M \mathcal{D}\varphi(t_E,x)\, e^{-I_E[\varphi(t_E,x)]}\,, \tag{2.9}$$

where M is the whole Euclidean spacetime. Note that the integral over $\phi(x)$ plays the role of sewing the two path integrals at their contact surface $t_E = 0$. We impose the normalization $\mathrm{Tr}[\rho_0] = \langle 0|0\rangle = 1$, that is, the coefficient Z is set to the partition function

$$Z = Z[M] = \int_M \mathcal{D}\varphi(t_E,x)\, e^{-I_E[\varphi(t_E,x)]}\,. \tag{2.10}$$

[2]You can also convince yourself of this expression by a following argument. The vacuum state would be obtained by a past infinite Euclidean time translation,

$$|0\rangle = \lim_{T\to\infty} \frac{e^{-HT}\,|\phi'(x); -T\rangle}{\| \, |e^{-HT}|\phi'(x); -T)\rangle \, \|}\,, \tag{2.1}$$

from any field operator eigenstate $|\phi'(x)\rangle$ that is not orthogonal to the vacuum, $\langle 0|\phi'(x)\rangle \neq 0$. The vacuum wave functional, $\Psi_0[\phi(x)] = \langle \phi(x)|0\rangle$, is then expressed as an Euclidean transition amplitude from $\phi'(x)$ at $t_E = -T$ to $\phi(x)$ at $t_E = 0$,

$$\Psi_0[\phi(x)] \propto \lim_{T\to\infty} \langle \phi(x); 0|e^{-HT}|\phi'(x); -T\rangle \tag{2.2}$$

$$\propto \lim_{T\to\infty} \int_{\varphi(-T,x)=\phi'(x)}^{\varphi(0,x)=\phi(x)} \mathcal{D}\varphi(t_E,x)\, e^{-I_E[\varphi(t_E,x)]}\,, \tag{2.3}$$

which reproduces the equation (2.4).

Next, let us move on to rewriting the density matrix ρ_0. Generally, for a pure state $|\psi\rangle$, matrix elements of the corresponding density matrix $\rho = |\psi\rangle\langle\psi|$ are just a product of two wave functionals, $\langle\phi_2(x)|\rho|\phi_1(x)\rangle = \Psi_\psi[\phi_2(x)]\Psi^*_\psi[\phi_1(x)]$, where $\Psi_\psi[\phi(x)] \equiv \langle\phi(x)|\psi\rangle$. And so once a wave functional admits a path integral representation like (2.4), we can also express the corresponding density matrix $\rho = |\psi\rangle\langle\psi|$ in a path integral form. Especially in the case of the vacuum density matrix,

$$\langle\phi_2(x)|\rho_0|\phi_1(x)\rangle = \Psi_0[\phi_2(x)]\Psi^*_0[\phi_1(x)] \tag{2.11}$$

$$= \frac{1}{Z}\int_{M,\, t_E\neq 0}^{\varphi(-0,x)=\phi_2(x),\, \varphi(+0,x)=\phi_1(x)} \mathcal{D}\varphi(t_E,x)\, e^{-I_E[\varphi(t_E,x)]}\,, \tag{2.12}$$

or,

$$\rho_0 = \int \mathcal{D}\phi_1(x)\mathcal{D}\phi_2(x)\ |\phi_2(x)\rangle\langle\phi_2(x)|\rho_0|\phi_1(x)\rangle\langle\phi_1(x)| \tag{2.13}$$

$$= \frac{1}{Z}\int \mathcal{D}\phi_1(x)\mathcal{D}\phi_2(x) \int_{M,\, t_E\neq 0}^{\varphi(-0,x)=\phi_2(x),\, \varphi(+0,x)=\phi_1(x)} \mathcal{D}\varphi(t_E,x)\, e^{-I_E[\varphi(t_E,x)]}\, |\phi_2(x)\rangle\langle\phi_1(x)|\ . \tag{2.14}$$

Now the boundary condition at $t_E = 0$ differs according to the direction from which we approach the boundary; the fields should satisfy $\varphi(-0,x) = \phi_2(x)$ in approaching from the past, and should satisfy $\varphi(+0,x) = \phi_1(x)$ in approaching from the future. In other words, the boundary condition forms a cut at $t_E = 0$. We can sew this cut by taking the trace, as $\mathrm{Tr}[|\phi_1(x)\rangle\langle\phi_2(x)|] = \langle\phi_2(x)|\phi_1(x)\rangle = \prod_x \delta(\phi_2(x)-\phi_1(x))$, and the resultant path integral reproduces the expression (2.8). One can extend the above discussions to states excited by local operators from the vacuum, $|\psi\rangle = TO(t_1,x_1)\ldots O(t_n,x_n)\,|0\rangle$, whose wave functionals have a path integral representation

$$\Psi_\psi[\phi(x)] = \frac{1}{\sqrt{Z'}}\int_{M,\, t_E<0}^{\varphi(0,x)=\phi(x)} \mathcal{D}\varphi(t_E,x)\, O(t_1,x_1)\ldots O(t_n,x_n)\, e^{-I_E[\varphi(t_E,x)]}\,. \tag{2.15}$$

Another important density matrix that admit a path integral representation is the thermal density matrix, $\rho_\beta \equiv e^{-\beta H}/Z$, which includes the vacuum density matrix as the $\beta = \infty$ case. Since Boltzmann factor $e^{-\beta H}$ is interpreted as an Euclidean time evolutor of time β, the matrix elements of ρ_β can be naturally understood as Euclidean transition amplitudes,

$$\langle\phi_2(x)|\rho_\beta|\phi_1(x)\rangle = \frac{1}{Z}\int_{\varphi(0,x)=\phi_1(x)}^{\varphi(\beta,x)=\phi_2(x)} \mathcal{D}\varphi(t_E,x)\, e^{-I_E[\varphi(t_E,x)]}\,. \tag{2.16}$$

One can transform the above expression into the same form with the vacuum case (2.12), by compactifying the Euclidean time direction of the spacetime M to a circle $\mathbb{S}^1$ of radius β. The vacuum case is included as the large radius limit $\beta \to \infty$. In the same way with the vacuum case, the normalization $\mathrm{Tr}[\rho_\beta] = 1$ set the coefficient Z to the partition function (2.10), though the Euclidean time direction of M is now compacitified.

As expected from the above observation that trace operations, $\rho \to \mathrm{Tr}[\rho]$, sew the cut in its path integral representation, partial trace operations, $\rho \to \rho_A = \mathrm{Tr}_{\bar{A}}[\rho]$, sew the cut partially only on the region $\bar{A}$, leaving the cut on the region A open.[3] Its matrix elements are given by partially tracing out the fields on $x_{\bar{A}} \in \bar{A}$,

$$\langle \phi_2(x_A)|\rho_A|\phi_1(x_A)\rangle = \int \mathcal{D}\phi(x_{\bar{A}})\, \langle \phi_2(x_A), \phi(x_{\bar{A}})|\rho|\phi_1(x_A), \phi(x_{\bar{A}})\rangle\,. \tag{2.17}$$

and this additional integral partially closes the cut of the total density matrix ρ (2.12),

$$\begin{aligned}
&\langle \phi_2(x_A)|\rho_A|\phi_1(x_A)\rangle \\
&= \frac{1}{Z}\int \mathcal{D}\phi(x_{\bar{A}}) \int_{M,\, t_E\neq 0}^{\varphi(-0,x)=\{\phi_2(x_A),\,\phi(x_{\bar{A}})\},\ \varphi(+0,x)=\{\phi_1(x_A),\,\phi(x_{\bar{A}})\}} \mathcal{D}\varphi(t_E,x)\, e^{-I_E[\varphi(t_E,x)]} &(2.18)\\
&= \frac{1}{Z}\int_{M,\,\{t_E,x\}\notin\{0\}\times A}^{\varphi(-0,x_A)=\phi_2(x_A),\,\varphi(+0,x_A)=\phi_1(x_A)} \mathcal{D}\varphi(t_E,x)\, e^{-I_E[\varphi(t_E,x)]}\,. &(2.19)
\end{aligned}$$

It then becomes obvious that in the path integral representation, indices of density matrices are represented by the location of cuts; the right and left indices correspond to the upper side $t_E = +0$ and the lower side $t_E = -0$ of the cut, respectively.

Generally, we can multiply density matrices by sewing the upper side of one cut and the lower side of the other cut,

$$\langle \phi_3(x_A)|\rho_A\sigma_A|\phi_1(x_A)\rangle = \int \mathcal{D}\phi_2(x_A)\, \langle \phi_3(x_A)|\rho_A|\phi_2(x_A)\rangle\, \langle \phi_2(x_A)|\sigma_A|\phi_1(x_A)\rangle\,, \tag{2.20}$$

which connects spacetimes of their path integral representations. To illustrate this multiplication, let us take reduced density matrices ρ_A and σ_A represented respectively by path integrals (2.19) over spacetimes M_ρ and M_σ, for simplicity. These spacetimes have cuts at $\{0\}\times A$, and according to (2.20), $\phi_3(x_A)$ is assigned to $\{-0\}\times A$ in M_ρ, $\phi_2(x_A)$ is assigned to both $\{+0\}\times A$ in M_ρ and $\{-0\}\times A$ in M_σ, and $\phi_3(x_A)$ is assigned to $\{-0\}\times A$ in M_ρ. The $\phi_2(x_A)$ integral in (2.20) then results in identifying $\{+0\}\times A$ in M_ρ and $\{-0\}\times A$ in M_σ,

$$\begin{aligned}
&\langle \phi_3(x_A)|\rho_A\sigma_A|\phi_1(x_A)\rangle \\
&= \frac{1}{Z[M_\rho]Z[M_\sigma]}\int \mathcal{D}\phi_2(x_A) \int_{M_\rho,\,\{t_E,x\}\notin\{0\}\times A}^{\varphi(-0,x_A)=\phi_3(x_A),\,\varphi(+0,x_A)=\phi_2(x_A)} \mathcal{D}\varphi(t_E,x) \\
&\qquad\qquad \int_{M_\sigma,\,\{t_E,x\}\notin\{0\}\times A}^{\varphi(-0,x_A)=\phi_2(x_A),\,\varphi(+0,x_A)=\phi_1(x_A)} \mathcal{D}\varphi(t_E,x)\ e^{-I_E[\varphi(t_E,x)]} &(2.21)\\
&= \frac{1}{Z[M_\rho]Z[M_\sigma]} \int_{M_\rho+M_\sigma,\,(+0,x_A)_{M_\rho}=(-0,x_A)_{M_\sigma},\,\{t_E,x\}\notin\{0\}\times A}^{\varphi((-0,x_A)_{M_\rho})=\phi_3(x_A),\,\varphi((+0,x_A)_{M_\sigma})=\phi_1(x_A)} \mathcal{D}\varphi(t_E,x)\, e^{-I_E[\varphi(t_E,x)]}\,. &(2.22)
\end{aligned}$$

[3]Here we assume that our Hilbert space $\mathcal{H}$ associated with the quantum fields $\phi(x)$ decomposes into a tensor product $\mathcal{H}_A \otimes \mathcal{H}_{\bar{A}}$, where $\mathcal{H}_A$ and $\mathcal{H}_{\bar{A}}$ are Hilbert spaces associated with the fields restricted to regions A and $\bar{A}$, $\phi(x)|_A$ and $\phi(x)|_{\bar{A}}$, respectively. This assumption is subtle in some cases, but would be reasonable at least for field theories that admit lattice regularization.

The resultant spacetime is a sum of M_σ and M_ρ glued at the cut.

Our goal of this subsection is to represent $\mathrm{Tr}[\rho_A^n]$ as a path integral. Let us take n copies of M with a cut in $\{0\} \times A$, and call them $M_1, \ldots, M_n$. The $(n-1)$ times multiplications in the n-th power $\rho_A^n = \rho_A \ldots \rho_A$ connect all these spacetimes, by sewing $\{+0\} \times A$ in M_i and $\{-0\} \times A$ in M_{i+1} for $i = 1, \ldots, n-1$,

$$\langle \phi_2(x_A)|\rho_A^n|\phi_1(x_A)\rangle = \frac{1}{Z[M]^n} \int_{\cup_i M_i,\, (+0,x_A)_{M_i}=(-0,x_A)_{M_{i+1}},\, \{t_E,x\}\notin\{0\}\times A}^{\varphi((-0,x_A)_{M_n})=\phi_2(x_A),\, \varphi((+0,x_A)_{M_1})=\phi_1(x_A)} \mathcal{D}\varphi(t_E,x)\, e^{-I_E[\varphi(t_E,x)]}\,. \tag{2.23}$$

Its remaining cuts at $\{-0\} \times A$ in M_n and $\{+0\} \times A$ in M_1 close by taking the trace, and finally we reach a simple formula

$$\mathrm{Tr}[\rho_A^n] = \frac{Z[M_{n,A}]}{Z[M]^n}\,, \tag{2.24}$$

where $M_{n,A}$ is a n-covering spacetime called *replica space*, a sum of $M_1, \ldots, M_n$ connected cyclicly by identifying $\{+0\}\times A$ in M_i with $\{-0\}\times A$ in M_{i+1} for $i = 1, \ldots, n$ ($M_{n+1} = M_1$).

This simple formula enables one to calculate Rényi entropies (1.4) as partition functions,

$$S_n(A) = -\frac{\log Z[M_{n,A}] - n \log Z[M]}{n-1}\,. \tag{2.25}$$

Originally n is a positive integer number, but it is usually assumed that we can analytically continue n and can take the limit $n \to 1$, yielding a formula for entanglement entropy (1.1)

$$S(A) = -\lim_{n\to 1} \frac{\log Z[M_{n,A}] - n \log Z[M]}{n-1} \tag{2.26}$$

$$= -(\partial_n - 1) \log Z[M_{n,A}]|_{n=1}\,. \tag{2.27}$$

2.1.2 Lattice discretization

If a field theory admit a lattice regularization, entropies can be calculated as the continuum limit of calculation results on lattices at least in principle. For vacuum states of free fields, this lattice calculation becomes simple enough that one can explicitly carry out the calculation numerically. This lattice technique [51, 52, 53] applies to both free scalars and free fermions, but here we take only free scalars for simplicity.

We start by constructing the vacuum density matrix on a lattice. By discretizing the space into a lattice, a free scalar theory normally becomes a system of coupled oscillators with a Hamiltonian of the form

$$H = \frac{1}{2}\sum_i \pi_i^2 + \frac{1}{2}\sum_{i,j} \phi_i K_{ij} \phi_j\,, \tag{2.28}$$

where i, j is the label of lattice sites and K is a real symmetric positive-definite matrix. This system can be seen as decoupled harmonic oscillators

$$H = \frac{1}{2} \sum_k \left({\pi'_k}^2 + \omega_k^2 {\phi'}_k \right) , \tag{2.29}$$

by diagonalizing K by a real orthogonal matrix O as $K_{ij} = O_{ki} \omega_k^2 O_{kj}$ with positive eigenvalues ω_k^2, and by a non-local field redefinition $\phi'_k \equiv O_{ki} \phi_i$ and $\pi'_k \equiv O_{ki} \pi_i$. The ground state of a simple Harmonic oscillator $H = (p^2 + \omega^2 x^2)/2$ has a Gaussian wave function $\psi(x) = (\omega/\pi)^{1/4} \exp(-\omega x^2/2)$, and so the vacuum of our scalar field ϕ has a multivariate Gaussian wave functional

$$\Psi[\phi] = \Psi(\phi_1, \phi_2, \dots) = \prod_k \left[\left(\frac{\omega_k}{\pi} \right)^{1/4} e^{-\omega_k {\phi'_k}^2/2} \right] = \left(\det \frac{W}{\pi} \right)^{1/4} e^{-\frac{1}{2} \sum_{i,j} \phi_i W_{ij} \phi_j} , \tag{2.30}$$

whose precision matrix $W = K^{1/2}$ is the positive square root of K with symmetric matrix elements $W_{ij} = O_{ki} \omega_k O_{kj}$. This matrix W and its inverse W^{-1} can be read off from the vacuum correlators as

$$X_{ij} \equiv \langle \phi_i \phi_j \rangle = \int \Big[\prod_i d\phi_i \Big] \, \Psi_0^*[\phi] \phi_i \phi_j \Psi_0[\phi] = \frac{1}{2} W^{-1}_{ij} , \tag{2.31}$$

$$P_{ij} \equiv \langle \pi_i \pi_j \rangle = \int \Big[\prod_i d\phi_i \Big] \, \Psi_0^*[\phi] \left(-i \frac{d}{d\phi_i} \right) \left(-i \frac{d}{d\phi_j} \right) \Psi_0[\phi] = \frac{1}{2} W_{ij} , \tag{2.32}$$

which satisfies $XP = 1/4$. From the expression (2.30), the vacuum density matrix is given by the product of the wave functionals,

$$\langle \phi' | \rho_0 | \phi \rangle = \Psi_0[\phi'] \Psi_0^*[\phi] = \left(\det \frac{W}{\pi} \right)^{1/2} e^{-\frac{1}{2} \sum_{i,j} (\phi_{2i} W_{ij} \phi_{2j} + \phi_{1i} W_{ij} \phi_{1j})} . \tag{2.33}$$

Note that although the above wave functional (2.30) appears to be a product state and so be disentangled in terms of the redefined field ϕ', it is really entangled in terms of the original field ϕ. In general, non-local field redefinitions do not preserve the original entanglement structure, as can be understood from the definition of entanglement entropy (1.1) requiring a spacial region A to be specified.

Now that a region A and its complement $\bar{A}$ are sets made up of lattice sites, we can perform the partial trace (2.17) over $\bar{A}$ just by integrating over $\phi_{\bar{\imath}}$ for all $\bar{\imath} \in \bar{A}$. To carry out this integration, let us divide the precision matrix W into 2×2 blocks,

$$W = \begin{pmatrix} W^{(A)} & W^{(A\bar{A})} \\ W^{(\bar{A}A)} & W^{(\bar{A})} \end{pmatrix} , \tag{2.34}$$

according to whether each matrix index is included in A or in $\bar{A}$. Since the matrix W is symmetric and positive definite, the submatrices $W^{(A)}$ and $W^{(\bar{A})}$, and their Schur complements,

$$W_{(A)} \equiv W^{(A)} - W^{(A\bar{A})} (W^{(\bar{A})})^{-1} W^{(\bar{A}A)} , \tag{2.35}$$

$$W_{(\bar{A})} \equiv W^{(\bar{A})} - W^{(\bar{A}A)} (W^{(A)})^{-1} W^{(A\bar{A})} , \tag{2.36}$$

are all symmetric and positive definite, where $W^{(A\bar{A})} = (W^{(\bar{A}A)})^T$. Restricting the indices i and j to the sites in A, the correlators (2.31) and (2.32) can be expressed as

$$X^{(A)} = \frac{1}{2} W_{(A)}^{-1}, \qquad P^{(A)} = \frac{1}{2} W^{(A)}, \tag{2.37}$$

thanks to the formula for the inverse of a block matrix,

$$W^{-1} = \begin{pmatrix} W_{(A)}^{-1} & -W_{(A)}^{-1} W^{(A\bar{A})} (W^{(\bar{A})})^{-1} \\ -W_{(\bar{A})}^{-1} W^{(\bar{A}A)} (W^{(A)})^{-1} & W_{(\bar{A})}^{-1} \end{pmatrix}. \tag{2.38}$$

They satisfy an uncertainty principle like inequality[4]

$$X^{(A)} P^{(A)} \geq \frac{1}{4}, \tag{2.39}$$

because a matrix $2P^{(A)} - (2X^{(A)})^{-1} = W^{(A)} - W_{(A)} = W^{(A\bar{A})} (W^{(\bar{A})})^{-1} W^{(\bar{A}A)}$ is non-negative definite due to the positivity of $W^{(\bar{A})}$.

Now we can evaluate the partial trace (2.17) explicitly as

$$\langle \phi^{(A)} | \rho_A | \phi'^{(A)} \rangle = \int \Big[\prod_{\bar{\imath} \in \bar{A}} d\varphi_{\bar{\imath}} \Big] \langle \phi^{(A)}, \varphi | \rho | \phi'^{(A)}, \varphi \rangle \,. \tag{2.40}$$

$$= \left(\det \frac{W}{\pi} \right)^{1/2} \int \Big[\prod_{\bar{\imath} \in \bar{A}} d\varphi_{\bar{\imath}} \Big] \tag{2.41}$$

$$\times \exp \left[-\frac{1}{2} \sum_{i,j \in A} (\phi_i W_{ij}^{(A)} \phi_j + \phi'_i W_{ij}^{(A)} \phi'_j) - \sum_{i \in A,\, \bar{\jmath} \in \bar{A}} (\phi_i + \phi'_i) W_{i\bar{\jmath}}^{(A\bar{A})} \varphi_{\bar{\jmath}} - \sum_{\bar{\imath}, \bar{\jmath} \in \bar{A}} \varphi_{\bar{\imath}} W_{\bar{\imath}\bar{\jmath}}^{(\bar{A})} \varphi_{\bar{\jmath}} \right] \tag{2.42}$$

$$= \frac{1}{\sqrt{\det(2\pi X^{(A)})}} \exp \left[-\frac{1}{4} \sum_{i,j \in A} \Big((\phi_i - \phi'_i)(2P^{(A)})_{ij} (\phi_j - \phi'_j) + (\phi_i + \phi'_i)((2X^{(A)})^{-1})_{ij} (\phi_j + \phi'_j) \Big) \right], \tag{2.43}$$

where we used a formula for determinants of block matrices,

$$\det W = \det W^{(A)} \det W_{(\bar{A})} = \det W_{(A)} \det W^{(\bar{A})} \,. \tag{2.44}$$

From this expression of the reduced matrix, in the same way as [51], we can obtain Rényi entropies and entanglement entropies,

$$S_n = \frac{1}{n-1} \mathrm{Tr} \log[(C + 1/2)^n - (C - 1/2)^n] \,, \tag{2.45}$$

$$S_A = \mathrm{Tr} \log[(C + 1/2) \log(C + 1/2) - (C - 1/2) \log(C - 1/2)] \,, \tag{2.46}$$

with $C \equiv \sqrt{X^{(A)} P^{(A)}}$. This result can also be derived by another method introducing some annihilation and creation operators [53, 52].

[4]For matrices X and Y, an inequality $X \geq Y$ stands for the non-negative definiteness of their difference $X - Y$.

2.2 Entanglements in field theories

2.2.1 General forms

It is known that in d-dimensional field theories, an entanglement entropy of an region A typically[5] takes the form of

$$S_A = \frac{s_{d-2}}{\epsilon^{d-2}} + \frac{s_{d-4}}{\epsilon^{d-4}} + \frac{s_{d-6}}{\epsilon^{d-6}} + \dots , \tag{2.47}$$

in the expansion of some UV cutoff length scale ϵ. One may wonder whether it is useful to think about such regularization ϵ dependent quantities, but once we understand how their ϵ dependence arises, from them we can construct quantities or combinations that are ϵ independent or are finite in the continuum $\epsilon \to 0$ limit.

The most dominant term is in the order of $O(1/\epsilon^{d-2})$, and is called as *area law* term, since its coefficient s_{d-2} is known to be proportional to the $(d-2)$-dimensional area of the entangling surface $\Sigma = \partial A$,

$$S_A = \alpha \frac{\text{Area}[\Sigma]}{\epsilon^{d-2}} + O\left(\frac{1}{\epsilon^{d-4}}\right) , \tag{2.48}$$

where α is an unimportant dimensionless constant given by the UV physics.

In the sub-leading orders, the power of $1/\epsilon$ decreases by two, and so the final term depends on whether the spacetime dimension is even or odd. In even dimensions, the expansion ends at a logarithmic term and a constant,

$$S_A^{(\text{even})} = \alpha \frac{\text{Area}[\Sigma]}{\epsilon^{d-2}} + \frac{s_{d-4}}{\epsilon^{d-4}} + \dots + \frac{s_2}{\epsilon^2} + C \log \frac{1}{\epsilon} + s \, , \tag{2.49}$$

while in odd dimensions, it ends at a constant term,

$$S_A^{(\text{odd})} = \alpha \frac{\text{Area}[\Sigma]}{\epsilon^{d-2}} + \frac{s_{d-4}}{\epsilon^{d-4}} + \dots + \frac{s_1}{\epsilon} - F \, . \tag{2.50}$$

In even dimensions, the logarithmic term $C \log(1/\epsilon)$ and the constant term s can be put together into one term $C \log(l/\epsilon)$ with some length scale l. As we will see, the most important quantity in these expansions is the dimensionless quantity C in even dimensions or F in odd dimensions, which can be interpreted to capture some degrees of freedom in the theory. In fact, ϵ independent quantities constructed form entropies, such as entropic c-functions, renormalized entanglement entropies or mutual information, pick out C or F somehow by getting rid of the power law terms $O(1/\epsilon^n)$.

Let us see this expansion in important dimensions, two, three, and four dimensions, which will appear in this thesis. In two dimensions, it is essentially one logarithmic term,

$$S_A^{(\text{2d})} = C \log \frac{1}{\epsilon} + s \, . \tag{2.51}$$

[5] This is not the case in special cases, for instance, when the entangling surface $\Sigma = \partial A$ has cusps.

Though the entangling surface Σ is zero-dimensional and just the end points of the region A in this dimension, this logarithmic term can be also regarded as the area law term for two dimensions, since the coefficient C of the $\log(1/\epsilon)$ is additive with respect to the end points and determined by the UV physics. In fact, C is $c/6$ for each one end point, where c is the central charge of the UV CFT_2; a half line has the coefficient $C = c/6$, an interval has $C = c/3$, and the union of two disjoint intervals has $C = 2c/3$. In three dimensions, it composes of the area law term and the constant term,

$$S_A^{(3\mathrm{d})} = \alpha \frac{\mathrm{Length}[\Sigma]}{\epsilon} - F\,. \tag{2.52}$$

Now the entangling surface Σ is just a one-dimensional curve, and its area means just its length. When the region A is a disk, there is a theorem called F-theorem stating that F monotonically decreases with along RG flows [54, 55]. In four dimensions, it is composed of the area law term and the logarithmic term,

$$S_A^{(4\mathrm{d})} = \alpha \frac{\mathrm{Area}[\Sigma]}{\epsilon^2} + C \log \frac{1}{\epsilon} + s\,. \tag{2.53}$$

Similar to two dimensions, the coefficient C is related to central charges or conformal anomaly coefficients a and c of the UV CFT via Solodukhin's formula [56, 57]:

$$C = -\frac{a}{2}\chi[\Sigma] - \frac{c}{2\pi}\int_\Sigma \left(\mathcal{R}_{aa} - \mathcal{R}_{abab} - \frac{\mathcal{R}}{3} + k^a_{\mu\nu}k^{\mu\nu}_a - \frac{1}{2}(k^{a\,\mu}_\mu)^2 \right)\,, \tag{2.54}$$

where $\chi[\Sigma]$ is the Euler characteristic, $\mathcal{R}$ is the Ricci scalar, $\mathcal{R}_{aa} = \mathcal{R}^{\mu\nu}n^a_\mu n^a_\nu$, $\mathcal{R}_{abab} = \mathcal{R}^{\mu\nu\rho\sigma}n^a_\mu n^b_\nu n^a_\rho n^b_\sigma$, and $k^a_{\mu\nu} = \gamma^\rho_\mu \gamma^\sigma_\nu \nabla_\rho n^a_\sigma$ is the extrinsic curvature for the normal vectors n^a_μ $(a = 1, 2)$ on Σ with the induced metric $\gamma_{\mu\nu} = g_{\mu\nu} - n^a_\mu n^a_\nu$.

2.2.2 CFT_2

Here we review entanglement entropies in the most well-known example, namely, two-dimensional CFT. We take the region A as an interval of length l, and the total state as the vacuum state and thermal states, which correspond to a plane $\mathbb{R}^2$ and a cylinder $\mathbb{S}^1 \times \mathbb{R}$, respectively. The period β of the Euclidean time direction $\mathbb{S}^1$ of the cylinder gives the inverse temperature of the thermal state $\rho_\beta = e^{-\beta H}/\mathrm{Tr}[e^{-\beta H}]$.

We can obtain entropies in CFT_2 in many ways, say, by introducing operators called *twist operators* $\sigma_n(z, \bar{z})$ and $\bar{\sigma}_n(z, \bar{z})$, by constructing modular Hamiltonian $-\log\rho$ from the energy momentum tensor $T_{\mu\nu}$, or by looking at how the free energy $\log Z[M_{n,A}]$ of the replica space changes with scaling of the region as a result of the conformal anomaly $\langle T^\mu_\mu \rangle = -\frac{c}{24}R$. Here we see how to calculate entropies using twist operators. Twist operators are local operators such that by going around them, fields obtain a phase factor, $e^{2\pi i/n}$ for a twist operator σ_n and $e^{-2\pi i n}$ for an anti-twist operator $\bar{\sigma}_n$, whose conformal weights are known to be

$$h = \bar{h} = \frac{c}{24}\left(n - \frac{1}{n}\right), \qquad \Delta = h + \bar{h} = \frac{c}{12}\left(n - \frac{1}{n}\right). \tag{2.55}$$

It is also known that the partition function $Z[M_{n,A}]$ of the replica space $M_{n,A}$ in (2.24) is equal to the two point function of twist operators inserted in both the endpoints, ∂A, in the original space M. For an interval $a \le x\,(=\mathrm{Re}[z]) \le b$ of length $l = b-a$ at $t\,(=\mathrm{Im}[z]) = 0$, the twist operators are inserted at $(z,\bar{z}) = (a,a)$ and (b,b) as

$$\mathrm{Tr}[\rho_A^n] = \frac{Z[M_{n,A}]}{Z[M]^n} = \langle \sigma_n(a,a)\bar{\sigma}_n(b,b)\rangle_{M=\mathbb{R}^2}\ , \tag{2.56}$$

$$= \left(\frac{\epsilon}{b-a}\right)^{2h}\left(\frac{\epsilon}{b-a}\right)^{2\bar{h}} = \left(\frac{\epsilon}{l}\right)^{\frac{c}{6}\left(n-\frac{1}{n}\right)}\ . \tag{2.57}$$

Here the length scale ϵ of the UV cutoff is introduced as the normalization to match physical dimensions. This is natural since there is no other scale, and since when the region A is as small as the UV cutoff, $l \simeq \epsilon$, then the reduced density matrix is almost the same as the total state, $\rho_A \simeq \rho$, and thus $\mathrm{Tr}[\rho_A^n] \simeq 1$. Taking its logarithm, we obtain Rényi entropy and entanglement entropy for an interval of length l in the flat space $\mathbb{R}^2$,

$$S_n = -\frac{1}{n-1}\log \mathrm{Tr}[\rho_A^n] = \frac{c}{6}\left(1+\frac{1}{n}\right)\log\frac{l}{\epsilon}\,, \tag{2.58}$$

$$S_A = \lim_{n\to 1} S_n = \frac{c}{3}\log\frac{l}{\epsilon}\,. \tag{2.59}$$

By mapping the z plane to a z' cylinder

$$z = e^{2\pi z'/\beta} \tag{2.60}$$

with the period $t'\,(=\mathrm{Im}[z']) \sim t' + \beta$, we can also obtain the entropy of an interval $[a', b']$ of length $l = b' - a'$ in a thermal state. By this map, the twist operator transforms as

$$\sigma(z',\bar{z}') = \left(\frac{\partial z}{\partial z'}\right)^h\left(\frac{\partial \bar{z}}{\partial \bar{z}'}\right)^{\bar{h}}\sigma(z,\bar{z}) = \left(\frac{2\pi}{\beta}e^{2\pi x'/\beta}\right)^{\frac{c}{12}\left(n-\frac{1}{n}\right)}\sigma(z,\bar{z})\,, \tag{2.61}$$

and thus their correlation function transforms as

$$\mathrm{Tr}[\rho_A^n] = \langle \sigma_n(a',a')\bar{\sigma}_n(b',b')\rangle_{\mathbb{S}^1\times\mathbb{R}}\ , \tag{2.62}$$

$$= \left(\frac{2\pi}{\beta}e^{\pi(a'+b')/\beta}\right)^{\frac{c}{6}\left(n-\frac{1}{n}\right)}\langle \sigma_n(a,a)\bar{\sigma}_n(b,b)\rangle_{\mathbb{R}^2}\ , \tag{2.63}$$

$$= \left(\frac{\pi\epsilon}{\beta\sinh(\pi l/\beta)}\right)^{\frac{c}{6}\left(n-\frac{1}{n}\right)}\ , \tag{2.64}$$

where $a = e^{2\pi a'/\beta}$ and $b = e^{2\pi a'/\beta}$. From this result, we can similarly read off the entropies for interval of length l in the thermal state,

$$S_n = \frac{c}{6}\left(1+\frac{1}{n}\right)\log\left(\frac{\beta}{\pi\epsilon}\sinh\frac{\pi l}{\beta}\right)\ , \tag{2.65}$$

$$S_A = \frac{c}{3}\log\left(\frac{\beta}{\pi\epsilon}\sinh\frac{l}{\beta}\right)\ . \tag{2.66}$$

In the low temperature or the small interval limit $\beta \gg l$, the logarithm becomes simple

$$\log\left(\frac{\beta}{\pi\epsilon}\sinh\frac{\pi l}{\beta}\right) \simeq \log\frac{l}{\epsilon}\,, \tag{2.67}$$

and the entropies reproduces the results in the vacuum. In the high temperature limit or the small interval limit $l \ll \beta$, the logarithm becomes a volume term and a constant,

$$\log\left(\frac{\beta}{\pi\epsilon}\sinh\frac{\pi l}{\beta}\right) \simeq \frac{\pi l}{\beta} + \log\frac{\beta}{2\pi\epsilon}\,. \tag{2.68}$$

In the entanglement entropy, the first volume term reproduces the thermal entropy

$$S = \frac{c}{3}\pi T l \tag{2.69}$$

for the box of size l.

2.2.3 Ball shaped regions in CFT$_d$

In CFT's, entanglement entropies of a ball of radius R can be computed by replica trick and by a nice conformal transformation from the Euclidean flat space $\mathbb{R}^d$ to a thermal hyperbolic space, $\mathbb{S}^1 \times \mathbb{H}^{d-1}$ [58]. Since there appears the conformal anomaly in even dimensions, here let us focus on odd dimensions d for simplicity. Let us take a radial coordinate in the flat space $\mathbb{R}^d$, and combine the radial coordinate r and Euclidean time direction t into a complex coordinate $w \equiv r + it$,

$$ds^2 = dt^2 + dr^2 + r^2 d\Omega_{d-2}^2 \tag{2.70}$$

$$= dw d\bar{w} + r^2 d\Omega_{d-2}^2\,, \tag{2.71}$$

where the physical region $r \geq 0$ is represented by the half plane $\mathrm{Re}[w] \geq 0$ in w plane. The transformation from w to a new complex coordinate z is given as

$$e^z = \frac{R+w}{R-w}\,, \qquad \text{or equivalently,} \qquad \frac{w}{R} = \tanh\frac{z}{2}\,. \tag{2.72}$$

Let us understand what happens in this transformation step by step. First, a transformation

$$z' = \frac{R+w}{R-w} \tag{2.73}$$

maps the half plane $\mathrm{Re}[w] \geq 0$ in w plane to the outer region of the unit circle $|z'| \geq 1$ in z' plane, while the entangling region, the point $w = R$ in w plane, is mapped to the infinity $z' = \infty$ in z' plane. Next, another transformation

$$z = \log z'\,, \tag{2.74}$$

maps the z' plane to a cylinder of z with the imaginary direction rolled up as $\mathrm{Im}[z] \sim \mathrm{Im}[z] + 2\pi$. By this transformation, the unit circle $|z'| \geq 1$ is mapped to the half $\mathrm{Re}[z] \geq 0$

of the cylinder, and the entangling region $z' = \infty$ is still mapped to the infinity $\mathrm{Re}[z] = \infty$. Introducing real coordinates $z = u + i\tau/R$, where $\tau \sim \tau + 2\pi R$ and $u \geq 0$, the resultant metric

$$ds^2 = R^2 e^{-2\sigma}(dzd\bar{z} + du^2 + \sinh^2 u d\Omega_{d-2}^2) \tag{2.75}$$

$$= e^{-2\sigma}\left(d\tau^2 + R^2(du^2 + \sinh^2 u d\Omega_{d-2}^2)\right) , \tag{2.76}$$

is conformally equivalent to the metric of a thermal hyperbolic space $\mathbb{S}^1 \times \mathbb{H}^{d-1}$,

$$ds^2_{\mathbb{S}^1\times\mathbb{H}^{d-1}} = d\tau^2 + R^2(du^2 + \sinh^2 u d\Omega_{d-2}^2) . \tag{2.77}$$

Here the conformal factor is given by

$$e^{-\sigma} = \frac{1}{2}\left|1 - \left(\frac{w}{R}\right)^2\right| = \frac{1}{2|\cosh^2(z/2)|} . \tag{2.78}$$

By this transformation, the entangling surface Σ at $w = R$ is mapped to the infinity $u = \infty$ of the hyperbolic space, and the direction going around the entangling surface Σ is mapped to the thermal cycle S^1. In fact, a small cycle $w = R + \epsilon e^{-i\theta}$ ($\epsilon \ll R$) around Σ is mapped to $u = \log(2R/\epsilon)$ ($\gg 1$) and $\tau = R\theta$.

Since the replica space M_n is just the n covering space going around the entangling surface n times, this transformation still maps M_n to a thermal hyperbolic space $\mathbb{S}^1 \times \mathbb{H}^{d-1}$ but with a different radius of $\mathbb{S}^1$, $\tau \sim \tau + 2\pi nR$, namely, a different temperature $\beta = 2\pi nR$. So in CFT's, the replica partition function is just the thermal partition function over the hyperbolic space

$$\log Z[M_n] = \log Z_{\beta=2\pi nR}[\mathbb{H}^{d-1}], \tag{2.79}$$

and the entanglement entropy is just the thermal entropy $S = \beta(E - F)$ of the hyperbolic space at the temperature $\beta = 2\pi R$,

$$S_n = -\frac{\log Z_{2\pi nR}[\mathbb{H}^{d-1}] - n \log Z_{2\pi R}[\mathbb{H}^{d-1}]}{n-1} , \tag{2.80}$$

$$S_A = \left(1 - \beta\frac{\partial}{\partial\beta}\right) \log Z_\beta[\mathbb{H}^{d-1}]\Big|_{\beta=2\pi R} . \tag{2.81}$$

We can get another useful expression for this entropy. By a further transformation, $\sinh u = \cos\theta$ with $0 \leq \theta \leq \pi/2$, we can conformally map the thermal hyperbolic space $\mathbb{S}^1 \times \mathbb{H}^{d-1}$ to Euclidean de Sitter space of radius R,

$$ds^2_{\mathrm{dS}_{\beta=2\pi nR}} = R^2(d\theta^2 + \cos^2\theta d\tau^2 + \sin^2\theta d\Omega_{d-2}^2) , \tag{2.82}$$

with an irregular temperature $\beta = 2\pi nR$, for $\tau \sim \tau + 2\pi nR$. When $n = 1$, The geometry corresponds to an ordinary sphere $\mathbb{S}^d$ of radius R. This map allows us to regard the replica partition function and the entanglement entropy as the thermal partition function and the thermal entropy of de Sitter space as well. Because the sphere $\mathbb{S}^d$ is conformally equivalent to the flat space $\mathbb{R}^d$, its total energy $E_{\mathbb{S}^d} = -\beta\partial_\beta \log Z[\mathrm{dS}_{\beta=2\pi nR}]|_{n=1}$ vanishes, and thus the entanglement entropy of a sphere $\mathbb{S}^{d-2}$ is given just as the partition function of the sphere $\mathbb{S}^d$ in the end,

$$S_A = \beta(E_{\mathbb{S}^d} - F_{\mathbb{S}^d}) = -\beta F_{\mathbb{S}^d} , \tag{2.83}$$

$$= \log Z[\mathbb{S}^d] . \tag{2.84}$$

2.2.4 Gapped theories

In theories with a mass gap of order m, it is proposed that the entanglement entropy of a region A has an expansion in powers of $1/m$ [59, 60]:

$$S_A = \alpha \frac{\ell_\Sigma}{\epsilon} + \beta\, m\, \ell_\Sigma - \gamma_\Sigma + \sum_{n=0}^{\infty} \frac{c_{2n+1}^\Sigma}{m^{2n+1}} \ , \tag{2.85}$$

with numerical constants α, β and the topological entanglement entropy γ_Σ [61, 62]. Here the constant β is a scheme-independent [63, 64], while the numerical constant α is scheme-dependent. The constant γ_Σ depends on only the topology of the entangling surface $\Sigma = \partial A$ and detects long-range order. For example, a free massive scalar field has $\beta = -1/12$ and $\gamma_\Sigma = 0$. The dimensionful coefficients c_{2n+1}^Σ are postulated [60] as local integrals of functions of the extrinsic curvature and its derivatives on Σ. In other words, entanglement contributing to c_{2n+1}^Σ localizes on the entangling surface in the large-m limit due to the short correlation length of order $1/m$. The coefficients c_{2n+1}^Σ are polynomials of the radii of order $-(2n+1)$. This expansion has no proof for its validity in general, and as will shown in chapter 3, this $1/m$ expansion would receive exponential corrections of the form $e^{-\#m\delta}$.

2.3 More on entanglements

2.3.1 UV cutoff independent measures of entanglements

Here we introduce new quantities, mutual information and renormalized entanglement entropy, which represent quantum entanglements in a more sophisticated and numerically more accessible manner than entanglement entropy.

The *mutual information* between two disjoint regions A and B is defined out of the entanglement entropies as

$$I(A,B) \equiv S_A + S_B - S_{AB} \,, \tag{2.86}$$

which measures how much quantum information is shared between the two regions. In field theories, this quantity is UV cutoff ϵ dependent because the ϵ dependence of an entanglement entropy S_A is known to be local with respect to its entangling surface $\Sigma = \partial A$, and thus cancels out in the combination (2.86). Generally, mutual information has an advantage in its ability to draw tiny non-local or non-additive terms in quantum entanglement, since terms additive with respect to the entangling surface cancel in its definition. This quantity can be seen as a special case of *relative entropy*,

$$S[\rho|\sigma] \equiv \mathrm{Tr}[\rho(\log\rho - \log\sigma)] \,, \tag{2.87}$$

originally defined for any density matrices ρ and σ, while mutual information corresponds to the case when $\rho = \rho_{AB}$ and $\sigma = \rho_A \otimes \rho_B$,

$$I(A,B) = S[\rho_{AB}|\rho_A \otimes \rho_B] \,. \tag{2.88}$$

We can eliminate the ϵ dependence in other ways. For entropies of a disk A of radius R_{disk},

$$S_A(R_{\text{disk}}) = \alpha \frac{2\pi R_{\text{disk}}}{\epsilon} - F\,, \tag{2.89}$$

a pragmatic regularization is proposed by Liu and Mezei [65] as the *renormalized entanglement entropy* (REE):

$$\mathcal{F}(R_{\text{disk}}) = (R_{\text{disk}}\partial_{R_{\text{disk}}} - 1)S_A(R_{\text{disk}})\ . \tag{2.90}$$

This quantity serves as a measure of degrees of freedom in field theories, in that REE monotonically decreases along RG flows, thanks to its characteristic mathematical property of monotonicity $\mathcal{F}'(R) \leq 0$, identifying the disk size with the inverse of the energy scale of renormalization [55]. The expression (2.84) tells that the value of REE for CFT_3 is just the free energy of a three-sphere, $F = -\log Z[\mathbb{S}^3]$ [58], which gives the proof of the F-theorem stating that $F_{\text{UV}} \geq F_{\text{IR}}$ for the free energies at the UV and IR conformal fixed points [66, 54, 67, 68]. Such a function is called F-function and is reminiscent of the Zamolodchikov's c-function [69], which monotonically decreases along RG flows as well and gives the central charge at conformal fixed points.

2.3.2 Mathematical inequalities for entanglements

Let us see some important mathematical properties of entanglement entropy (1.1). First of all, it is not additive but sub-additive

$$S_A + S_B \geq S_{AB}\,, \tag{2.91}$$

with joining regions. This *sub-additivity* of entanglement entropy is equivalent to the non-negativity of mutual information (2.86),

$$I(A, B) \geq 0, \tag{2.92}$$

which holds since relative entropy is known to be non-negative, $S[\rho|\sigma] \geq 0$, and mutual information is a special case of relative entropy as explained before.

In fact, entanglement entropy satisfies a more strong inequality, called the *strong sub-additivity* [70]

$$S_{AC} + S_{BC} \geq S_C + S_{ABC}\,, \tag{2.93}$$

or equivalently,

$$S_A + S_B \geq S_{A\cup B} + S_{A\cap B}\,, \tag{2.94}$$

in a symmetric form, and the sub-additivity (2.91) is reproduced by taking C as $\emptyset$ in (2.93) or taking $A \cap B = \emptyset$ in (2.94). This inequality (2.93) is equivalent to the statement that mutual information monotonically increases with joining regions,

$$I(A, B \cup C) \geq I(A, C)\,, \tag{2.95}$$

which follows form the fact that relative entropy decreases monotonically under partial traces,

$$S[\rho|\sigma] \geq S[\mathrm{Tr}_B\rho|\mathrm{Tr}_B\sigma]\,, \tag{2.96}$$

by taking $\rho = \rho_{ABC}$ and $\sigma = \rho_A \otimes \rho_{BC}$ in this case. Less importantly, we can regard it as the non-negativity of a more complicated quantity called the conditional mutual information,

$$\begin{aligned} I(A,B|C) &\equiv S_{A|C} + S_{B|C} - S_{AB|C}\,, \\ &= S_{AC} + S_{BC} - S_{ABC} - S_C\,, \end{aligned} \tag{2.97}$$

where $S_{X|Y} \equiv S_{XY} - S_Y$ is called the conditional entropy. In field theories, the strong subadditivity is utilized for proving that some quantity serves as a measure of physical degrees of freedom in the sense that it monotonically decreases along RG flows, for quantities such as the entropic c-function in two dimensions [71] and the F-function (2.90) in three dimensions [55] introduced already.

2.4 Entanglements in holographic theories

2.4.1 AdS space

As AdS/CFT correspondence says, quantum gravity on AdS_{d+1} is equivalent to a CFT_d on its boundary, that is, their partition functions $Z = Z[J]$ are just the same [21, 22],

$$Z_{\text{Quantum Gravity on AdS}_{d+1}} = Z_{\mathrm{CFT}_d}\,. \tag{2.98}$$

And as explained in chapter 1, as a first step to study this holographic relation, we usually take the classical limit in the bulk side so that we can approximate the bulk partition function as the dominant classical contribution,

$$Z_{\text{Quantum Gravity on AdS}_{d+1}} \sim e^{-I_{\text{gravity}}}\,, \tag{2.99}$$

where I_{gravity} is the on-shell classical gravity action. These fundamental holographic relations will play an important role in deriving the holographic formula for entropies.

Here we review the *AdS_{d+1} space*, which is the maximally symmetric solution of Einstein equation

$$R_{\mu\nu} - \frac{1}{2}g_{\mu\nu}R + \Lambda g_{\mu\nu} = 0\,, \tag{2.100}$$

in the vacuum, namely, without any energy momentum tensor of matters, with a negative cosmological constant $\Lambda < 0$. In the vacuum, the Ricci tensor $R_{\mu\nu}$ and thus Ricci scalar R are determined by the cosmological constant as

$$R_{\mu\nu} = \frac{2}{d-1}\Lambda g_{\mu\nu}, \qquad\qquad R = \frac{2(d+1)}{d-1}\Lambda\,. \tag{2.101}$$

In the maximally symmetric case, where the Riemann tensor $R_{\mu\nu\alpha\beta}$ (or equivalently the curvature 2-form $\Omega^{\mu}{}_{\nu} \equiv \frac{1}{2} R^{\mu}{}_{\nu\alpha\beta} dx^{\alpha} \wedge dx^{\beta}$) takes the form of

$$R_{\mu\nu\alpha\beta} = 2k g_{\mu\alpha} g_{\nu\beta} \qquad (\Omega^{\mu}{}_{\nu} = k dx^{\mu} \wedge dx_{\nu}) \,, \tag{2.102}$$

with some constant k, its trace $R = kD(D-1)$ determines the whole Riemann tensor via

$$k = \frac{R}{d(d+1)} = \frac{2\Lambda}{d(d-1)} \,. \tag{2.103}$$

The metric is given as

$$ds^2 = -(1 - kr^2) dt^2 + \frac{dr^2}{1 - kr^2} + r^2 d\Omega_{d-1}^2 \,, \tag{2.104}$$

$$= -\left(1 + \frac{r^2}{L^2}\right) dt^2 + \frac{dr^2}{1 + r^2/L^2} + r^2 d\Omega_{d-1}^2 \,, \tag{2.105}$$

where we introduced AdS radius $L \equiv \sqrt{-1/k}$, the typical length scale of the geometry. This coordinate is called *static coordinate*. When the cosmological constant is positive $\Lambda > 0$, this metric gives de Sitter space with Hubble constant $H \equiv \sqrt{k}$, and has a Hubble horizon at $r = 1/H$ where the coefficient of dt^2 vanishes.

To obtain other useful coordinates of AdS_{d+1} space, let us see how the space can also be realized as an embedding in $(d+2)$-dimensions. In fact, AdS_{d+1} can be given as a time-like vector

$$-L^2 = -X_{-1}^2 - X_0^2 + X_1^2 + \cdots + X_d^2 \tag{2.106}$$

in the flat space $\mathbb{R}^{2,d}$ with an additional time direction,

$$ds^2 = -dX_{-1}^2 - dX_0^2 + dX_1^2 + \cdots + dX_d^2. \tag{2.107}$$

From this representation, we can easily see that AdS_{d+1} space has the isometry $\mathrm{SO}(d,2)$, which is identified with the conformal symmetry of the dual CFT_d. By taking polar coordinates for both the two-dimensional time and d-dimensional space,

$$X_{-1} = L \cosh \frac{\rho}{L} \cos \frac{t}{L} \,, \tag{2.108}$$

$$X_0 = L \cosh \frac{\rho}{L} \sin \frac{t}{L} \,, \tag{2.109}$$

$$X_i = L \sinh \frac{\rho}{L} \, \Omega_i, \tag{2.110}$$

where $\rho \geq 0$ is the radial direction and Ω_i are angular coordinates of $\mathbb{S}^{d-1}$ with $\sum_{i=1}^{d} \Omega_i^2 = 1$, we arrive at a coordinate called *global coordinate*,

$$ds^2 = d\rho^2 - \cosh^2 \frac{\rho}{L} \, dt^2 + L^2 \sinh^2 \frac{\rho}{L} \, d\Omega_{d-1}^2. \tag{2.111}$$

The time direction t is originally periodic, but we take the universal covering of the space by extending the cycle $\mathbb{S}^1$ to a line $\mathbb{R}$, to avoid closed time-like curves. This global

coordinate and the static coordinate are equivalent and related by the redefinition of the radial coordinate, $r/L = \sinh \rho/L$. Another redefinition $r/L = \tan\theta$ compactifing the radial direction into $0 \leq \theta \leq \pi/2$, gives another coordinate called *conformal coordinate*,

$$ds^2 = \frac{-dt^2 + d\theta^2 + \sin^2\theta d\Omega_{d-1}^2}{\cos^2\theta}, \tag{2.112}$$

whose t-θ plane is conformal to the flat metric $-dt^2 + d\theta^2$. We can see that the spacetime is a cylinder, sometimes called AdS cylinder, whose boundary $\mathbb{R} \times \mathbb{S}^{d-1}$ at $\theta = \pi/2$ is sometimes called AdS boundary. The dual CFT is interpreted to be located at this boundary, where the angular coordinates Ω_i are identified with the coordinates of the CFT.

While the dual CFT lives on a cylinder $\mathbb{R} \times \mathbb{S}^{d-1}$ in the above coordinates, we can also study the dual CFT located on a flat space $\mathbb{R}^{1,d-1}$ by taking a patch called *Poincaré patch*. Poincaré patch covers only half the spacetime $U_+ > 0$ (or $U_+ < 0$), where $U_\pm \equiv X_{-1} \pm X_d$ is the light-cone coordinate in the embedded space $\mathbb{R}^{2,d-1}$. Deleting the other light-cone coordinate U_- by the constraint (2.106) and rescaling the remaining X coordinates as

$$(x^0, \ldots, x^{d-1}) \equiv \frac{L}{U_+}(X_0, \ldots, X_{d-1}), \tag{2.113}$$

the metric (2.107) becomes

$$ds^2 = \frac{L^2}{U_+^2} dU_+^2 + \frac{U_+^2}{L^2} dx^2_{\mathbb{R}^{1,d-1}} = L^2 \frac{dx^2_{\mathbb{R}^{1,d-1}} + dz^2}{z^2}, \tag{2.114}$$

where $dx^2_{\mathbb{R}^{1,d-1}} = -(dx^0)^2 + (dx^1)^2 + \cdots + (dx^{d-1})^2$ is the flat metric and $z \equiv L^2/U_+$. We usually take $z > 0$ patch corresponding to $U_+ > 0$ patch, while $z < 0$ patch corresponds to $U_+ < 0$ patch. The AdS boundary is now located at $z = 0$, and whose shape is now a flat space $\mathbb{R}^{1,d-1}$. The flat coordinates x's are identified with the coordinates of CFT, and the additional holographic z direction is naturally interpreted as the length scale in dual field theories. In fact, the scaling symmetry included in $\mathrm{SO}(d,2)$ acts on both z and x directions as $(x, z) \to (e^\sigma x, e^\sigma z)$, while the Poincaré symmetry $\mathrm{SO}(d-1,1) \ltimes \mathbb{R}^{d-1,1} (\subset \mathrm{SO}(d,2))$ does not act on z and acts only on x directions as $(x^\mu, z) \to (\Lambda^\mu{}_\nu x^\nu + a^\mu, z)$. Generally, the additional holographic direction in the bulk side is interpreted to represent the length scale in the boundary side; the bulk geometry can be interpreted as a geometrical representation of the RG flow of the dual field theory. Its UV physics is encoded near the AdS boundary in the bulk, while its IR physics is encoded deeply inside the bulk.

Let us take the Euclidean version of AdS_{d+1} space, which is now realized as a time-like vector

$$-L^2 = -X_{-1}^2 + X_0^2 + X_1^2 + \cdots + X_d^2 \tag{2.115}$$

in the flat space $\mathbb{R}^{1,d+1}$. We can then also study the dual CFT located on a thermal hyperbolic space $\mathbb{S}^1 \times \mathbb{H}^{d-1}$, by taking a coordinate called *hyperbolic coordinate* or *topological black hole coordinate*,

$$ds^2 = \left(\frac{L}{R}\right)^2 \left(\frac{R^2}{r^2 - R^2} dr^2 + \frac{r^2 - R^2}{R^2} d\tau^2 + r^2 (du^2 + \sinh^2 u d\Omega_{d-2}^2) \right), \tag{2.116}$$

which follows from the introduction of the coordinates

$$X_{-1} = L\frac{r}{R}\cosh u\,, \qquad X_i = L\frac{r}{R}\sinh u\,\Omega_{i-1} \quad (i = 2, \ldots, d)\,, \tag{2.117}$$

$$X_0 = L\sqrt{(r/R)^2 - 1}\sin(\tau/R)\,, \qquad X_1 = L\sqrt{(r/R)^2 - 1}\cos(\tau/R)\,. \tag{2.118}$$

This metric has a black hole horizon at $r = R$, whose temperature $\beta = 2\pi R$ is the period of the τ cycle.

2.4.2 Holographic formulae for entanglements

As explained already in chapter 1, for static systems holographically dual to asymptotically AdS spaces with Einstein gravity, the entanglement entropy of a region A is holographically related to the area of the codimension-two bulk minimal surface γ_A anchored at the entangling surface $\Sigma = \partial A$ on the boundary, via the *holographic entanglement entropy formula* or Ryu-Takayanagi (RT) formula (1.2) [41, 42],

$$S_A = \min_{\partial\gamma_A = \partial A} \frac{\mathrm{Area}[\gamma_A]}{4G_N}\,. \tag{2.119}$$

It is proved that this formula fulfils the strong sub-additivity (2.93) expectedly [72, 73, 74], and its proof relies only on geometric discussions utilizing the minimality of the surfaces, providing a geometrical interpretation to the quantum mechanical constraint. The proof then suggests a profound way of the emergence of the spacetime geometry from the quantum mechanical degrees of freedom. More inequalities that the formula satisfies were studied to characterize the quantum theories which have a gravity dual [75, 76].

Many checks and studies have been performed for the holographic formula after its proposal, while it took a while for the formula to be derived by [77]. The derivation employs so-called Lewkowycz-Maldacena prescription, applying the replica trick explained at (2.1.1) to holographic systems, and was extended to more general holographic formulae, such as the formula for time-dependent systems [78, 79], for Rényi entropies [80], and for higher derivative theories [81]. Let us review the former two extensions.

In the formula (1.2), the surface γ_A has the minimum area within the bulk time slice whose normal vector is the timelike Killing vector of the static bulk geometry. It would be meaningless to minimize the area of a surface in the whole bulk spacetime, since we can reduce the area to any negative value by bending the surface into the timelike direction. And so this formula originally applies only to static situations, but was generalized to a covariantized formula called the *covariant holographic entanglement entropy formula* or Hubeny-Rangamani-Takayanagi (HRT) formula [78],

$$S_A = \operatorname*{ext}_{\partial\gamma_A = \partial A} \frac{\mathrm{Area}[\gamma_A]}{4G_N}\,, \tag{2.120}$$

where the codimension-two bulk surface γ_A is now just the extremal surface instead of the minimal surface. While RT formula takes the surface (called RT surface) with the minimum area within the bulk time slice, HRT formula takes the surface (called HRT

surface) with the extremal area in the whole bulk spacetime,[6] and now applies to time-dependent cases as well. If there are multiple extremal surfaces, we should choose the one with the minimum area among them.

The holographic formula (1.2) is also generalized to Rényi entropies [80]. In fact, it gives not Rényi entropy $S_{n,A}$ (1.4) itself but some related quantity,

$$\tilde{S}_{n,A} \equiv n^2 \partial_n \left(\frac{n-1}{n} S_{n,A} \right) , \tag{2.121}$$

$$= (1 - n\partial_n) \log \mathrm{Tr}[\rho_A^n] , \tag{2.122}$$

$$= \partial_{1/n} \left(\frac{1}{n} \log \mathrm{Tr}[\rho_A^n] \right) , \tag{2.123}$$

which is recently named as *modular entropy* in [79]. Its holographic formula resembles to the one for entanglement entropy, but is more intricate as the entropy is given by the area of a cosmic brane with a tension depending on the parameter n, which is extremized in the backreacted geometry. Similarly to the holographic entanglement entropy formula, the modular entropy $\tilde{S}_n$ of a region A is given by the area of some codimension-two surface $C_A^{(n)}$ in the dual gravity theory as

$$\tilde{S}_n = \left. \frac{\mathrm{Area}[C_A^{(n)}]}{4G_N} \right|_{\delta I = 0,\, \partial C_A^{(n)} = \partial A} , \tag{2.124}$$

where the surface $C_A^{(n)}$ is anchored on ∂A on the asymptotic boundary of the bulk spacetime as well. Unlike the formula for entanglement entropies, however, the surface $C_A^{(n)}$ is to be fixed by minimizing an n-dependent Euclidean action $I = I_{\mathrm{bulk}} + I_{\mathrm{brane}}$. Here I_{bulk} is the original bulk action in the dual gravity theory consisting of the Einstein-Hilbert action, the cosmological constant term and matter terms

$$I_{\mathrm{bulk}}[G_{\mu\nu}(X), \psi(X)] = I_{\mathrm{EH}}[G_{\mu\nu}(X)] + I_{\Lambda}[G_{\mu\nu}(X)] + I_{\mathrm{matters}}[G_{\mu\nu}(X), \psi(X)] , \tag{2.125}$$

where $G_{\mu\nu}(X)$ the bulk metric, $\psi(X)$ matter fields, and X^μ ($\mu = 0, \ldots, d$) is the bulk coordinate. If we extremize the codimension-two surface with this bulk action, we end up with the RT surface γ_A for the holographic entanglement entropy. A new ingredient of the prescription for the Rényi entropy is a cosmic brane action I_{brane} of $C_A^{(n)}$,

$$I_{\mathrm{brane}}[G_{\mu\nu}(X), X^\mu(y)] = T_n \, \mathcal{A}[G_{\mu\nu}(X), X^\mu(y)] , \tag{2.126}$$

which is just the product of a brane tension T_n given by

$$T_n = \frac{1}{4G_N} \frac{n-1}{n} , \tag{2.127}$$

[6] There are many equivalent constructions of this surface γ_A, which look different. The extremal surface explained above (called $\mathcal{W}$ in the original paper [78]), the surface with vanishing traces of extrinsic curvatures ($\mathcal{Y}_{ext}$), and a surface constructed by using light-sheets ($\mathcal{Y}^{min}_{\mathcal{A}_t}$), are eventually all equivalent. See the original paper for the detail.

and the area of the surface $C_A^{(n)}$

$$\mathcal{A} \equiv \text{Area}[C_A^{(n)}] = \int_{C_A^{(n)}} d^{d-1}y\sqrt{g(y)}\,. \tag{2.128}$$

Here $X^\mu(y)$ specify the embedding of the surface into the bulk, y^i $(i = 1, \ldots, d-1)$ the embedding coordinate, and $g_{ij}(y)$ the induced metric on C_n,

$$g_{ij}(y) = G_{\mu\nu}(X(y))\frac{\partial X^\mu}{\partial y^i}\frac{\partial X^\nu}{\partial y^j}\,. \tag{2.129}$$

The main difference from the formula for entanglement entropies arises from the backreaction of the codimension-two surface to the bulk metric $G_{\mu\nu}$. Namely we extremize the action including the cosmic brane:

$$0 \;= \frac{\delta I}{\delta G_{\mu\nu}(X)} = \frac{\delta I_{\text{bulk}}}{\delta G_{\mu\nu}(X)} + T_n\,\frac{\delta \mathcal{A}}{\delta G_{\mu\nu}(X)}\,, \tag{2.130}$$

where the first term is the original bulk equation of motion, and the second term is essentially the energy-momentum tensor of the cosmic brane $C_A^{(n)}$. Note that $C_A^{(n)}$ is still a minimal surface as the equation of motion for the embedding $X^\mu(y)$ shows:

$$\frac{\delta I}{\delta X^\mu(y)} = T_n\,\frac{\delta \mathcal{A}}{\delta X^\mu(y)} = 0\,. \tag{2.131}$$

This equation should be evaluated on the backreacted bulk metric $G_{\mu\nu}$. When there are matter fields ψ, we also have to solve

$$\frac{\delta I}{\delta \psi} = \frac{\delta I_{\text{matters}}}{\delta \psi} = 0\,, \tag{2.132}$$

in the backreacted background $G_{\mu\nu}$. The holographic entanglement entropy formula (1.2) is recovered from (2.124) in the limit $n \to 1$ where the brane tension T_n vanishes and we can neglect the backreaction of the brane.

2.4.3 Derivation of the holographic formula

Here we review the derivation of the formula (2.124) for modular entropy, which thus includes the derivation of the formula (1.2) for entanglement entropy as the special case when $n = 1$. To derive it, we employ the replica trick (2.24),

$$\log \text{Tr}[\rho_A^n] = \log Z[M_{n,A}] - n \log Z[M_{1,A}]\,, \tag{2.133}$$

where $M_{n,A}$ is the n-fold cover branched over the region A. In the classical gravity regime, there exists a regular solution B_n of the Einstein equation holographically dual to the field theory on the replica manifold $M_{n,A}$ such that $\partial B_n = M_{n,A}$. The partition function Z is equated to the on-shell bulk action on B_n:

$$Z[M_n] = Z_{\text{bulk}} \sim e^{-I_{\text{bulk}}[B_n]}\,. \tag{2.134}$$

The parameter n has been supposed to be an integer up to now, but we analytically continue it to an arbitrary real number. Such an analytic continuation can be performed in the bulk side by defining the "bulk per replica" manifold

$$\hat{B}_n = B_n/\mathbb{Z}_n, \tag{2.135}$$

under the assumption that the replica symmetry $\mathbb{Z}_n$ extends to the on-shell bulk solution B_n [77].[7] This quotient geometry $\hat{B}_n$ has a conical singularity at a codimension-two fixed locus $C_A^{(n)}$ of the $\mathbb{Z}_n$ symmetry with a deficit angle

$$\Delta\phi = 2\pi(1-1/n)\,. \tag{2.136}$$

The fixed locus $C_A^{(n)}$ extends to the AdS boundary and touches on the entangling surface ∂A which is also fixed locus of the replica symmetry.

Next, let us define "bulk action per replica" I for the quotient $\hat{B}_n$, just by dividing the bulk on-shell action $I_{\rm bulk}[B_n]$ by n,

$$I \equiv I_{\rm bulk}[B_n]/n\,. \tag{2.137}$$

This action I differs from $I_{\rm bulk}[\hat{B}_n]$ of the quotient bulk $\hat{B}_n$, and has an additional contribution from the singularity at $C_A^{(n)}$.[8] Bearing in mind that $\hat{B}_n$ is locally the same as the original bulk B_n away from the conical singularity $C_A^{(n)}$, the Ricci scalar $R(X)$ of $\hat{B}_n$ takes the following form [83]

$$\sqrt{G(X)}R(X)|_{\hat{B}_n} = \sqrt{G(X)}R(X)|_{B_n} + 2\Delta\phi\int_{C_A^{(n)}} d^{d-1}y\sqrt{g}\,\delta^{d+1}(X-X(y))\,. \tag{2.138}$$

Thus in the Einstein gravity $I_{\rm EH} = -\frac{1}{16\pi G_N}\int d^{d+1}X\sqrt{G(X)}R(X)$,

$$\begin{aligned} I_{\rm bulk}[\hat{B}_n] &= I_{\rm bulk}[B_n]/n - \frac{\Delta\phi}{8\pi G_N}\int_{C_A^{(n)}} d^{d-1}y\sqrt{g}\,, \\ &= I - \frac{1-1/n}{4G_N}\mathcal{A}\,, \end{aligned} \tag{2.139}$$

which means that the action I includes the area term

$$I = I_{\rm bulk}[\hat{B}_n] + T_n\,\mathcal{A}\,, \tag{2.140}$$

with the correct brane tension (2.127)

$$T_n = \frac{\Delta\phi}{8\pi G_N} = \frac{1-1/n}{4G_N}\,, \tag{2.141}$$

[7] See [82] for the discussion on the replica symmetry $\mathbb{Z}_n$ breaking.

[8] Here our notation of $I_{\rm bulk}[\hat{B}_n]$ is different from that in other literatures such as [80]. Our $I_{\rm bulk}[\hat{B}_n]$ includes the contribution from the conical singularity $C_A^{(n)}$, while their $I_{\rm bulk}[\hat{B}_n]$ means $I_{\rm bulk}[\hat{B}_n\backslash C_A^{(n)}] = I_{\rm bulk}[B_n]/n = I$ without the contribution from $C_A^{(n)}$.

and the area $\mathcal{A}$ (2.128) as desired.

A point of caution is that not $I_{\rm bulk}[\hat{B}_n]$ itself, but the combination $I = I_{\rm bulk}[\hat{B}_n] + T_n\,\mathcal{A}$ is on-shell with respect to the bulk fields $G_{\mu\nu}(X)$ and $\psi(X)$. This is clear from the relation (2.137) and B_n being the regular solution for the action $I_{\rm bulk}[B_n]$.

The replica symmetry would constrain the embedding $X^\mu(y)$ to be the minimal surface, $\delta\mathcal{A}/\delta X^\mu(y) = 0$.[9] We promote the embedding $X^\mu(y)$ to a dynamical variable and minimize the action I with respect to $X^\mu(y)$ in order to analytically continue n to a real number.

Combining the replica trick (2.133) and the holographic relation (2.134) together with the definition of the action I (2.137), we have the expression

$$\begin{aligned} \log {\rm Tr}[\rho_A^n] &= -(I_{\rm bulk}[B_n] - n\, I_{\rm bulk}[B_1])\,, \\ &= -n(I - I|_{n=1})\,, \end{aligned} \tag{2.142}$$

where the second term $-I|_{n=1}$ ensures the normalization $\log {\rm Tr}[\rho_A] = 0$. Then the expression (2.123) gives This succinct form is convenient to derive the entropy $\tilde{S}_n$

$$\tilde{S}_n = -\partial_{1/n} I \tag{2.143}$$

$$= -\partial_{1/n}\left(I_{\rm bulk}[\hat{B}_n] + \left(1 - \frac{1}{n}\right)\frac{\mathcal{A}}{4G_N}\right) \tag{2.144}$$

$$= -\frac{\delta I[\phi]}{\delta\phi}\frac{\delta\phi}{\delta(1/n)} + \frac{\mathcal{A}}{4G_N}\,, \tag{2.145}$$

where the first and second terms come from the variation of all the bulk fields $\phi = \{G_{\mu\nu}(X), \psi(X), X^\mu(y)\}$ and the tension $T_n = (1-1/n)/4G_N$, respectively. Imposing the equations of motion, the first term vanishes $\delta I/\delta\phi = 0$, and we reach the holographic Rényi entropy formula (2.124)

$$\tilde{S}_n = \frac{\mathcal{A}}{4G_N}\,. \tag{2.146}$$

The derivation explains why one has to take into account the backreaction of the cosmic brane to the geometry while extremizing the area.

2.4.4 Area law in holographic theories

Holographically, the area law term (2.48) of the entanglement entropy arises from the infiniteness of AdS spaces. We can see it in any coordinate, but let us take Poincaré patch (2.114) for simplicity. The spacetime volume of AdS space diverges in approaching

[9] We could justify this statement somewhat by a following rough argument. Consider how the area $\mathcal{A}$ would change in the leading order of a perturbation $\epsilon^\mu(y)$ of the embedding $X^\mu(y)$, in the bulk $\hat{B}_n$. In the original bulk B_n, where n copies of $\hat{B}_n$ are glued at the surface, let us call the vector $\epsilon^\mu(y)$ toward the i-th copy of $\hat{B}_n$ as $\epsilon_i^\mu(y)$. Since the original surface $X^\mu(y)$ is invariant under the replica $\mathbb{Z}_n$ symmetry shifting $\epsilon_i^\mu(y)$ to $\epsilon_{i+1}^\mu(y)$, the variation of the area $\frac{\delta\mathcal{A}}{\delta X^\mu}\epsilon_i^\mu$ does not depend on the label i and in fact $\frac{\delta\mathcal{A}}{\delta X^\mu}\epsilon_i^\mu = \frac{\delta\mathcal{A}}{\delta X^\mu}\epsilon^\mu$. On the other hand, the sum of these vectors vanishes $\sum_{i=1}^n \epsilon_i^\mu = 0$ because of the symmetry. Then $0 = \frac{\delta\mathcal{A}}{\delta X^\mu}\sum_{i=1}^n \epsilon_i^\mu = n\frac{\delta\mathcal{A}}{\delta X^\mu}\epsilon^\mu$ means that the area is minimal $\frac{\delta\mathcal{A}}{\delta X^\mu} = 0$.

$z \to 0$, and thus it is convenient to introduce a small IR cutoff $z = \epsilon$ to regulate its volume. Since z direction corresponds to the length scale in field theory side, this IR cutoff in the bulk corresponds to the length scale of UV cutoff in the dual field theory. The area of the surface γ_A in the holographic entanglement entropy formula also diverges in $z \to 0$ and is regulated by this IR cutoff $z = \epsilon$. Let us see how the holographic entanglement entropy behaves in the limit $\epsilon \to 0$. The main contribution of its area comes from the region near the boundary $z \sim \epsilon$,

$$\text{Area}[\gamma_A] \sim L^{d-1}\text{Area}[\Sigma]\int_\epsilon \frac{dz}{z^{d-1}} \sim \text{Area}[\Sigma]\frac{L^{d-1}}{\epsilon^{d-2}}, \tag{2.147}$$

and thus the holographic entanglement entropy behaves as

$$S_A \sim \frac{L^{d-1}}{G_N}\frac{\text{Area}[\Sigma]}{\epsilon^{d-2}}, \tag{2.148}$$

which reproduces the area law term (2.48).

2.4.5 $\mathbf{AdS_3/CFT_2}$

Let us see the simplest example, the holographic entanglement entropy of an interval $A = [-R, R]$ of length $l = 2R$ at $t = 0$ in CFT_2. This interval is located at $z = 0$ of the dual AdS_3,

$$ds^2 = L^2\frac{-dt^2 + dx^2 + dz^2}{z^2}\,. \tag{2.149}$$

The corresponding minimal surface γ_A is the geodesic connecting two points $x = \pm R$ at $t = 0$ and $z = 0$, and is just a semi-circle

$$z^2 + x^2 = R^2\,, \tag{2.150}$$

on which the induced metric is given as

$$ds^2 = L^2\frac{R^2dz^2}{z^2(R^2 - z^2)}. \tag{2.151}$$

From this expression, the length of the geodesic is explicitly calculated as

$$S_A = \frac{1}{4G_N}\int_{\gamma_A} ds = \frac{L}{2G_N}\int_\epsilon^{l/2}\frac{Rdz}{z\sqrt{R^2 - z^2}} = \frac{L}{2G_N}\log\frac{l}{\epsilon}\,. \tag{2.152}$$

This entropy exactly reproduces the CFT_2 result (2.59), thanks to Brown-Henneaux formula [84]

$$c = \frac{3L}{2G_N}, \tag{2.153}$$

known for $\text{AdS}_3/\text{CFT}_2$ correspondence.

2.4.6 Ball shaped regions in $\mathbf{AdS}_{d+1}/\mathbf{CFT}_d$

Let us see the next simplest example, the holographic entanglement entropy of an ball $r < R$ of radius R at $t = 0$ in CFT_d. This ball is located at $z = 0$ of the dual AdS_d,

$$ds^2 = L^2 \frac{-dt^2 + dr^2 + r^2 d\Omega_{d-2}^2 + dz^2}{z^2} \,. \tag{2.154}$$

The corresponding minimal surface γ_A is just a semi-sphere

$$r^2 + z^2 = R^2 \,, \tag{2.155}$$

on which the induced metric is given as

$$ds^2 = L^2 \left(\frac{R^2 dz^2}{z^2(R^2 - z^2)} + \frac{R^2 - z^2}{z^2} d\Omega_{d-2}^2 \right) . \tag{2.156}$$

From this expression, the length of the geodesic is explicitly calculated as

$$S_A = \frac{1}{4G_N} \int_{\gamma_A} dA = \frac{\mathrm{Vol}(\mathbb{S}^{d-2}) L^{d-1}}{4G_N} \int_{\epsilon/R}^1 \frac{(1-y^2)^{\frac{d-3}{2}} dy}{y^{d-1}} \tag{2.157}$$

$$= \frac{\mathrm{Vol}(\mathbb{S}^{d-2}) L^{d-1}}{4G_N} \left(\frac{1}{d-2} \left(\frac{R}{\epsilon} \right)^{d-2} + \frac{d-1}{2(d-2)} \left(\frac{R}{\epsilon} \right)^{d-4} + \dots \right) \tag{2.158}$$

where $y \equiv z/R$. This entropy expectedly has the area law term and sub-leading terms whose power of R/ϵ decreases by two. This entropy has the constant term

$$(-)^{\frac{d-1}{2}} \frac{\mathrm{Vol}(\mathbb{S}^{d-2}) L^{d-1}}{4G_N} \frac{B(\frac{d-1}{2}, \frac{1}{2})}{2} \,, \tag{2.159}$$

in odd dimensions, and has the logarithmic term

$$(-)^{\frac{d-2}{2}} \frac{\mathrm{Vol}(\mathbb{S}^{d-2}) L^{d-1}}{4G_N} \frac{B(\frac{d-1}{2}, \frac{1}{2})}{\sqrt{2\pi}} \log \frac{R}{\epsilon} \,, \tag{2.160}$$

in even dimensions.

There is another method to calculate these ball entropies, by using the topological black hole coordinate (2.116) [58]. The minimal surface is now given by the horizon $r = R$ of the black hole, and thus the holographic entanglement entropy is given by the horizon area,

$$S_A = \frac{\mathrm{Vol}(\mathbb{H}^{d-1}) L^{d-1}}{4G_N} \,, \tag{2.161}$$

namely, just the black hole entropy as Bekenstein-Hawking formula tells. The volume integral of the hyperbolic space,

$$\mathrm{Vol}(\mathbb{H}^{d-1}) = \mathrm{Vol}(\mathbb{S}^{d-2}) \int_0^{\log(2R/\epsilon)} du \ \sinh^{d-2} u \,, \tag{2.162}$$

exactly reproduces the y integral (2.157) via a change of the variable, $y = 1/\cosh u$. This story is exactly the gravity dual of the CFT calculation (2.81) using a conformal map to a thermal hyperbolic space $\mathbb{S}^1 \times \mathbb{H}^{d-1}$, which is located at the boundary of the topological black hole coordinate.

Chapter 3

A New Universality of Entanglement in Gapped Theories and Holography

In gapped theories with a mass gap m, the $1/m$ expansion formula of entanglement entropy (2.85) is proposed and numerically checked up to the order of $1/m^3$ for a disk region in free massive theories [85, 86]. However, this $1/m$ expansion seems peculiar since it implies that entropies in gapped theories are totally additive with respect to entangling surfaces, while entropies are generally just sub-additive as (2.91). We checked how this $1/m$ expansion is valid by studying mutual information in gapped theories, because mutual information can pick up non-additive terms and is easy to obtain numerically thanks to its independence from the UV cutoff ϵ. If the $1/m$ expansion formula is exactly correct, the mutual information would vanish. We take one of the simplest setup to realize meaningful mutual information, namely, the mutual information $I(B, C)$ between the inner disk B and the compliment C of the outer disk of an annulus A, in three dimensions (see Fig. 3.1).

We numerically calculate the mutual information in a free field theory and a strongly coupled theory holographically dual to a capped-off geometry, consulting literatures on annular entropies in conformal field theories. In both cases, it is nonzero and decays exponentially with the mass gap m as

$$I(B, C) \sim e^{-\#m\delta} \ , \tag{3.1}$$

where δ is the width of the annulus. We speculate that this exponential behaviour is universal for mutual informations in any gapped theory. Since mutual information is composed of entanglement entropies, this speculation means that the $1/m$ expansion of entanglement entropy should have exponential corrections,

$$S_A = \alpha \frac{\ell_\Sigma}{\epsilon} + \beta\, m\, \ell_\Sigma - \gamma_\Sigma + \sum_{n=0}^{\infty} \frac{c_{2n+1}^\Sigma}{m^{2n+1}} + O(\exp[-m\delta]) \ , \tag{3.2}$$

where δ would be proportional to the shortest distance between disjoint entangling surfaces and $\delta \propto R_2 - R_1$ for the annulus. This term has not been noticed so far because of its smallness, and is somewhat non-local in that it is not additive with respect to the entangling surfaces.

This chapter is based on the author's work [1] with T. Nishioka.

3.1 Mutual information across an annulus

In this section, we review general properties of the mutual information I across an annulus A in gapped systems and CFT's, explaining how it is obtained from the entanglement entropy of the annulus.

We take B and C to be two regions outside A, namely, a disk of radius R_1 and the complement of a disk of radius R_2, respectively (see Fig. 3.1). We can interpret this mutual information as how much quantum information is shared by B and C across the annulus A. Since the entanglement entropy of a given region is equal to that of the complement in pure states, S_C and $S_{B\cup C}$ equal the entropies of a disk of radius R_2 and an annulus of inner and outer radii R_1 and R_2, respectively. The mutual information I across the annulus A then reduces to

$$I(R_1, R_2) \equiv I(B, C) = S_{\text{disk}}(R_1) + S_{\text{disk}}(R_2) - S_A(R_1, R_2) \ . \tag{3.3}$$

In this setup, the monotonicity of mutual information (2.95) translates into the monotonicity with respect to the radii R_1, R_2:

$$\frac{\partial}{\partial R_1} I(R_1, R_2) \geq 0 \ , \qquad \frac{\partial}{\partial R_2} I(R_1, R_2) \leq 0 \ . \tag{3.4}$$

In the following, let us review these entropies in CFT's and in gapped theories, respectively.

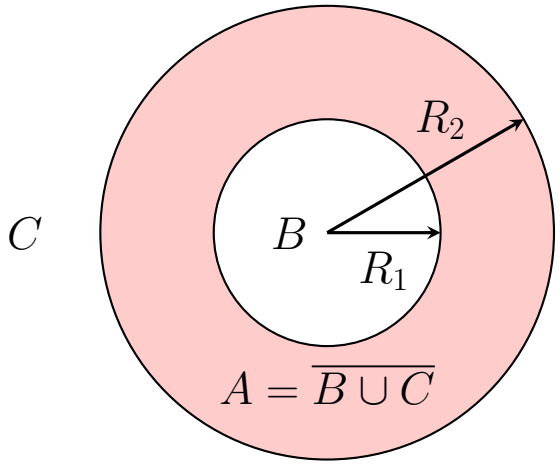

Figure 3.1: The entangling regions for the mutual information. The region B is a disk of radius R_1. The region C is the complement of a disk of radius R_2. The complement of the union of the two regions $\overline{B \cup C}$ is the annulus A in the red colored region.

3.1.1 Mutual information in CFT's

In CFT's, as mentioned in chapter 2, the entanglement entropy for a disk of radius R takes a form of

$$S_{\text{disk}}(R) = \alpha \frac{2\pi R}{\epsilon} - F \ , \tag{3.5}$$

where the second term is a constant $F = -\log Z[\mathbb{S}^3]$. The form of the entropy for an annulus A of the inner radius R_1 and the outer radius R_2 is also fixed by the conformal symmetry as

$$S_A(R_1, R_2) = \alpha \frac{2\pi(R_1 + R_2)}{\epsilon} - f(R_2/R_1) \ , \tag{3.6}$$

where the first term is just the area law (2.48) and the second term f is a function of the ratio $R_2/R_1 (> 1)$ of the radii. This function f should be monotonically decreasing and convex

$$f'(\rho) \leq 0 \ , \qquad f''(\rho) \geq 0 \ , \tag{3.7}$$

with respect to the new variable $\rho = \log(R_2/R_1)(> 0)$, due to the strong subadditivity

$$S_B + S_C \geq S_{B\cup C} + S_{B\cap C} \ . \tag{3.8}$$

In what follows, we review the derivation of (3.7) given by [87].

Let the regions B and C be a disk of radius R_2 and an annulus of radii R_1 and R_3 with $R_1 < R_2 < R_3$ as in Fig. 3.2 (a). The strong subadditivity (3.8) together with (3.6) and (3.5) yields the monotonicity in (3.7):

$$f(R_3/R_1) \leq f(R_2/R_1) \ . \tag{3.9}$$

The convexity in (3.7) can be derived similarly by taking both B and C as an annulus of radii R_2 and R_4, and an annulus of radii R_1 and R_3 satisfying $R_1 < R_2 < R_3 < R_4$ as in Fig. 3.2 (b). In the $R_4 \to R_3$ limit, the strong subadditivity

$$f(R_4/R_2) + f(R_3/R_1) \leq f(R_4/R_1) + f(R_3/R_2) \ , \tag{3.10}$$

reduces to the monotonicity of $f'(\rho)$.

As a result, in CFT's, the mutual information becomes

$$I_{\rm CFT}(R_2/R_1) = f(R_2/R_1) - 2F \ , \tag{3.11}$$

with the constant F in the disk entropy (3.5), and the inequality $I'(R_2/R_1) \leq 0$ (3.4) are equivalent to the monotonicity of f that was already derived in (2.93).

3.1.2 Mutual information in gapped theories

In gapped theories, if the $1/m$ expansion (2.85) is valid, the entanglement entropies of a disk and an annulus would take the form of

$$\begin{aligned} S_{\rm disk}(R, m) &= \alpha \frac{2\pi R}{\epsilon} + 2\pi\beta\, mR - \gamma_{\Sigma_R} + \sum_{n=0}^{\infty} \frac{c_{2n+1}^{\Sigma_R}}{m^{2n+1}} \ , \\ S_A(R_1, R_2, m) &= \alpha \frac{2\pi(R_1 + R_2)}{\epsilon} + 2\pi\beta\, m\,(R_1 + R_2) - \gamma_{\Sigma_{R_1,R_2}} + \sum_{n=0}^{\infty} \frac{c_{2n+1}^{\Sigma_{R_1,R_2}}}{m^{2n+1}} \ , \end{aligned} \tag{3.12}$$

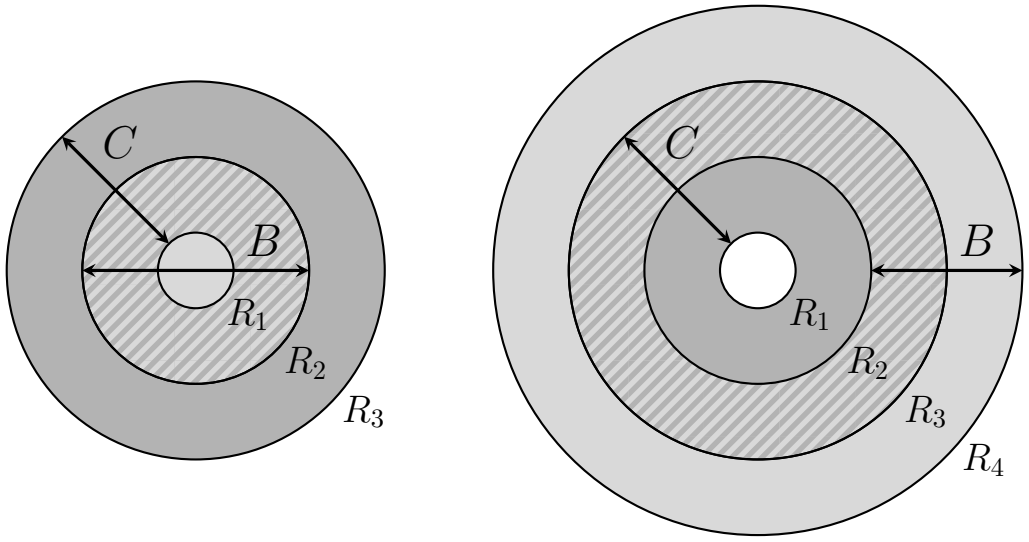

(a) (b)

Figure 3.2: The subsystems B (in light gray) and C (in dark gray) to prove the monotonicity (a) and the convexity (b) of the function f in (3.6). The striped regions are the intersections $B \cap C$.

where Σ_R is a circle of radius R and $\Sigma_{R_1,R_2} = \Sigma_{R_1} + \Sigma_{R_2}$ is two concentric circles of radii R_1 and R_2. Because all the terms are additive with respect to entangling surfaces Σ, they cancel out in the combination of the mutual information, and so the $1/m$ expansion predicts that the mutual information vanishes,

$$I_{\text{gapped}}(mR_1, mR_2) = 0 \ . \tag{3.13}$$

In the following sections, we will use these mutual informations (3.11) and (3.13) to determine the function f in CFT and to check the validity of the large mass expansion formula (2.85) in the case of the annulus.

3.2 Mutual information for a free massive scalar

Let us apply the general discussion on the mutual information in section 3.1 to a free massive scalar field whose action is defined by

$$I = \frac{1}{2} \int d^3x \left[(\partial_\mu \phi)^2 + m^2 \phi^2 \right] \ . \tag{3.14}$$

In this case, the coefficients β and γ in the entropy (3.12) are known to be $\beta = -1/12$ and $\gamma = 0$.[1] The coefficients c^{Σ}_{2n+1} are calculated [85, 86] up to $n = 1$, being local integrals

[1] The topological entanglement entropy vanishes because the massive scalar theory reduces to an empty theory in the IR limit.

of functions of the extrinsic curvature κ and κ's derivatives on the Σ. For example,

$$c_1 = -\frac{n_0 + 3n_{1/2}}{480} \int_\Sigma ds\, \kappa^2 \ , \tag{3.15}$$

for n_0 free scalar fields and $n_{1/2}$ free Dirac fermions. In the present case, the entangling surface Σ_{R_1,R_2} is two disjoint disks of radii R_1, R_2 whose extrinsic curvatures are $\kappa = 1/R_1, 1/R_2$. Thus $c_1^{\Sigma_{R_1,R_2}} = -\frac{\pi}{240}(1/R_1 + 1/R_2)$ for a single free scalar field. The constant term F of the disk entropy (3.5) is analytically calculated as the free energy on a three-sphere, $F_{\text{scalar}} = (\ln 2)/8 - 3\zeta(3)/16\pi^2 \simeq 0.0638$ [54]. The mutual informations (3.11) and (3.13) are

$$I_{\text{massless}} = f(R_2/R_1) - 2F_{\text{scalar}} \ , \tag{3.16}$$

$$I_{\text{massive}} = 0 \ . \tag{3.17}$$

3.2.1 Numerical results for the mutual information

We perform the numerical calculation by putting a free scalar field on the radial lattice following [51, 59], whose details can be found in Appendix A.1. The main results are presented in Fig. 3.3 and 3.4.

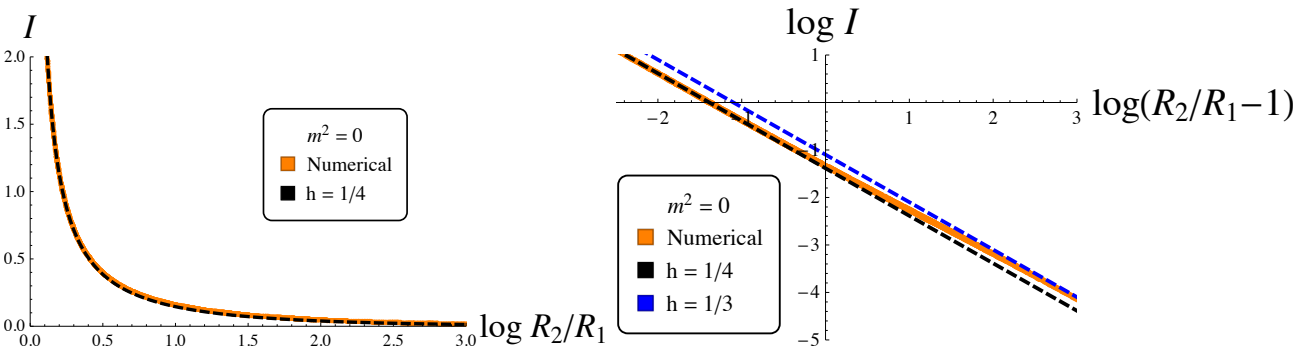

(a) (b)

Figure 3.3: The mutual informations I across the annulus of radii R_1 and R_2 for the free massless scalar field. (a) The mutual information I (the orange line) has the desired monotonicity and convexity, and is well fitted by $h/(R_2/R_1 - 1)$ (the black dotted line). (b) However, this coefficient h is not a constant and increases with R_2/R_1 from $h \simeq 1/4$ (the black dotted line) to $h \simeq 1/3$ (the blue dotted line).

Fig. 3.3 shows the mutual information I (3.16) for the free massless scalar field. The function f satisfies the desired monotonicity and convexity (2.93) with respect to $\rho = \log(R_2/R_1)$ as is clear in Fig. 3.3 (a). The mutual information I asymptotically vanishes for large R_2/R_1, which means that the function f has a finite constant term $2F_{\text{scalar}}$. This suggests that the finite constant term is topological and additive for each connected component of the entangling surfaces, namely, proportional to the 0-th Betti number $b_0[\Sigma]$

of Σ. The numerical function $I = I(R_2/R_1)$ is well approximated by $h/(R_2/R_1 - 1)$ with $h \simeq 1/4$ for small width, but h monotonically increases to $h \simeq 1/3$ for large R_2/R_1 (see Fig. 3.3 (b)). We therefore propose that f is given by

$$f(R_2/R_1) = \frac{h(R_2/R_1)}{R_2/R_1 - 1} + 2F_{\text{scalar}} \ , \tag{3.18}$$

where $h(R_2/R_1)$ is a mild monotonically increasing function of R_2/R_1 such that $h \simeq 1/4$ for $R_2/R_1 \sim 1$ and $h \simeq 1/3$ for $R_2/R_1 \gg 1$. These asymptotic values are consistent with previous works [88, 89] as will be explained in the next subsections.

The mutual information (3.16) for the free massive scalar field is displayed in Fig. 3.4. It is monotonically decreasing with the mass (i.e., decreasing with mR_2 or mR_1 while R_2/R_1 being fixed), and almost vanishes for large mass (Fig. 3.4 (a)) as is consistent with (3.17). In fact, Fig. 3.4 (b) demonstrates that the mutual information decays exponentially with a "dimensionless width" $m(R_2 - R_1)$,

$$I_{\text{massive}} \propto m(R_2 + aR_1) \exp[-b\, m(R_2 - R_1)] \ , \tag{3.19}$$

with constants a and b. This exponential behaviour satisfies the expected monotonicity (3.4). We will find similar decay even in the holographic model in section 3.3 and discuss their possible universality in a gapped phase in section 3.4.

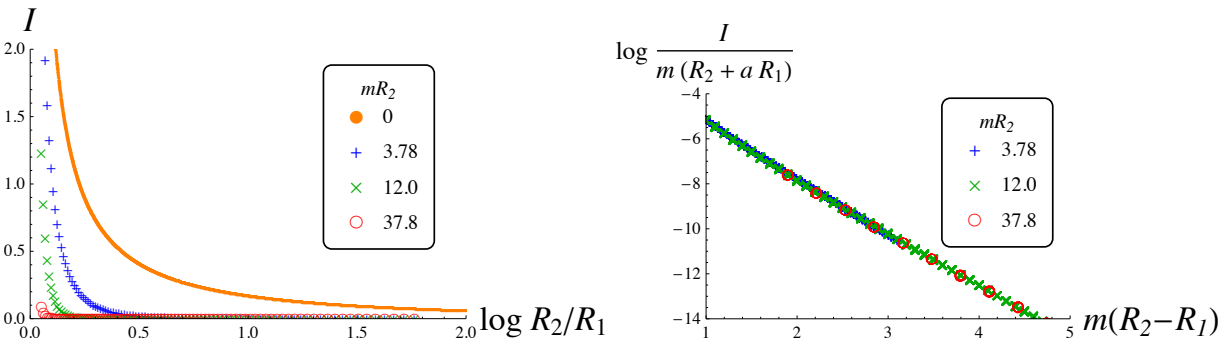

(a) (b)

Figure 3.4: The mutual informations I across the annulus of radii R_1 and R_2 for scalar fields with different masses m. (a) I monotonically decreases with the mass m (orange→blue→green→red). (b) In fact, it exponentially decreases with the dimensionless width $m(R_2 - R_1)$. For $m(R_2 - R_1) \gtrsim 1$, it shows $I \propto m(R_2 + aR_1) \exp[-b\, m(R_2 - R_1)]$ with $a \simeq 2 \sim 5$ ($a = 3$ in the figure) and $b \simeq 2.5$.

3.2.2 Small and large width limits in CFT

The annulus with small width ($R_2/R_1 \approx 1$) can be approximated by a thin strip of width $R_2 - R_1$ extending along a circle of radius $2\pi R_1$ as in Fig. 3.5.[2] The mutual information

[2]We thank T. Takayanagi for drawing our attention to this point.

for the thin strip of width δ is shown to obey [88, 53]

$$I \simeq \kappa \frac{\mathcal{A}}{\delta} \ , \tag{3.20}$$

where $\mathcal{A}$ is the area of the plane bounding the strip. This behavior was derived by dimensionally reducing the thin strip to an interval in $(1+1)$ dimensions for free fields and summing the mutual informations over the Kaluza-Klein modes.

The coefficient κ is calculated for a free massless scalar field [88] to be $\kappa = 0.0397$. Applying (3.20) to our case, we find

$$I \simeq 0.0397 \frac{2\pi R_1}{R_2 - R_1} = \frac{0.249}{R_2/R_1 - 1} \ , \tag{3.21}$$

which fits our numerical result in the small width limit ($h \simeq 1/4$ in (3.18)) very well. One may wonder if the small width limit of the mutual information (3.20) is universal and the coefficient κ counts the number of degrees of freedom in any QFT. We will come back to this point in section 3.4 where we calculate κ in a holographic model.

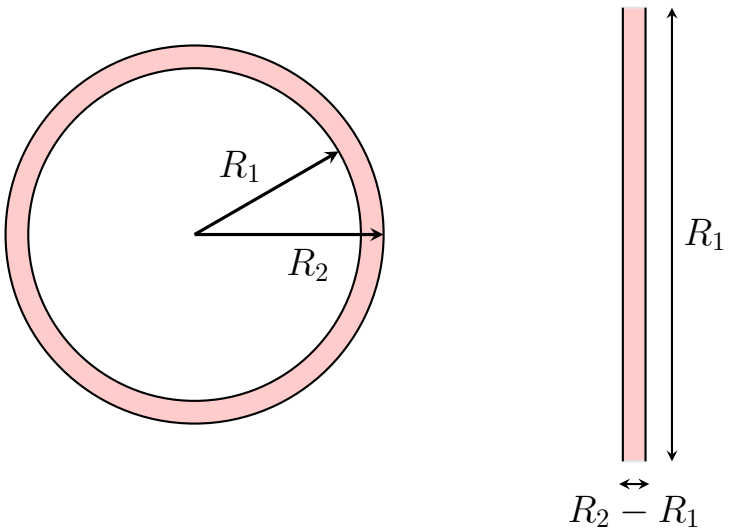

Figure 3.5: A thin annulus (a) can be approximated by a thin strip (b) with compactified direction.

Next, consider the opposite limit where the width is large. Let w_i, z_i $(i = 1, 2)$ be the two-dimensional Cartesian coordinates related by an inversion transformation

$$(z - z_0)_i = R_T^2 \frac{(w - w_0)_i}{|w - w_0|^2} \ , \tag{3.22}$$

where w_0 is the inversion point. The inverse map is obtained by exchanging the role of w and z in the transformation with the inversion point at $z = z_0$. R_T is a constant which we can tune arbitrarily.

Consider an annulus in the w-coordinates whose center is at the origin with radii $R_1 < R_2$. Let the points at $w_2 = 0$ on the outer circle be p_1, p_2 and on the inner circle be q_1, q_2. We choose the inversion points w_0 and z_0 on the real axes at $(w_1, w_2) = (R_0, 0)$ and $(z_1, z_2) = (R'_0, 0)$, respectively. We assume w_0 is inside the annulus, $R_1 < R_0 < R_2$. Under the transformation (3.22), the annulus is mapped to two disjoint circles[3] (see Fig. 3.6) and the points p_1, p_2 and q_1, q_2 are at the intersections of the real axis and circles of radii R'_1 and R'_2 given by

$$R'_1 = R_T^2 \frac{R_1}{R_0^2 - R_1^2} , \qquad R'_2 = R_T^2 \frac{R_2}{R_2^2 - R_0^2} . \tag{3.23}$$

The distance between the centers of the two circles is

$$r' = R_T^2 R_0 \frac{R_2^2 - R_1^2}{(R_2^2 - R_0^2)(R_0^2 - R_1^2)} . \tag{3.24}$$

The conformal symmetry implies that the cross ratio[4] x is invariant under the conformal transformation,

$$x = \frac{|p_1 - p_2||q_1 - q_2|}{|p_1 - q_2||p_2 - q_1|} , \tag{3.25}$$

which in our case is

$$x = \frac{4R_1 R_2}{(R_1 + R_2)^2} = \frac{4R'_1 R'_2}{r'^2 - (R'_1 - R'_2)^2} . \tag{3.26}$$

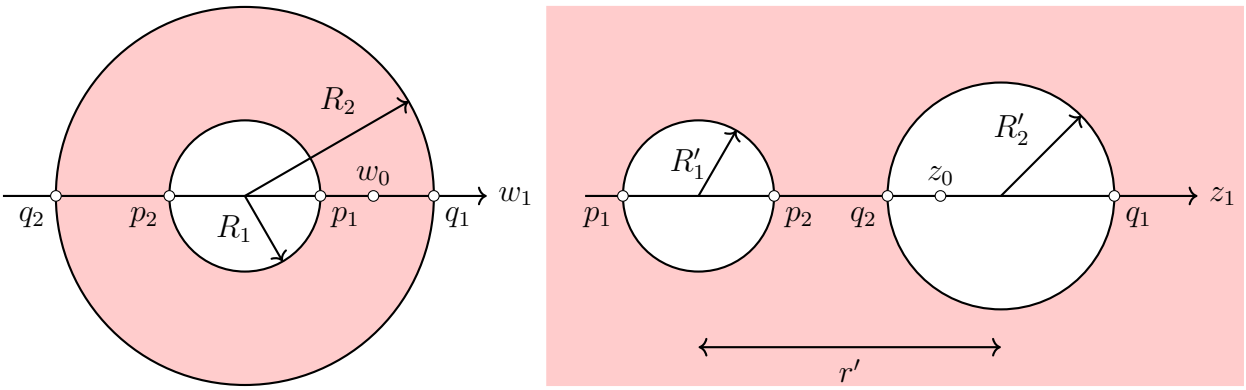

Figure 3.6: The inversion map of an annulus to two disjoint circles. The region inside the annulus in red color is mapped to the outside of the two circles in red color.

[3] We thank K. Ohmori and Y. Tachikawa for the discussions on this map.

[4] There are two cross ratios for four points. The other one is

$$y = \frac{|p_1 - p_2||q_1 - q_2|}{|p_1 - q_1||p_2 - q_2|} .$$

In this way, we can calculate the entanglement entropy of two disjoint circles from that of the corresponding annulus. The former was studied in [90, 91, 89] in the widely separated limit for a free massless scalar field. The mutual information between the two circles is [89]

$$I = \frac{1}{3}\frac{R_1' R_2'}{r'^2} + O\left((R_1' R_2'/r'^2)^2\right) \ . \tag{3.27}$$

The inversion maps (3.23) and (3.24) convert it to the mutual information of the annulus,

$$I = \frac{1}{3}\frac{1}{R_2/R_1} + \cdots \ , \tag{3.28}$$

in the large width limit ($R_2/R_1 \gg 1$). What we observed in the previous subsection is nothing but this asymptotic form consistent with numerical result shown in Fig. 3.3.

3.3 Holographic mutual information

In this section, we examine the mutual information across an annulus in CFT_3 and a gapped system holographically described by Einstein gravity in the (asymptotically) AdS_4 space. The essential device to gain the holographic mutual information is the holographic formula of entanglement entropies (1.2). If there are multiple extremal surfaces, we always pick one of them with least area, which yields a transition between minimal surfaces as we vary a parameter such as a gap scale. In this sense, each extremal surface can be regarded as a phase in QFT as we will see in the following.

3.3.1 In CFT_3 dual to AdS_4 background

We start with CFT_3 dual to the AdS_4 background

$$ds^2 = L^2 \frac{dz^2 - dt^2 + dr^2 + r^2 d\theta^2}{z^2} \ , \tag{3.29}$$

with the AdS radius L. The original CFT_3 is interpreted to live on the boundary $z = 0$ (or at $z = \epsilon \ll 1$ if UV regularization is needed).

The extremal surface respecting the rotational symmetry of the annulus is a solution to the equation of motion for the action

$$I[r(z)] = \frac{\pi L^2}{2G_N} \int dz \, \frac{r(z)\sqrt{1 + r'(z)^2}}{z^2} \ , \tag{3.30}$$

with the boundary conditions $r(0) = R_i$ $(i = 1, 2)$ on its ends. There are two possible extremal surfaces depending on their topologies:

- **Two disk phase** (Fig. 3.7 (2)): γ_A is the superposition of disconnected two disks, each of them being given by

  $$r(z) = \sqrt{R_i^2 - z^2} \ , \qquad (i = 1, 2) \ , \tag{3.31}$$

  respectively. This solution always exists independent of the size of the annulus.

- **Hemi-torus phase** (Fig. 3.7 (1)): γ_A is a connected extremal surface. The analytic solution is obtained in the following way [92, 93, 94]. It consists of two branches in the (r, z)-plane as

$$r = \begin{cases} R_1 \exp\left[-f_-(z/r)\right] \ , \\ R_2 \exp\left[-f_+(z/r)\right] \ , \end{cases} \tag{3.32}$$

where the functions $f_\pm(x)$ are defined using the incomplete elliptic integrals[5] by

$$f_\pm(x) = \frac{1}{2}\log(1+x^2) \pm \eta\, x_m \left[\mathbb{F}\left(\omega(x)|\eta^2\right) - \Pi\left(1-\eta^2, \omega(x)|\eta^2\right)\right] \ , \tag{3.34}$$

with the range $0 \le x \le x_m \equiv \sqrt{\frac{2\eta^2-1}{1-\eta^2}}$ and $\omega(x) = \arcsin\left[\frac{x/x_m}{\sqrt{1-\eta^2(1-x/x_m)}}\right]$. The parameter η in the range $\eta \in [1/\sqrt{2}, 1]$ is related to the ratio R_2/R_1 of the inner and outer radii of the annulus as

$$\log(R_2/R_1) = 2\eta\sqrt{\frac{2\eta^2-1}{1-\eta^2}}\left[\mathbb{K}(\eta^2) - \Pi(1-\eta^2|\eta^2)\right] \ . \tag{3.35}$$

This solution is available only for $(1 \le) R_2/R_1 < 2.724$.

The two disk phase is realized for the large width $R_2/R_1 > 2.724$ where it is the unique solution, while it compete with the hemi-torus phase when $R_2/R_1 < 2.724$. In order to fix the location of the phase transition, we calculate the mutual information I across the annulus defined by (3.3). It is clear in the holographic setup that $I > 0$ signifies the hemi-torus phase because $I = 0$ in the two disk phase.[6] We benefit from the relevant result of [94] to get the mutual information in the hemi-torus phase[7]

$$I_{\text{hemi-torus}} = \frac{\pi L^2}{G_N}\left[\frac{\mathbb{E}(\eta^2) - (1-\eta^2)\mathbb{K}(\eta^2)}{\sqrt{2\eta^2-1}-1} - 1\right] \ , \tag{3.37}$$

[5]The definitions of the incomplete elliptic integrals used here are

$$\begin{aligned} \mathbb{F}(x|m) &\equiv \int_0^x d\theta \frac{1}{\sqrt{1-m\sin^2\theta}} \ , \\ \Pi(n,x|m) &\equiv \int_0^x d\theta \frac{1}{(1-n\sin^2\theta)\sqrt{1-m\sin^2\theta}} \ , \end{aligned} \tag{3.33}$$

and $\mathbb{K}(m) \equiv \mathbb{F}(\pi/2|m)$ and $\Pi(n|m) \equiv \Pi(n, \pi/2|m)$.

[6]The mutual information can vanish only in the large-N limit and there are $O(1/N)$ corrections [95, 96] for finite N. More generally, the mutual information is bounded from below.

[7]The elliptic integral of the second kind is defined by

$$\mathbb{E}(m) \equiv \int_0^{\pi/2} d\theta \sqrt{1-m\sin^2\theta} \ . \tag{3.36}$$

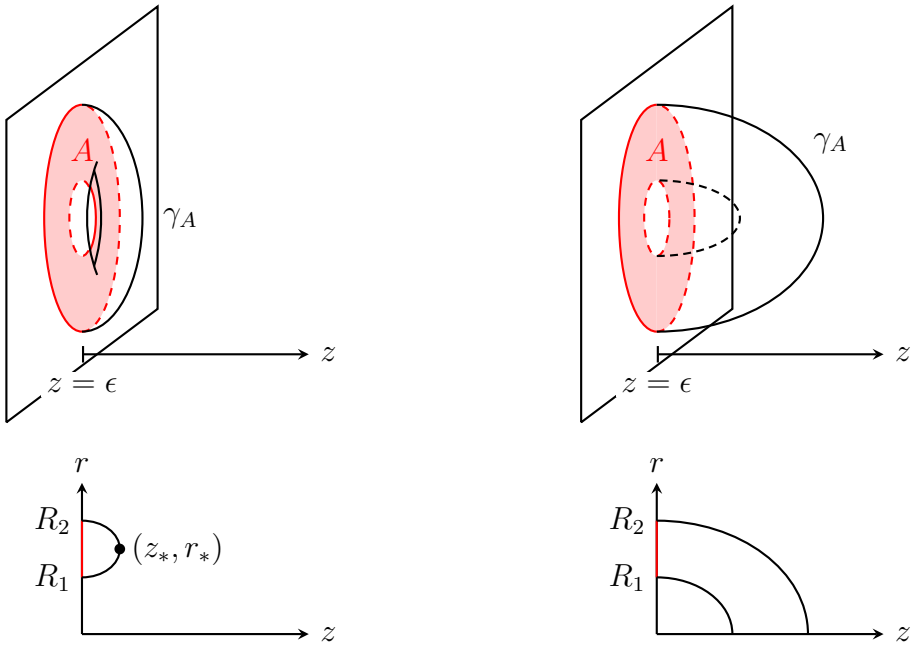

(1) Hemi-torus phase

(2) Two disk phase

Figure 3.7: Two phases for the minimal surface in the AdS_4 background: connected hemi-torus phase (1) and disconnected two disk phase (2). Here the time t direction is suppressed.

whose plot is displayed in orange color in Fig. 3.8. It is a two-valued function whose lower branch is always negative and the upper branch intersects with $I = 0$ at $R_2/R_1 = (R_2/R_1)_{\text{critical}} \approx 2.4$. Since the holographic formula (1.2) selects the non-negative I, the physical mutual information is given by $I_{\text{hemi-torus}}$ for $R_2/R_1 < (R_2/R_1)_{\text{critical}}$ and $I = 0$ for $(R_2/R_1)_{\text{critical}} < R_2/R_1$. It has a kink at $R_2/R_1 = (R_2/R_1)_{\text{critical}}$ caused by the phase transition of the extremal surface γ_A. Comparing with the general form (3.11) of the mutual information in CFT, Fig. 3.8 demonstrates the monotonicity and convexity (2.93) of the function f with respect to $\rho = \log(R_2/R_1)$. In other words, the holographic entanglement entropy of an annulus satisfies the strong subadditivity as guaranteed by the holographic proof based on the minimality of the surfaces [72].

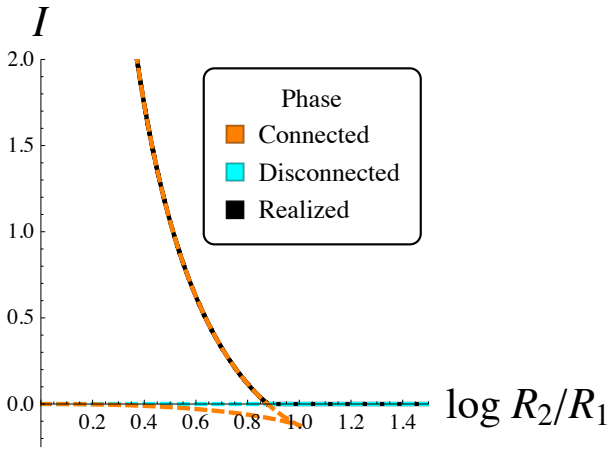

Figure 3.8: The holographic mutual information I across the annulus of radii R_1 and R_2 for CFT. This mutual information $I = I(R_2/R_1)$ has a phase transition at $(R_2/R_1)_{\text{critical}} \simeq 2.4$, and vanishes for $R_2/R_1 > (R_2/R_1)_{\text{critical}}$ because the disconnected two disk phase is realized.

3.3.2 In a gapped system dual to the CGLP background

We move onto a gapped theory described by an asymptotically AdS geometry whose IR region (away from the boundary) is capped off. As a concrete example, we use the CGLP background [27] in M-theory dual to a $(2+1)$-dimensional QFT with a gap scale.

The CGLP background is a $(3+1)$-dimensional geometry times a seven-dimensional internal manifold, which asymptotes to the AdS_4 space times the Stiefel manifold $V_{5,2}$. In the Einstein frame, the metric is given by

$$ds^2 = \alpha(u)\left[du^2 + \beta(u)\left(-dt^2 + dr^2 + r^2 d\theta^2\right)\right] + g_{ij}dy^i dy^j \ , \tag{3.38}$$

where u is the holographic coordinate of the AdS_4 ranging from the IR capped-off point 0 to the UV fixed point ∞. y^i $(i = 1, \cdots, 7)$ are the coordinates of the internal manifold

with a volume

$$V(u) = \int \prod_{i=1}^{7} dy^i \sqrt{\det g} \ , \tag{3.39}$$

vanishing at $u = 0$. The functions in the metric are given by

$$\begin{aligned}
\alpha(u) &= \frac{H(u)^{1/3} c^2(u)}{4} \ , \qquad \beta(u) = \frac{4}{H(u) c^2(u)} \ , \\
V(u) &= \frac{3^{17/8} \pi^4 \varepsilon^{21/4}}{2} H^{7/6}(u) (2 + \cosh u)^{3/8} \sinh^{3/2}\left(\frac{u}{2}\right) \sinh^{3/2} u \ , \\
H(u) &= \frac{L^6}{\varepsilon^{9/2}} 2^{3/2} 3^{11/4} \int_{(2+\cosh u)^{1/4}}^{\infty} \frac{dt}{(t^4-1)^{5/2}} \ , \\
c^2(u) &= \frac{3^{7/4} \varepsilon^{3/2} \cosh^3(u/2)}{2(2+\cosh u)^{3/4}} \ ,
\end{aligned} \tag{3.40}$$

with two dimensionful parameters L and ε. The parameter L is the AdS radius near the boundary, determined by the number of M2-branes N and the Planck length ℓ_p as $L \equiv 3^{-2/3} 2 \pi^{1/3} \ell_p N^{1/6}$. The parameter ε, defining the size of deformation [97], has mass dimension $-4/3$, letting H be dimensionless. V appears to depend on ε, but does not indeed. By rescaling the boundary coordinates (t, r) appropriately, one can remove ε completely from the metric if one wishes.

Let us take a look at the UV behavior of the metric (3.38) for a moment. When u is close to the UV cutoff $u \to \Lambda \gg 1$, the function $H(u)$ becomes

$$H(u) \to 2^{15/4} 3^{3/4} \, L^6 \, e^{-9u/4} \ , \tag{3.41}$$

and the other functions approach

$$\begin{aligned}
\alpha(u) &\to \frac{9}{16} L^2 \ , & \beta(u) &\to 2^{3/2} 3^{-5/2} \, L^{-6} \, e^{3u/2} \ , \\
V(u) &\to 3^3 \pi^4 L^{21/2} \ , & c^2(u) &\to 2^{-13/4} 3^{7/4} e^{3u/4} \ .
\end{aligned} \tag{3.42}$$

The transformation $z = 2^{5/4} 3^{1/4} L^3 e^{-3u/4}$ takes the metric to the Poincaré coordinates of the AdS_4 space near the boundary

$$ds^2 \to L^2 \frac{dz^2 - dt^2 + dr^2 + r^2 d\theta^2}{z^2} + \cdots \ . \tag{3.43}$$

Since the extremal surface for a small annulus localizes near the boundary, the entanglement entropy remains to have the previous two phases shown in Fig. 3.7 in the CGLP background. In addition, there are new phases for a large annulus whose minimal surfaces can reach and terminate on the IR cap-off as we describe below. These are superpositions of disk- and cylinder-type solutions for a disk region [65, 85] depicted in Fig. 3.9. They have different topologies as the names suggest, and the cylinder-type solution only exists and dominates for a large radius. This resembles the situation for a strip region

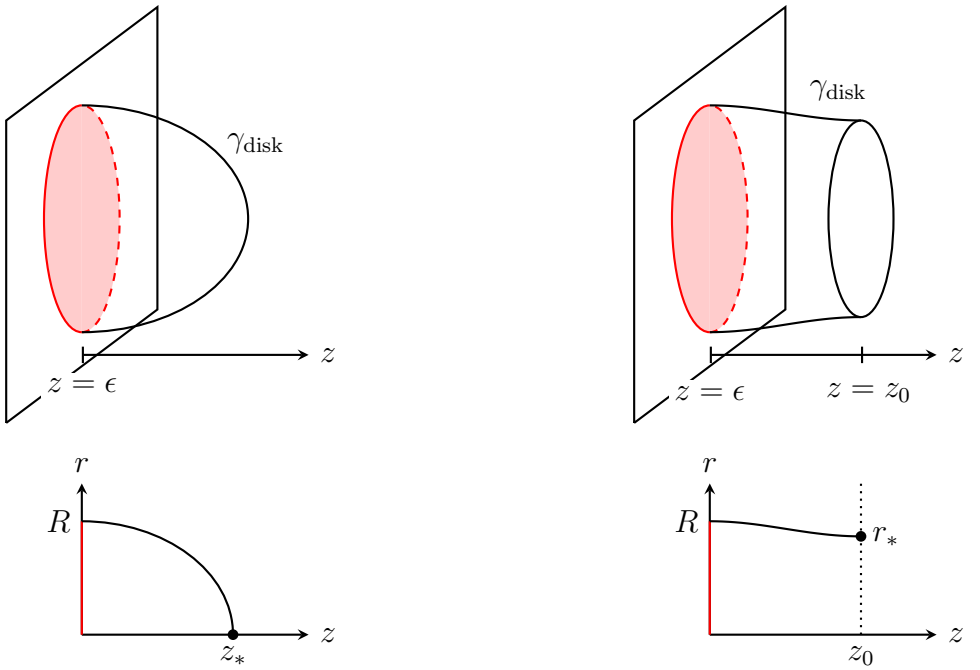

(a) disk phase (b) cylinder phase

Figure 3.9: Two phases of the extremal surface in calculating holographic entanglement entropy of disks in the CGLP background: disk phase (a) and cylinder phase (b). In the Poincaré coordinate $z = 2^{5/4}3^{1/4}L^3e^{-3u/4}$, the UV boundary $u = \Lambda$ corresponds to $z = \epsilon = 2^{5/4}3^{1/4}L^3e^{-3\Lambda/4}$ and the IR capped-off point $u = 0$ corresponds to $z = z_0 = 2^{5/4}3^{1/4}L^3$. In the cylinder phase, the extremal surface terminates on the IR capped-off point $z = z_0$.

in a gapped system, which is interpreted as a confinement/deconfinement phase transition [98, 99]. In the present case, the minimal surface switches from the disk-type to the cylinder-type at the critical radius $R = R_{\text{critical}} \simeq 0.72/m$, where $m = \varepsilon^{-3/4}$ is the gap scale determined by the CGLP metric. Taking into account these facts, we end up with three superposed phases; two disk phase, one disk and one cylinder (disk-cylinder) phase, and two cylinder phase. The first one has already appeared for CFT in the previous subsection (see Fig. 3.7). The second and third ones are drawn in Fig. 3.10. In total, there are the four phases for the annulus in the CGLP background:

(1) the hemi-torus phase (Fig. 3.7 (1)) for $R_2 - R_1 \lesssim 1/m$.

(2) the two disk phase (Fig. 3.7 (2)) for $R_1, R_2 < R_{\text{critical}}$,

(3) the disk-cylinder phase (Fig. 3.10 (3)) for $R_1 < R_{\text{critical}} < R_2$,

(4) the two cylinder phase (Fig. 3.10 (4)) for $R_{\text{critical}} < R_1, R_2$,

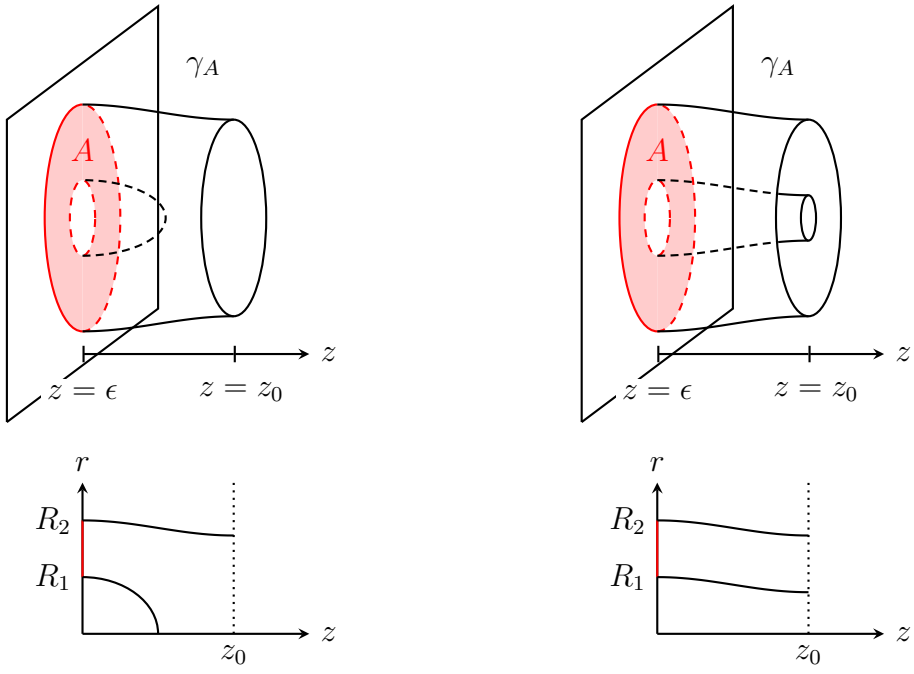

(3) Disk-cylinder phase (4) Two cylinder phase

Figure 3.10: Two new disconnected phases for the minimal surface in the CGLP background: disk-and-cylinder phase (3) and two cylinders phase (4). In the Poincaré coordinate $z = 2^{5/4}3^{1/4}L^3e^{-3u/4}$, the UV boundary $u = \Lambda$ corresponds to $z = \epsilon = 2^{5/4}3^{1/4}L^3e^{-3\Lambda/4}$ and the IR capped-off point $u = 0$ corresponds to $z = z_0 = 2^{5/4}3^{1/4}L^3$.

There are apparently overlaps between the first phase and the others, where the one with the least entropy is realized. To classify the phase structure, we calculate the holographic entanglement entropy in a similar way to the previous pure AdS case. The rotational symmetry lets us assume the radial coordinate r of the extremal surface γ_A as a

(two-branched) function $r_\pm = r_\pm(u)$ of the holographic coordinate u. The area functional becomes

$$I\left[r(u)\right] = \frac{\pi}{2G_N}\sum_{\pm}\int du\, r_\pm(u)\, g(u)\sqrt{1+\beta(u)(r'_\pm(u))^2}\ , \tag{3.44}$$

with $g(u) = V(u)\alpha(u)\beta^{1/2}(u)$. The extremal surface $r = r(u)$ should satisfy the equation of motion

$$2\, g(u)\sqrt{1+\beta(u)(r'(u))^2} = \partial_u\left[\frac{r(u)g(u)\beta(u)r'(u)}{\sqrt{1+\beta(u)(r'(u))^2}}\right]\ , \tag{3.45}$$

with the boundary conditions $r_+(\infty) = R_2$ and $r_-(\infty) = R_1$. In contrast to the CFT case, the analytic solution remains to be known. Instead, we employ the numerical calculation by the "shooting method".

- In the hemi-torus phase, we solve the equation of motion (3.45) from the tip $(r, u) = (r_*, u_*)$ where the two branches meet and have an expansion

  $$r_\pm(u) = r_* \pm 2\sqrt{\frac{g(u_*)}{g(u_*)\beta'(u_*) + 2g'(u_*)\beta(u_*)}}\sqrt{u-u_*} + O((u-u_*)^{3/2})\ . \tag{3.46}$$

  The radii of the annulus $(R_2, R_1) = (r_+(u=\infty), r_-(u=\infty))$ are functions of (r_*, u_*), respectively.

- In the three disconnected phases, the extremal surfaces γ_A for the annulus are obtained just by summing the two extremal surfaces $\gamma_{\mathrm{disk}(R_1)}$ and $\gamma_{\mathrm{disk}(R_2)}$ for two disks of radii R_1 and R_2. The extremal surface $\gamma_{\mathrm{disk}(R)}$ for a disk in the CGLP metric was obtained [85] as follows. The disk-type solution can be constructed by solving the equation of motion (3.45) from the tip of the disk $(r, u) = (0, u_*)$, where the extremal surface shrinks as

  $$r(u) = 2\sqrt{\frac{2g(u_*)}{2\beta(u_*)g'(u_*) + g(u_*)\beta(u_*)}}\sqrt{u-u_*} + O((u-u_*)^{3/2})\ . \tag{3.47}$$

  On the other hand, the cylinder-type solution extends to the IR capped-off point $u = 0$ and we solve the equation of motion (3.45) from $(r, u) = (r_*, 0)$ where the extremal surface terminates and behaves as

  $$r(u) = r_* + \frac{1}{8r_*\beta(0)}u^2 + O(u^3)\ . \tag{3.48}$$

  The disk radius $R = r(\infty)$ is given as a function of u_* or r_*, respectively.

After solving the equation of motion numerically, we compare the holographic entanglement entropies (3.44) between the four phases. The resulting phase diagram is presented in Fig. 3.11. It shows that the hemi-torus phase is realized when the width of

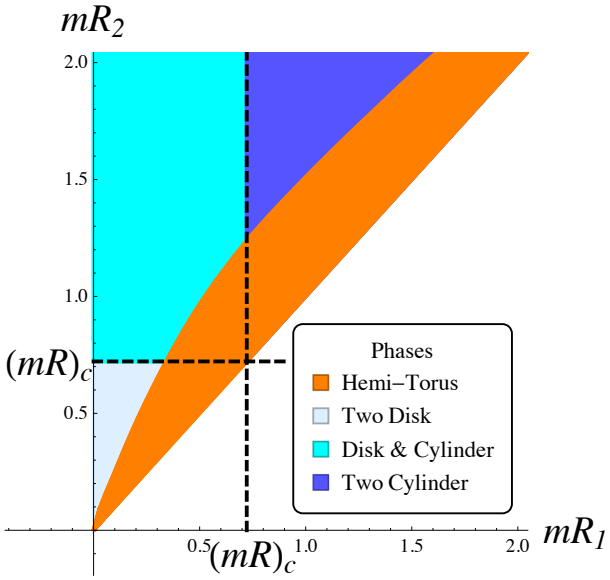

Figure 3.11: The phase diagram of the entanglement entropy for an annulus of radii R_1 and R_2. The hemi-torus phase is favored when the width of the annulus is small compared to the gap scale.

the annulus is small against the gap scale. Note that there is no phase for $R_2/R_1 < 1$ since R_2 is the outer radius of the annulus.

The mutual information (3.3) across the annulus vanishes in all the disconnected phases, and $I > 0$ only in the hemi-torus phase. Fig. 3.12 shows I as a function of $\log(R_2/R_1)$ with mR_2 fixed. It is positive and decreases as R_2/R_1 becomes large, but vanishes at some point due to the phase transition from the hemi-torus phase to a disconnected phase. It is also monotonically decreasing with the mass for a fixed R_2/R_1, and as shown in Fig. 3.13, it exhibits the same exponential decay (3.19) as in the massive free scalar with different constants a, b.

3.4 Universal behaviors of quantum entanglements

In the last two sections, we have dealt with the mutual informations $I(R_1, R_2)$ across the annulus or the annulus entropies $S_A(R_1, R_2)$ for the free massive scalar theory and the holographic model. In this section, we will compare these two cases, and attempt to identify universal behaviors of quantum entanglement.

First we consider the small width limit of the mutual information in CFT. From the field theory result, we anticipate (3.20) holds even in the holographic model. Since the hemi-torus phase is always favored in the small width limit, we can make use of the relations (3.35) and (3.37). A short calculation yields the small width behavior (3.20)

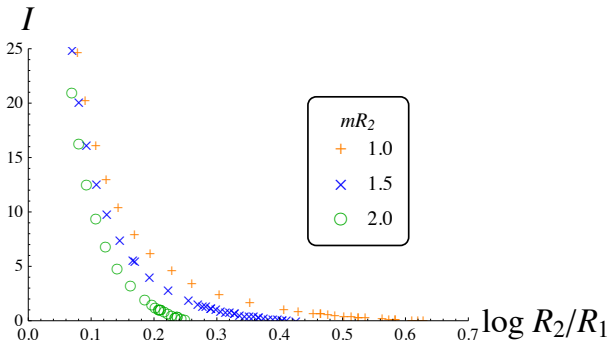

Figure 3.12: The holographic mutual information I across the annulus of radii R_1 and R_2 in a gapped theory holographically described by CGLP metric. $I = I(mR_1, mR_2)$ vanishes for large R_2/R_1 because the phase becomes disconnected, and monotonically decreases with the mass m increased.

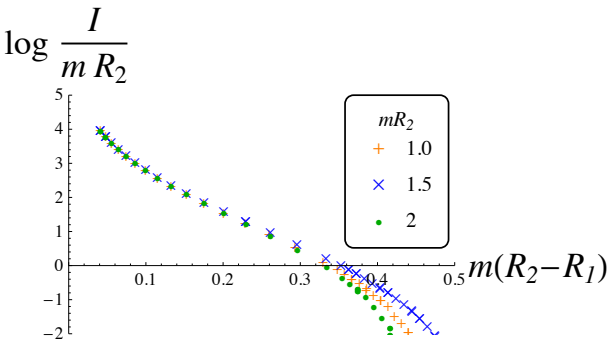

Figure 3.13: The exponential decay of the holographic mutual information I with the dimensionless width $m(R_2 - R_1)$. For $0.1 \lesssim m(R_2 - R_1) \lesssim 0.3$, it shows $I \propto mR_2 \exp[-b'\, m(R_2 - R_1)]$ with $b' \simeq 10$. For $m(R_2 - R_1) \gtrsim 0.3$, this exponential behavior ends because of the phase transition to the disconnected phases with $I = 0$.

with the coefficient $\kappa_{\rm hol}$ given by[8]

$$\kappa_{\rm hol} \equiv \frac{L^2\Gamma[3/4]^4}{2\pi G_N} \ . \tag{3.49}$$

It is plausible that κ in (3.20) counts the effective degrees of freedom in a given QFT because it is proportional to the number of fields in free field theories which characterize the UV fixed point detected by the small width limit of the mutual information. Indeed, the $\kappa_{\rm hol}$ in the holographic model decreases under any RG flow thanks to the holographic c-theorem [101, 102, 67, 68] that provides the constraint $L_{\rm UV} \geq L_{\rm IR}$ for the AdS radii in the UV and IR fixed points. Similar story may hold for the mutual information through two concentric $(d-2)$-sphere separated by a short distance δ which behaves as $I \simeq \kappa\, {\rm Area}(S^{d-2})/\delta^{d-2}$ in $d \geq 4$ dimensions [88, 53]. We do not explore this possibility in this thesis, but hope to investigate it in the future.

In gapped systems, we observed the exponential decay of the mutual information (3.19), both for the free massive scalar field and the strongly coupled theory described by CGLP background, in spite of their difference in the coupling strength. These observations indicates that this exponential behaviour would be universal for mutual informations in gapped theories. It implies the existence of an exponentially suppressed correction to the proposal (2.85),

$$S_A = \alpha\frac{\ell_\Sigma}{\epsilon} + \beta\, m\, \ell_\Sigma - \gamma_\Sigma + \sum_{n=0}^{\infty} \frac{c^\Sigma_{2n+1}}{m^{2n+1}} + O(\exp[-m\delta]) \ , \tag{3.50}$$

where δ is the typical length scale of the region A and would be proportional to the shortest distance between disjoint entangling surfaces. We conjecture that this is a universal property of entanglement entropy in any gapped system. This resembles the universal thermal corrections in entanglement entropy [103, 104, 105, 106, 107] and it would be intriguing to find a relationship between them.

[8] See [100] as a recent related work.

Chapter 4

Time-dependent Entanglement and Holography

The holographic formula (1.2) applies only to static situations, and was generalized to the covariantized formula (2.120), which now applies to time-dependent cases as well. Some studied black hole dynamics holographically with this formula, by some clever but mysterious tricks to obtain time-dependent situations in static black hole geometries, AdS-Schwarzschild black holes and BTZ black holes [108]. The resultant quantum states are interpreted as thermalizing states, and they found that a certain type of entanglement entropies grow linearly with time as expected from field theories calculations of global quench processes [109], and they attributed the linear growth to the growth of the volume of time slice or wormhole through a black hole in the bulk side. On the other hand, our study takes a concrete time-dependent growing black hole geometry from the first, namely, the three-dimensional time-dependent Janus black hole geometry [15, 16, 110] [1], which is one parameter generalization of BTZ black hole and whose dual thermalizing CFT state was proposed already. With this setup, we demonstrate that entanglement entropies can grow linearly with time even without growth of time slice or wormhole in the bulk side, and speculate that what is truly needed for entropies to grow linearly is the invasion of the corresponding bulk surface into the event horizon of black holes.

This chapter is based on the author's work [2] with N. Ogawa and T. Ugajin.

4.1 The time-dependent Janus black hole

Here we review the properties of the three dimensional time-dependent Janus black hole with emphasis on its causal structure and dual CFT interpretation.

[1] There is also a static type of Janus deformation of BTZ black hole [110].

4.1.1 The metric

The Janus black hole has the metric

$$ds^2 = L^2 \, \frac{d\mu^2 - d\tau^2 + r_0^2 \cos^2 \tau d\theta^2}{g(\mu)^2} \,, \tag{4.1}$$

where we take its horizon radius as Lr_0 so that the only dimensionful quantity is the AdS radius L. The conformal factor

$$g(\mu) = \frac{\mathrm{cn}(\kappa_+ \mu, k^2)}{\kappa_+ \, \mathrm{dn}(\kappa_+ \mu, k^2)} \tag{4.2}$$

depends on Janus deformation parameter γ via subsidiary constants

$$\kappa_\pm \equiv \sqrt{\frac{1 \pm \sqrt{1 - 2\gamma^2}}{2}} \,, \qquad\qquad k \equiv \frac{\kappa_-}{\kappa_+} \,. \tag{4.3}$$

The parameter takes a value within $0 \leq \gamma \leq 1/\sqrt{2}$, and controls the strength of the time dependence of the geometry. This geometry of non-zero γ is time-dependent in that it has no timelike Killing vector, and it becomes static only when $\gamma = 0$ with $g(\mu) = \cos \mu$, reducing to just BTZ black hole with an inverse temperature

$$\beta = \frac{2\pi}{r_0} \,, \tag{4.4}$$

in the unit of the AdS radius L. And so the Janus black hole is a one-parameter generalization of BTZ black hole. Its Penrose diagram drawn in the conformally flat (μ, τ) directions is shown in Figure 4.1. The conformal boundaries $g(\mu) = 0$ are still two-sided and located at $\mu = \pm\mu_0$, where $\mu_0 \equiv K(k^2)/\kappa_+$ and $K(k^2)$ is the complete elliptic integral of the 1st kind, $K(k^2) \equiv \int_0^{\pi/2} d\theta / \sqrt{1 - k^2 \sin^2 \theta}$. As a consequence of the time dependence, its apparent horizons,

$$\tan \tau = -\frac{d}{d\mu} \log g(\mu) \,, \tag{4.5}$$

which are defined in each constant time τ slice, differs from its event horizon, $\tau - \pi/2 = \mu - \mu_0$. Since the width $2\mu_0$ between the two conformal boundaries in the μ coordinate increases with γ, the diagram becomes wider than that of BTZ black hole.

In the result, the Janus black hole with non-zero $\gamma > 0$ has a finite region causally disconnected from the conformal boundaries $\mu = \pm\mu_0$. It is an interesting question how the boundary theory encodes information on such a bulk region causally inaccessible from the boundary, which is called causal shadow region [111, 112]. It is known that HRT surface can invade the event horizon while RT surface cannot, and so HRT surface can probe causal shadow region. This indicates that we can draw some information on causal shadow holographically from time-dependent entanglement entropies.

This metric is a solution of the three-dimensional Einstein gravity with a scalar ϕ,

$$S = \frac{1}{16\pi G} \int d^3x \sqrt{g} \left(R - g^{ab} \partial_a \phi \partial_b \phi + \frac{2}{L^2} \right) , \tag{4.6}$$

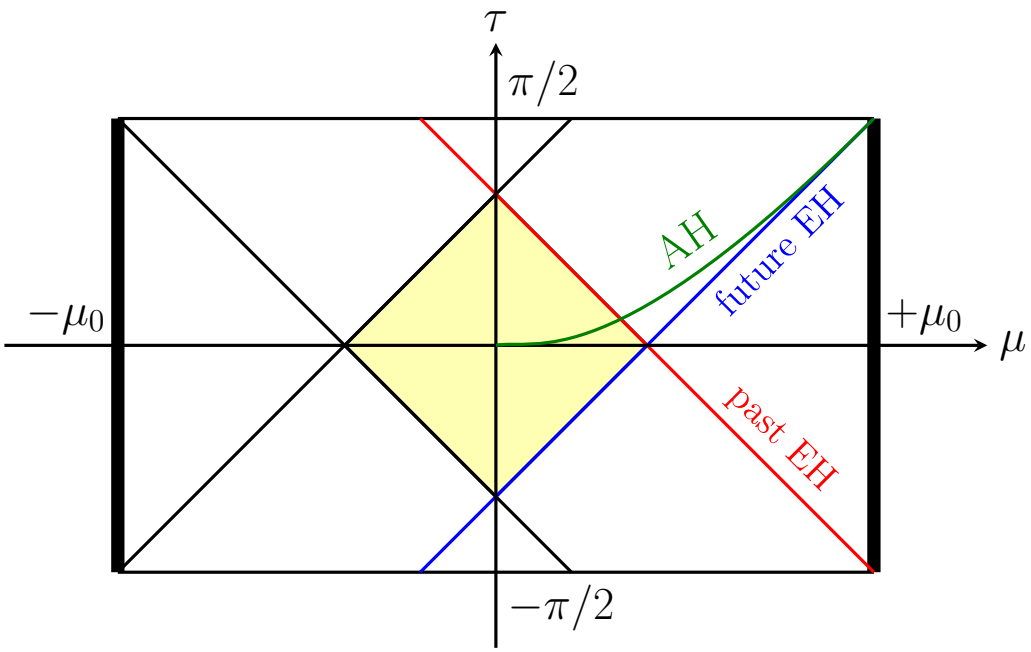

Figure 4.1: Penrose diagram of the three-dimensional time-dependent Janus black hole. The two conformal boundaries are located at $\mu = \pm\mu_0$ (thick lines), and the diagram is a wide rectangle because $\mu_0 \geq \pi/2$. The blue and red lines represent, respectively, the future and past event horizons which intersect with the right hand side boundary. The yellow shaded region corresponds to the "causal shadow" region, which is causally disconnected from the both boundaries. The apparent horizons (green line) in time slices $\tau = \text{const.}$ are located inside the future event horizon.

where the scalar field has a configuration monotonically changing in the holographic direction,

$$\begin{aligned}\phi &= \phi_0 + \sqrt{2}\left(\tanh^{-1}(k\,\mathrm{sn}(\kappa_+\mu, k^2)) + \log\sqrt{1-k^2}\right) \\ &= \phi_0 + \sqrt{2}\left(\tanh^{-1}(k\tanh y) + \log\sqrt{1-k^2}\right). \end{aligned} \tag{4.7}$$

The scalar field values $\phi_\pm \equiv \phi(y = \pm\infty)$ on the right and left boundaries then differ by a γ dependent value

$$\phi_+ - \phi_- = 2\sqrt{2}\tanh^{-1} k = \sqrt{2}\tanh^{-1}\sqrt{2}\gamma\,. \tag{4.8}$$

This three-dimensional system can be embedded in type IIB supergravity in ten dimensions with an appropriate ansatz [15]. Then in the same way as the standard D1-D5 black hole [19, 20, 8], the boundary CFTs are given as the IR fixed points of the two-dimensional $\mathcal{N} = (4,4)$ supersymmetric $\mathrm{SU}(N_1) \times \mathrm{SU}(N_5)$ quiver field theories, which turn out to be σ-models on the instanton moduli space $\mathcal{M} = M_4^{N_1 N_5}/S_{N_1 N_5}$. The bulk scalar field ϕ is identified with the dilaton field, and hence the boundary values $\phi_\pm$ are related to the coupling constants $g_\pm$ of those boundary quiver theories [15]. In terms of the IR σ-models,

this difference in the boundary values leads to the difference in the overall coefficients of the actions on the two boundaries.

4.1.2 The CFT interpretation

In applying AdS/CFT techniques, another time coordinate t related to τ as

$$\tanh r_0 t \equiv \sin \tau \tag{4.9}$$

is useful, because the flat metric $-dt^2 + d\theta^2$ of the dual CFT becomes manifest in its metric,

$$ds^2 = L^2 \left[dy^2 + \frac{r_0^2}{\tilde{g}(y)^2 \cosh^2 r_0 t}(-dt^2 + d\theta^2) \right]. \tag{4.10}$$

Here we have also introduced another radial coordinate y related to μ as

$$\tanh y \equiv \mathrm{sn}(\kappa_+ \mu, k^2)\,, \tag{4.11}$$

which measures the proper length, $dy = d\mu/g(\mu)$, and we have rewritten the factor $g(\mu)$ in terms of this new coordinate y as

$$\tilde{g}(y) \equiv g(\mu(y)) = \frac{1}{\kappa_+ \sqrt{(1-k^2)\cosh^2 y + k^2}} = \sqrt{\frac{2}{1 + \sqrt{1-2\gamma^2}\cosh 2y}}\,. \tag{4.12}$$

The conformal boundaries $\mu = \pm\mu_0$ are mapped to the infinities, $y \to \pm\infty$, while the origin $\mu = 0$ corresponds to the origin $y = 0$. Moving on to the conformal boundaries $y \to \pm\infty$, the metric (4.10) approaches to Poincaré patch of the pure AdS space,

$$ds^2 = L^2 \frac{dz^2 - dt^2 + d\theta^2 + \mathcal{O}(z)}{z^2}\,, \tag{4.13}$$

with an identification

$$z \equiv \frac{2}{\sqrt[4]{1-2\gamma^2}\, r_0} e^{-|y|} \cosh r_0 t\,. \tag{4.14}$$

Hence the UV cutoff ϵ_{CFT} of the CFT is given as

$$\epsilon_{\mathrm{CFT}} = \frac{2}{\sqrt[4]{1-2\gamma^2}\, r_0} e^{-y_\infty} \cosh r_0 t_\infty\,, \tag{4.15}$$

where $y_\infty (\gg 1)$ is the corresponding bulk volume regulator and t_∞ represents the time coordinate t for the CFT located at $y = \pm y_\infty$.

Next, let us review the quantum state dual to the Janus black hole. In the case when $\gamma = 0$, it reduces to just BTZ black hole, which is known to be dual to the thermofield double state of the inverse temperature β (4.4) [12, 113],

$$|\Psi\rangle = \frac{1}{\sqrt{Z}} \sum_n e^{-\frac{\beta}{2} E_n} |E_n\rangle |E_n\rangle\,. \tag{4.16}$$

As explained in the previous subsection, if we turn on the parameter γ, the Hamiltonians $H_\pm$ on the right and left boundaries become different, and so it is conjectured [16] that the Janus black hole is dual to a state that is a natural extension of the thermofield double state,

$$|\Psi\rangle = \frac{1}{\sqrt{Z}} \sum_{m,n} e^{-\frac{\beta}{4}(E_n^- + E_m^+)} \langle E_m^+ | E_n^- \rangle |E_m^+\rangle |E_n^-\rangle \,, \tag{4.17}$$

where $E_n^\pm$'s are eigenvalues of $H_\pm$. This state can also be constructed by Euclidean path integral in the same way as the themofield double state. This conjecture has passed some nontrivial checks. For example, the one point function of the Lagrangian density was computed in both the bulk and boundary sides, which agrees up to the second order in γ [15, 16].

4.2 The holographic EE of an interval

In this section, we compute the entanglement entropy of an interval A holographically in the Janus black hole via the covariant holographic entanglement entropy formula (2.120), and study its time dependence. The interval A is taken as $-\theta_\infty \le \theta \le \theta_\infty$ in the right CFT, at a fixed time $t = t_\infty$ (see Figure 4.2). The extremal surface γ_A can be obtained by solving Euler-Lagrange equations for the area functional,

$$A[t(y), \theta(y)] \equiv L \int_{y_*}^{y_\infty} dy \sqrt{1 + \frac{r_0^2}{\tilde{g}(y)^2 \cosh^2 r_0 t}(-\dot{t}^2 + \dot{\theta}^2)} \tag{4.18}$$

with dynamical variables $t(y)$ and $\theta(y)$ as for the "time" parameter y, where the dot ($\dot{}$) denotes the "time" derivative, d/dy. As shown in Fig. 4.2, the surface is just a geodesic in the right region $y > 0$ and thus its one-dimensional area or length A is given as a y integral from the boundary $y = y_\infty$ to the returning point $y = y_*$, at which the derivative $\dot{\theta}$ of the surface $(t, \theta) = (t(y), \theta(y))$ diverges. Now the bulk volume regulator y_∞ also regulates the area functional. The location (y_*, t_*) of the returning point is determined by the boundary coordinates $(t_\infty, \theta_\infty)$, and so we can represent the area A as a function of the boundary coordinates as $A = A(t_\infty, \theta_\infty)$, by substituting the expression $y_* = y_*(t_\infty, \theta_\infty)$ into the integral (4.18).

We will see that this extremal surface can invade the event horizon, and its area depends on the boundary time t_∞.

4.2.1 Area of the extremal surface

Surprisingly, we can solve the Euler-Lagrange equations for $t(y)$ and $\theta(y)$ in the following way. The action (4.18) has a conserved charge J associated to its θ translation symmetry,

$$J \equiv \frac{\delta A/L}{\delta \dot{\theta}} = \frac{1}{\tilde{g}(y) \cosh r_0 t} \frac{r_0^2 \dot{\theta}}{\sqrt{\tilde{g}(y)^2 \cosh^2 r_0 t + r_0^2(-\dot{t}^2 + \dot{\theta}^2)}} \,, \tag{4.19}$$

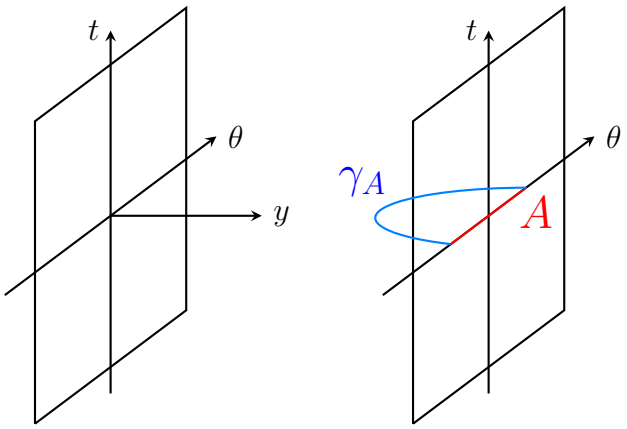

Figure 4.2: The subsystem A (the red line) is taken as one interval of the length $\Delta\theta = 2\theta_\infty$ in the right boundary (the right black square). The extremal surface γ_A (the blue curve) is located totally in the right side $y > 0$.

which can also be expressed by the location (y_*, t_*) of the returning point as

$$J = \frac{r_0}{\tilde{g}(y_*)\cosh r_0 t_*}\,, \tag{4.20}$$

since $\dot{\theta}$ in (4.19) diverges at the returning point. Utilizing this constant J, we can rewrite the equation of motion for $t(y)$ into an equation for $t(\theta)$ as

$$\frac{d}{dy}\frac{\delta A}{\delta \dot{t}} - \frac{\delta A}{\delta t} = 0 \Leftrightarrow \frac{d}{dy}\left(J\frac{\dot{t}}{\dot{\theta}}\right) = Jr_0\frac{-\dot{t}^2+\dot{\theta}^2}{\dot{\theta}}\tanh r_0 t \tag{4.21}$$

$$\Leftrightarrow \frac{d^2t}{d\theta^2} = r_0\left[1-\left(\frac{dt}{d\theta}\right)^2\right]\tanh r_0 t\,, \tag{4.22}$$

without any appearance of the "time" y. Its general solution is given by $\sinh r_0 t = \sinh A\cosh r_0(\theta + B)$ with some constants A and B, which are determined by geometrical conditions $\theta|_{y=y_*} = 0$ and $dt/d\theta|_{y=y_*} = 0$ as

$$\sinh r_0 t = \sinh r_0 t_* \cosh r_0\theta\,. \tag{4.23}$$

This relation allows us to erase the dynamical variable θ, and the equation for the conservation of J (4.19) gives a first order differential equation for the remaining variable t,

$$\dot{t} = \frac{\cosh r_0 t}{r_0\tilde{g}(y_*)\cosh r_0 t_*}\sqrt{\frac{\cosh^2 r_0 t - \cosh^2 r_0 t_*}{1-(\tilde{g}(y)/\tilde{g}(y_*))^2}}, \tag{4.24}$$

which has a unique solution

$$\sqrt{1-\frac{\sinh^2 r_0 t_*}{\sinh^2 r_0 t}}\ (=\tanh\theta) = \cosh r_0 t_*\tanh\left[\int_{y_*}^{y} dy\ \frac{\tilde{g}(y)^2}{\sqrt{\tilde{g}(y_*)^2-\tilde{g}(y)^2}}\right]\,, \tag{4.25}$$

under the initial condition $t(y_*) = t_*$. This expression gives the solution $(t(y), \theta(y))$ in terms of the location (y_*, t_*) of the returning point, which is determined by the boundary value $(t_\infty, \theta_\infty)$ via the boundary condition $t(y_\infty) = t_\infty$, $\theta(y_\infty) = \pm\theta_\infty$ and equations (4.23), (4.25) as

$$\sinh r_0 t_* = \frac{\sinh r_0 t_\infty}{\cosh r_0 \theta_\infty}\,, \tag{4.26}$$

$$\sinh\left[\int_{y_*}^{y_\infty} dy\, \frac{\tilde{g}(y)^2}{\sqrt{\tilde{g}(y_*)^2 - \tilde{g}(y)^2}}\right] = \frac{\sinh r_0 \theta_\infty}{\cosh r_0 t_\infty}\,. \tag{4.27}$$

Note that there are bulk points which cannot be returning points for any boundary value $(t_\infty, \theta_\infty)$, and so there exists a region which cannot be reached by the extremal surfaces (see Fig. 4.3). It would be interesting if generally HRT surface can invade the event horizon but cannot invade the apparent horizon.

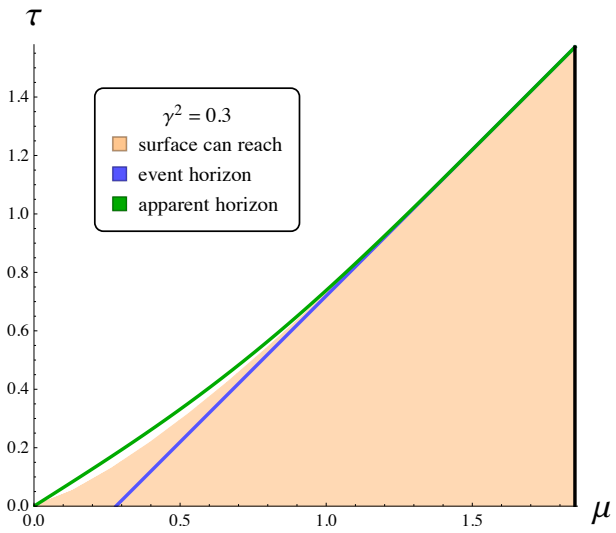

Figure 4.3: How deeply the extremal surfaces can go inside the Janus black hole (with $\gamma^2 = 0.3$ in the figure). The shaded orange region represents where the extremal surfaces can pass through. The extremal surfaces can go beyond the event horizon (blue line), but cannot go beyond the apparent horizon (green line).

Now we can represent the area (4.18) of the solution as a function of the boundary value $(t_\infty, \theta_\infty)$,

$$A(t_\infty, \theta_\infty)/L = 2\int_{y_*}^{y_\infty} dy\, \frac{\tilde{g}(y_*)}{\sqrt{\tilde{g}(y_*)^2 - \tilde{g}(y)^2}}\,, \tag{4.28}$$

by plugging (4.23) and (4.24) into its definition, where y_* is implicitly determined by $(t_\infty, \theta_\infty)$ via the relation (4.27). This area has a UV divergence $-2\log\epsilon_{\mathrm{CFT}}$, because

approaching to each boundary, $\tilde{g}(y) \to 0$ and so

$$A/L \to 2\int^{y_\infty} dy \sim 4y_\infty = 2\log\frac{2\cosh r_0 t_\infty}{\sqrt[4]{1-2\gamma^2}\, r_0 \epsilon_{\rm CFT}}\,. \tag{4.29}$$

This UV divergence can be regularized as

$$\begin{aligned} A^{(\rm reg)}/L &\equiv A/L + 2\log\epsilon_{\rm CFT} \\ &= A/L - \frac{1}{2}\log(1-2\gamma^2) + 2\log\frac{2\cosh r_0 t_\infty}{r_0} - 2y_\infty\,. \end{aligned} \tag{4.30}$$

4.2.2 Some special limits

It is generally difficult to obtain the explicit expression of the surface area A in terms of the boundary value $(t_\infty, \theta_\infty)$, but there are some limits in which it is explicitly obtainable:

- A large interval ($\theta_\infty \gg r_0^{-1}$) in the early time ($t_\infty \ll \theta_\infty$)
- A large interval ($\theta_\infty \gg r_0^{-1}$) in the late time ($t_\infty \gg \theta_\infty$)
- A small Janus deformation ($\gamma \ll 1$)

A large interval in the early time

In this parameter region, the returning point (y_*, t_*) is very close to the origin $(0,0)$, as can be seen in a following way. The t_* is determined by (4.26) as

$$r_0 t_* \simeq 2e^{-r_0\theta_\infty}\sinh r_0 t_\infty \quad (\ll 1)\,, \tag{4.31}$$

where we used $\cosh r_0\theta_\infty \simeq e^{r_0\theta_\infty}/2$ and $\sinh r_0 t_* \simeq r_0 t_*$. The y_* is determined by (4.27) as

$$r_0\theta_\infty - \log\cosh r_0 t_\infty \simeq \int_{y_*}^{y_\infty} dy\, \frac{\tilde{g}(y)^2}{\sqrt{\tilde{g}(y_*)^2 - \tilde{g}(y)^2}} \quad (\gg 1)\,. \tag{4.32}$$

This situation means $y_* \ll 1$, because the left hand side of (4.32) is very large while the integral of the right hand side increases monotonically with decreasing y_* and diverges in the limit $y_* \to 0$. In fact, in the limit $y_* \to 0$, the integral of the right hand side can be evaluated as

$$r_0\theta_\infty - \log\cosh r_0 t_\infty \simeq -\frac{1}{\sqrt{\kappa_+^2 - \kappa_-^2}}\log\left[\frac{\kappa_+ + \sqrt{\kappa_+^2 - \kappa_-^2}}{4} y_*\right]\,, \tag{4.33}$$

by changing the integration variable from y to $z \equiv \tanh y$. This expression gives y_* explicitly in terms of $(t_\infty, \theta_\infty)$, and allows us to delete y_* in the area integral and express the regularized area as a function of $(t_\infty, \theta_\infty)$,

$$A^{(\mathrm{reg})}(t_\infty, \theta_\infty)/L \simeq 2\kappa_+ r_0 \theta_\infty + 2(1-\kappa_+)\log\cosh r_0 t_\infty - 2\log\left[\frac{\kappa_+ + \sqrt{\kappa_+^2 - \kappa_-^2}}{2} r_0\right], \tag{4.34}$$

where we used a relation

$$\begin{aligned}&\int_{y_*}^{y_\infty} dy\ \frac{\tilde{g}(y_*)}{\sqrt{\tilde{g}(y_*)^2 - \tilde{g}(y)^2}} \\ &\simeq -\frac{\kappa_+}{\sqrt{\kappa_+^2 - \kappa_-^2}} \log\left[\frac{\kappa_+ + \sqrt{\kappa_+^2 - \kappa_-^2}}{4} y_*\right] - \log\left[\frac{\kappa_+ + \sqrt{\kappa_+^2 - \kappa_-^2}}{\sqrt{\kappa_+^2 - \kappa_-^2}}\right] + y_\infty \end{aligned} \tag{4.35}$$

which holds in the limit $y_* \to 0$. Note that the area linearly grows with both t_∞ and θ_∞, in this parameter region, though their coefficients are different.

A large interval in the late time

In this parameter region, (4.26) and (4.27) lead to

$$2e^{-r_0 t_*} \simeq \int_{y_*}^{y_\infty} \frac{\tilde{g}(y)^2 dy}{\sqrt{\tilde{g}(y_*)^2 - \tilde{g}(y)^2}} \simeq e^{r_0(\theta_\infty - t_\infty)} \quad (\ll 1)\,, \tag{4.36}$$

where we used $\sinh x \simeq \cosh x \simeq e^x/2$ for $x \gg 1$ and $\sinh x \simeq x$ for $x \ll 1$. This expression in turn implies $y_* \gg 1$, therefore the integrals in (4.36) and (4.28) can be respectively approximated as

$$\int_{y_*}^{y_\infty} \frac{\tilde{g}(y)^2 dy}{\sqrt{\tilde{g}(y_*)^2 - \tilde{g}(y)^2}} \simeq \frac{2}{\sqrt[4]{1-2\gamma^2}} e^{-y_*}\,, \tag{4.37}$$

$$\int_{y_*}^{y_\infty} \frac{\tilde{g}(y_*) dy}{\sqrt{\tilde{g}(y_*)^2 - \tilde{g}(y)^2}} \simeq y_\infty - y_* + \log 2\,, \tag{4.38}$$

where we also used $y_\infty - y_* \gg 1$. By substituting (4.38) into (4.28), and by erasing y_∞ and y_* with the aid of (4.15), (4.36) and (4.37), we can evaluate the regularized area $A^{(\mathrm{reg})}$ (4.30) as

$$A^{(\mathrm{reg})}(t_\infty, \theta_\infty)/L \simeq 2(r_0\theta_\infty - \log r_0)\,, \tag{4.39}$$

which does not depend on either of γ or t_∞. Then in particular, it coincides with the result for BTZ black hole ($\gamma^2 = 0$).

Expansion with the deformation γ^2

So far, we have seen the early time $t_\infty \ll \theta_\infty$ and the late time $\theta_\infty \ll t_\infty$ behavior of the extremal surface area for general γ, but the surface phase transition discussed in the next section typically occurs at the intermediate time region $t_\infty \sim \theta_\infty$. To obtain an analytic expression applicable to the whole time region, let us evaluate the surface area up to the lowest order of the deformation γ^2. By expanding the relation (4.27) and the area integral (4.28) up to the order of γ^2, we get

$$A^{(\mathrm{reg})}/L = 2\log\left(\frac{2}{r_0}\sinh r_0\theta\right) - \frac{1}{2}\left(\frac{3F^2+2}{2\sqrt{1+F^2}}\coth^{-1}\left(\sqrt{1+F^2}\right) - \frac{3}{2}\right)\gamma^2 + \mathcal{O}(\gamma^4)\,, \tag{4.40}$$

where

$$F(t,\theta) = \frac{\cosh r_0 t_\infty}{\sinh r_0\theta_\infty}\,. \tag{4.41}$$

The detail of this calculation is explained in Appendix B.1. Note that when $\gamma = 0$, it reduces to the usual thermal result for BTZ black hole. In the early ($F \ll 1$) and late ($F \gg 1$) time limits, it respectively reproduces the results (4.34) and (4.39) for large intervals.

4.2.3 Time dependence

Let us summarize the typical time dependence of our holographic entanglement entropy of one interval. Take a large interval $\theta_\infty \gg r_0^{-1}$ for simplicity. As seen in the previous subsection, its entropy starts at nonzero value $2\kappa_+ r_0\theta_\infty$ with the corresponding extremal surface reaching at the origin $(0,0)$. The surface starts to depart from the origin toward the right boundary, and the entropy grows linearly with the time t_∞ with the speed of $2(1-\kappa_+)r_0$. About after the surface escapes from the event horizon, the geometry around the surface is almost just the pure AdS space and so the entropy becomes saturated at the value of BTZ, $2r_0\theta_\infty$.

This time-dependent behavior is very similar to the one in [108], which constructed a time-dependent situation by applying some tricks to BTZ black hole. Both entropies grow linearly at first, where the extremal surface is invading the event horizon, and become saturated at the value of the thermal entropy at a time proportional to the region size, where the extremal surface is almost the same as the one in pure AdS space. However, our setup has significant differences from that old work:

- The surface invades the right horizon but does not go through the left horizon to the other asymptotic region; it does not connect the two asymptotic regions. Then the linear growth of its entropy is not related to any nice time slice or wormhole connecting the two asymptotic regions, which the old work attributes the reason of the linear growth to.

- The speed $2(1-\kappa_+)r_0$ at which the entropy grows is slower than one $2r_0$ of the old work. The growing speed increases with γ, as is expected from the property of

the geometry that the strength of its time dependence is controlled by the Janus deformation γ.

- There is an initial entropy $2\kappa_+ r_0\theta_\infty$, which decreases with γ. The entropy grows from $2\kappa_+ r_0\theta_\infty$ to $2r_0\theta_\infty$ at the speed of $2(1-\kappa_+)r_0$, and so the time for the entropy to be saturated can be estimated as the size of the interval θ_∞. This time is independent of γ, and is the same as that old work.

- Based on many numerical calculations, we found that the transition from the linearly growing period to the saturated period is smoothed and not so sharp as in the old work.

From the comparison between our work and the old work, we speculate that the origin of the linear growth of the holographic entanglement entropies is not the growth of any nice time slice or wormhole but is the invasion of the surface into the horizon.

4.3 HEE of two intervals and the phase transition

As explained before, one can also construct a holographic model displaying linear growing entropies from just static BTZ black hole, by a clever and mysterious trick, namely, by taking two intervals located separately in each CFT and by taking the time direction of one CFT opposite [108]. With our time-dependent Janus black hole, here we also investigate the one parameter γ generalization of that work, by taking two intervals separated in each CFT and by taking the time direction opposite, in the same way. This entanglement can be interpreted as some entanglement between the left and right CFT's.

4.3.1 Two phases

We take our region A to be two disjoint same intervals $-\theta_\infty \leq \theta \leq \theta_\infty$ in each of the left and right CFT's at a fixed time $t = t_\infty$, that is, $A = \{(\pm y_\infty, t_\infty, \theta); -\theta_\infty \leq \theta \leq \theta_\infty\}$ (see Figure 4.4). In the same way as the BTZ black hole, its corresponding extremal surface still can take two types of topologies (see Figure 4.4), "connected phase" and "disconnected phase", even in the Janus black hole geometry (4.10).

The disconnected type consists of two disjoint geodesics which start from and end at the same boundary (see Figure 4.4 (a)); starting from $(\pm y_\infty, t_\infty, -\theta_\infty)$, turning around at $(\pm y_*, t_*, 0)$ and ending at $(\pm y_\infty, t_\infty, \theta_\infty)$. This surface is just the two copies of the surface we have studied already for one interval, where the new copy is a mirror image of the original copy constructed by parity transformation $y \to -y$; one copy is located in the right region $y > 0$ and the other is in the left region $y < 0$. Consequently, in the disconnected phase, the area of the corresponding extremal surface is just the two times the area we studied already for one interval:

$$A_{dc} = 2A\,. \tag{4.42}$$

The connected type is a new ingredient, consisting of two geodesics which connect the two boundaries (see Figure 4.4 (b)); starting from $(y_\infty, t_\infty, \pm\theta_\infty)$ and ending at $(-y_\infty, t_\infty, \pm\theta_\infty)$.

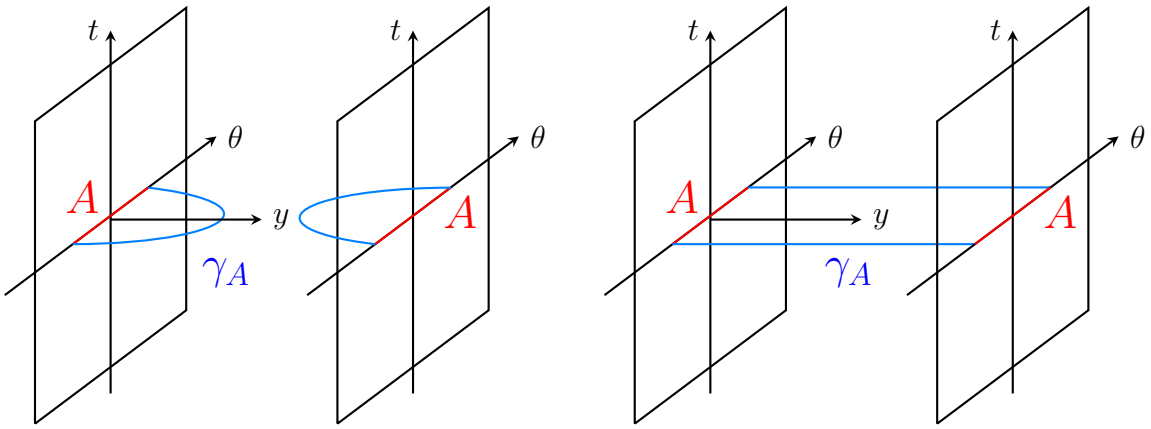

(a) disconnected phase (b) connected phase

Figure 4.4: The subsystem A (two red lines) is taken as two disjoint intervals of the same length $\Delta\theta = 2\theta_\infty$ in the right and left boundary (two black squares). The extremal surface γ_A (blue lines) has two phases: disconnected phase (a) and connected phase (b).

Let us study the area functional of this type of surface. The area functional is extremized when $\theta = \text{const.}$ ($= \pm\theta_\infty$), and then the area functional (4.18) becomes

$$A[t(y)]/L = \int_{-y_\infty}^{y_\infty} dy \sqrt{1 - \frac{r_0^2\, \dot{t}^2}{\tilde{g}(y)^2 \cosh^2 r_0 t}}\,, \tag{4.43}$$

for each of the two pieces of the surface ($\theta = \pm\theta_\infty$). This functional has a conserved charge E associated to its t-translation symmetry,

$$\begin{aligned} E \equiv \frac{\delta A/L}{\delta \dot{t}} &= \frac{-r_0^2\, \dot{t}}{\tilde{g}(y) \cosh r_0 t \sqrt{\tilde{g}(y)^2 \cosh^2 r_0 t - r_0^2\, \dot{t}^2}} \\ \Leftrightarrow \quad \dot{t} &= \frac{-E\, \tilde{g}(y)^2 \cosh^2 r_0 t}{\sqrt{r_0^2 + E^2\, \tilde{g}(y)^2 \cosh^2 r_0 t}}\,. \end{aligned} \tag{4.44}$$

This charge E vanishes, however, because $\dot{t}$ cannot change its sign and we have the boundary condition $\int_{-y_\infty}^{y_\infty} \dot{t}\, dy = t_\infty - t_\infty = 0$. In the result, the total area of the connected extremal surface can be explicitly calculated as

$$\begin{aligned} A_c(t_\infty, \theta_\infty)/L &= 2 \times 2y_\infty \\ &= 4 \log \frac{2 \cosh r_0 t_\infty}{r_0 \epsilon_{\text{CFT}}} - \log(1 - 2\gamma^2)\,, \end{aligned} \tag{4.45}$$

where we used the relation between the regulator y_∞ and the CFT cutoff ϵ_{CFT} (4.15). We

can regulate the UV divergence similarly as

$$\begin{aligned} A_c^{(\mathrm{reg})}/L &\equiv A_c(t_\infty, \theta_\infty)/L + 4\log\epsilon_{\mathrm{CFT}} \\ &= 4\log\frac{2\cosh r_0 t_\infty}{r_0} - \log(1-2\gamma^2)\,. \end{aligned} \tag{4.46}$$

Note that the Janus deformation γ only appears in the constant term, and does not affect the growing speed of the entropy, $4r_0$, in the connected phase. One interesting point is that the constant term becomes arbitrarily large in $\gamma^2 \to \frac{1}{2}$ limit. This illuminates the fact that the length of the wormhole behind the Janus black hole becomes infinitely long in this limit.

4.3.2 Phase transition

Here we discuss the whole time-dependent behavior of the holographic entanglement entropy of the two intervals. Since there are two extremal surfaces in the bulk geometry, the holographic entanglement entropy S_A is given by the area of the surface with the smaller area,

$$S_A = \frac{1}{4G_N}\,\min\{A_c, A_{dc}\}\,, \tag{4.47}$$

where A_c and A_{dc} are given by (4.45) and (4.28) respectively. We saw that both the surface can invade the event horizon, and their areas depend on the boundary time t_∞. The surface to be realized then depends on the time, and a phase transition can occur at some time between these two phases. As we will see below, the time dependent behavior of the entropy S_A varies according to the deformation parameter γ.

$\gamma = 0$ When $\gamma = 0$, the spacetime reduces to the BTZ black hole, and does not contain any causal shadow region. The connected and disconnected surface areas are respectively given by

$$A_c(t_\infty, \theta_\infty)/L = 4\log\left(\frac{2\cosh r_0 t_\infty}{r_0\epsilon_{\mathrm{CFT}}}\right)\,, \qquad A_{dc}(t_\infty, \theta_\infty)/L = 4\log\left(\frac{2\sinh r_0\theta_\infty}{r_0\epsilon_{\mathrm{CFT}}}\right)\,. \tag{4.48}$$

Let us take a sufficiently large subsystem $r_0\theta_\infty \gg 1$. The entropy initially grows linearly with time because the connected surface is chosen in accordance with $A_c < A_{dc}$, and stops growing at a critical time $t_\infty = t_c \simeq \theta_\infty$. After the critical time, it ends up with a constant value, double the value of the thermal entropy, because the disconnected surface becomes chosen in accordance with $A_{dc} < A_c$.

This time-dependent behavior such as the sharp phase transition can be also observed on the CFT side, since the time-scale of the transition is given by β [108] and now $r_0\theta \gg 1$ implies $t_c \gg \beta$. Furthermore, the initial entanglement entropy at $t_\infty = 0$ can be identified with the contribution from the boundary of A (4 points). In CFT side, the time-dependent behavior can be intuitively understood in the so-called quasi-particle picture [109]. In this

picture, we assume that a pair creation of entangled quasi-particles occurs at every spatial point at the initial time, and that they propagate in opposite directions at the speed of light. A pair contributes to the entanglement entropy when one of the pair is inside the region and the other of the pair is outside the region. This picture correctly reproduces the linear growth and saturation of the entanglement entropy.

$0 < \gamma^2 \ll \frac{1}{2}$ When $0 < \gamma^2 \ll \frac{1}{2}$, the story is quite similar to the BTZ case, $\gamma = 0$. The entanglement entropy grows up until a critical time $t_\infty = t_c \simeq \theta_\infty$, and at the critical time, the areas of the two surfaces become equal and a phase transition takes place. In this case, the growth rate of the entanglement entropy suddenly decreases discontinuously, but does not immediately become zero, unlike the BTZ case. The entanglement entropy continues to grow very slowly and converges to a constant independent of γ. Hence the final value is identical with that of the BTZ case, $\gamma = 0$, in particular.

Another important difference from the BTZ black hole case is that the initial entanglement entropy includes an additional positive constant term $(-\frac{L}{4G_N}\log(1-2\gamma^2))$. This term can be regarded as a kind of boundary entropy, which is the contribution of defects in the system [114] (see also [115] for the holographic realization). Note that in our system the defect is localized along the Euclidean time direction.

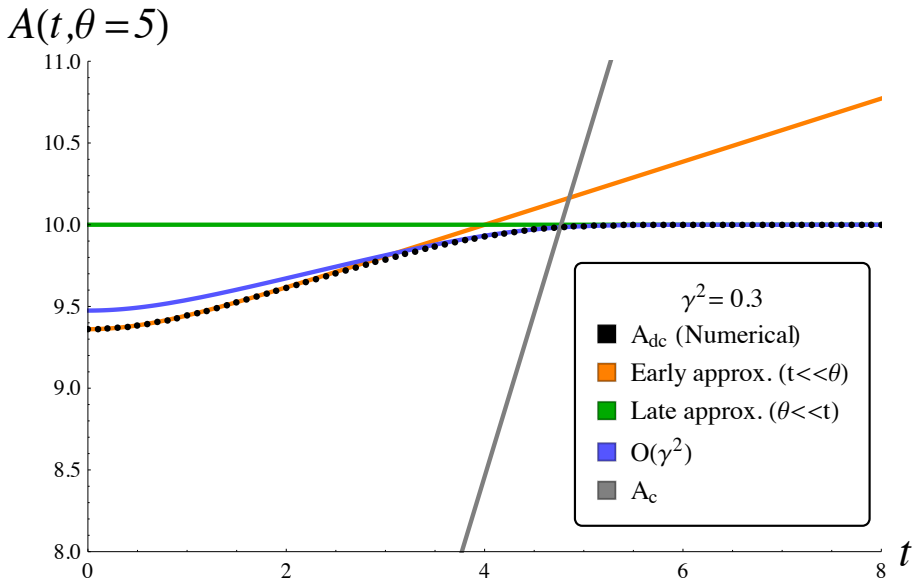

Figure 4.5: The time t dependence of the extremal surface area A for a subsystem $\theta = 5$, in the disconnected phase (black dotted line, numerically obtained) and in the connected phase (gray line). The phase transition from the connected phase to the disconnected phase occurs at their intersection point $t = t_c$. The disconnected phase surface area A_{dc} is initially well approximated by the early time limit approximation (4.34) (orange line), and finally well approximated by the late time limit approximation (4.39) (green line). The whole time-dependence of A_{dc} is qualitatively reproduced by the calculation (4.40) up to $\mathcal{O}(\gamma^2)$ (blue line).

It is difficult to determine the critical time t_c analytically for arbitrary γ and θ_∞, because one need to evaluate the disconnected surface area (4.28) around the time region $t_\infty \sim \theta_\infty$ for which it is difficult to evaluate the areas explicitly. Here we evaluate it perturbatively around $\gamma = 0$ up to the second order. The detail of the calculation is given in Appendix B.1. By equating (4.45) and (4.40), we obtain

$$t_c \simeq \theta_\infty - 2.058\gamma^2 + \mathcal{O}(\gamma^4)\,. \tag{4.49}$$

Note that the coefficient of γ^2 does not depend on the size of the subsystem θ_∞ or r_0.

We can also solve the equations of motion for the disconnected extremal surface numerically, to obtain the accurate time-dependence of A_{dc}. The result is plotted in Fig. 4.5, together with the results of the γ^2-perturbation, the early time and late time approximations discussed in the last section. The figure shows that the γ^2-perturbation gives quite a good approximation around $t_\infty \sim t_c$.

$\gamma^2 \to \frac{1}{2}$ When γ^2 is very close to $\frac{1}{2}$, the time evolution of the entanglement entropy does not exhibit a phase transition for a large range of θ_∞. The minimal value θ_c of the subsystem size θ_∞ necessary for the phase transition to happen is determined by solving

$$A_{dc}(t_\infty = 0, \theta_\infty = \theta_c, \gamma^2) = A_c(t_\infty = 0, \gamma^2)\,. \tag{4.50}$$

By using the early-time expression (4.34) for the left hand side, we can solve this equation as[2]

$$\theta_c \simeq \frac{1}{2\sqrt{2}r_0}\left(-\log\left(1-2\gamma^2\right) - 2\log 2\right)\,. \tag{4.51}$$

When $\theta \leq \theta_c$, the disconnected surface is realized from the initial time $t_\infty = 0$. Furthermore, the initial entanglement entropy is proportional to the size of the subsystem ($\propto \theta$), which can be also seen by using the early-time approximation. This is one of the very peculiar point in the $\gamma^2 \to \frac{1}{2}$ limit.

Let us summarize the time dependence of the entropies when introducing Janus deformation. In BTZ black hole geometry, the connected surface is initially realized, then after the critical time t_c which is proportional to the size of the subsystem, the disconnected surface becomes realized. Although the behavior in the Janus black hole geometry shares many similarities to the BTZ case, there are two notable differences. First of all, we showed that the critical time is shorter than that in the BTZ case. Intuitively, this is because the Janus black hole has a longer wormhole region, therefore the length of the connected surface becomes longer than that of the BTZ black hole. We computed this critical time up to the second order of the deformation parameter γ. Secondly, we found that the disconnected surface is always realized when γ^2 gets sufficiently close to $1/2$ with the size of the region fixed, namely, when the wormhole region is sufficiently long.

In Fig. 4.3, we numerically plotted the bulk region where the disconnected surface can arrive, and found that outside the apparent horizon, there exists a barrier which any

[2]We dropped subleading terms for $1-2\gamma^2$, because in (4.34) we already used the $r_0\theta \gg 1$ approximation, which in turn implies $1-2\gamma^2 \ll 1$ here.

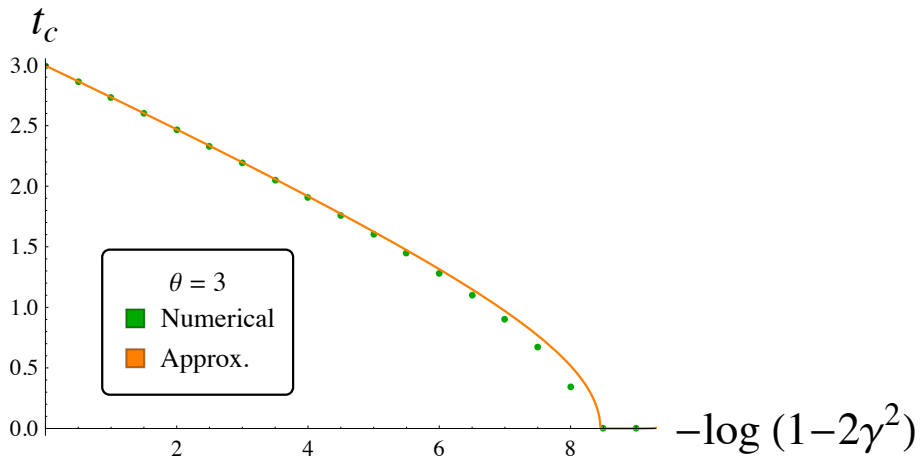

Figure 4.6: The γ^2 dependence of the transition time t_c of a subsystem $\theta = 3$. The green dots are obtained by calculating the disconnected phase surface area A_{dc} numerically. The approx line (orange line) is obtained by substituting the disconnected phase surface area A_{dc} (4.40) calculated up to $\mathcal{O}(\gamma^2)$. The transition time t_c decreases with $-\log(1/2-\gamma^2)$ almost linearly, and the connected phase disappears with sufficiently large γ^2.

disconnected surface cannot invade. As a result, after the phase transition, the black hole interior region that the extremal surfaces can probe is rather limited. This limitation is especially strong in the above case when γ^2 is close to $1/2$.

It would be also interesting to see the time evolution of the mutual information between intervals $-\theta_\infty < \theta < \theta_\infty$ in the right and left CFTs. The mutual information eventually vanishes in the disconnected phase, $t_\infty \geq t_c$. For BTZ black holes, this critical time is given by half the size of the subsystem $t_c^{(\mathrm{BTZ})} = \theta_\infty$ in the high temperature limit. In [116], they considered the perturbation of BTZ black holes by a shock wave sent from one boundary, and found that the critical time becomes shorter by so called scrambling time. Here we see that our γ-deformation also leads to earlier critical times. The main difference from our results is that the deviation of the critical time from the BTZ value $t_c - t_c^{(\mathrm{BTZ})}$ is proportional to the inverse temperature β in their case, while it is not in our case.

4.4 Discussions

In [111], it was shown that if we take the region A to be the total space of the left CFT, the extremal surface which computes the holographic entanglement entropy has to be located in the causal shadow. This property is necessary for the holographic entanglement entropy formula to respect the causality of the dual boundary theory. We can easily check this condition in the Janus black hole, because in the large θ_∞ limit the corresponding extremal surface localizes at the origin $(y, t) = (0, 0)$ (or $(\mu, \tau) = (0, 0)$ in the coordinate (4.1)).

There are several outlooks for this work. It would be interesting to calculate the

entanglement entropy on the dual CFT side. One candidate CFT is a free fermion system [117], for which the explicit form of the twist operator is known [118]. Fig. 4.3 seems to show that it is not possible for the disconnected surface to penetrate the apparent horizon of the Janus black hole, and it would be interesting to prove this directly like [119].

Chapter 5

Renormalized Entanglement Entropy on a Curved Space

Renormalized entanglement entropy (REE) has an advantage in its ability to capture physical degrees of freedom directly, in the sense that it monotonically decreases along renormalization group (RG) flows [55]. To figure out how quantum entanglement encodes physical degrees of freedom as REEs, and to clarify what is the essence in its definition to capture physical degrees of freedom, we extended its definition from the flat space to the simplest curved space, a sphere $\mathbb{S}^2$. There are naively two possible ways to extend its definition, and so we tried both definitions in an example. As a consequence, we found that the one in the more natural definition monotonically decreases along RG flow expectedly at least in our example, while the other one does not.

This chapter is based on the author's work [3] with S. Banerjee and T. Nishioka.

5.1 Renormalized entanglement entropy

5.1.1 Two REE's on cylinder

Entanglement entropy is always accompanied by UV divergences in QFT. The leading part is well-known as the area law term (2.48) diverging as $1/\epsilon^{d-2}$ in d dimensions for the UV cutoff $\epsilon \ll 1$. For this reason, the bare entropy is scheme-dependent and needs to be renormalized so as to be free from the UV divergences. One possible regularization is to renormalize the divergences to parameters in the background gravity theory such as the Newton and cosmological constants as is usually done in QFTs on curved spaces [120].

A simpler regularization was proposed by Liu and Mezei [65] for a spherical or any scalable entangling region on a flat space-time. They define the renormalized entanglement entropy (REE) by acting a differential operator of the radius of the sphere on the EE. In three dimensions, the REE of a disk of radius R_{disk} becomes (2.90) which subtracts the UV divergence of the EE, as explained in chapter 2. Moreover it has been shown that the REE defined in this way is monotonically decreasing along any RG flow in three dimensions [55], known as the F-theorem [66, 54].

In this chapter, we will consider a theory on a cylinder $\mathbb{R} \times \mathbb{S}^{d-1}$ with the metric given

by

$$ds^2 = -dt^2 + R^2 \left(d\theta^2 + \sin^2\theta \, d\Omega_{d-2}^2 \right) \ , \tag{5.1}$$

and divide the $\mathbb{S}^{d-1}$ by a codimension-two hypersurface Σ at $t = 0$ and $\theta = \theta_0$ to a subsystem A within $0 \leq \theta \leq \theta_0$ and its compliment $\bar{A}$ within $\theta_0 \leq \theta \leq \pi$. The angle θ_0 can be restricted to be $0 \leq \theta_0 \leq \pi/2$ for the entropy is symmetric with respect to the exchange of A and $\bar{A}$ when we concentrate only on the vacuum state of the theory.

In our case we can define two types of REEs on the cylinder. First we note that the finite part of the EE of the cap-like region A on $\mathbb{S}^2$ equals to that of a disk on $\mathbb{R}^2$, $F = -\log Z[\mathbb{S}^3]$, if the theory is conformal. Thus the entropy $S_A(\theta_0)$ for CFT_3 on the cylinder takes the form:

$$S_A(\theta_0)|_{\mathrm{CFT}} = \alpha \frac{2\pi R \sin\theta_0}{\epsilon} - F \ , \tag{5.2}$$

with a non-universal coefficient α. The first term, fixed by requiring the area law, is proportional to the circumference $R\sin\theta_0$ of the entangling surface.

A straightforward generalization of (2.90) is to define the REE on the cylinder as

$$\mathcal{F}_{\mathrm{LM}}(R, \theta_0) = (R\partial_R - 1) S_A(R)|_{\theta_0} \ , \tag{5.3}$$

where the derivative with respect to R is taken at fixed angle θ_0. It is finite and becomes $\mathcal{F}_{\mathrm{LM}} = F$ at any RG fixed point thanks to the relation (5.2). We will see in section 3.2 that for a massive scalar field of mass m, the REE $\mathcal{F}_{\mathrm{LM}}(mR)$ is monotonically decreasing in the small and large mR regions as mR increases at fixed θ_0. At $mR = 0$ it takes the value F_{scalar} for a scalar field in three dimensions and decreases to 0 as $mR \to \infty$, while it is not stationary[1] as a function of $(mR)^2$ at the UV fixed point as will be shown in the next section. However, numerical calculations show that it does not decrease monotonically in the intermediate regime $1 \ll mR \ll \infty$ of the RG flow at least for the massive scalar field theory.

The second way to renormalize the UV divergence of the entropy is to define the REE on the cylinder as

$$\mathcal{F}_{\mathrm{C}}(R, \theta_0) \equiv (\tan\theta_0 \, \partial_{\theta_0} - 1) \, S_A(\theta_0)|_R \ , \tag{5.4}$$

where the derivative with respect to θ_0 is taken at fixed R. As the definition implies, $\mathcal{F}_{\mathrm{C}}$ is always finite for the differential operator kills the area law divergence. Also it coincides with the finite part of the $\mathbb{S}^3$ free energy F at a conformal fixed point. We will see in the next section for a free massive scalar field of mass m that $\mathcal{F}_{\mathrm{C}}$ decreases monotonically as a function of $(mR)^2$ at fixed θ_0 and it is also stationary as a function of $(mR)^2$ at the UV fixed point. Then the REE $\mathcal{F}_{\mathrm{C}}$, obtained from EE on the cylinder, serves as an F-function in three dimensions. It decreases monotonically from the UV to the IR and is stationary

[1]The REE for a relevant perturbation of CFT is called stationary if the first derivative with respect to the coupling constant vanishes at a conformal fixed point. The REE of a disk (2.90) is known to be non-stationary [121, 122] for a massive free scalar theory.

at the UV fixed point for a massive scalar field. This is analogous to the Zamolodchikov's c-function in two dimensions, at least for a massive scalar field.

Before closing this section, we comment on the flat space limit of the cylinder EE. The cylinder metric (5.6) reduces to the flat space in the $R \to \infty$ and $\theta \to 0$ limits with $r \equiv R\,\theta$ held fixed, and the cap-like entangling region A turns into the disk of radius $R_{\rm disk} \equiv R\,\theta_0$. It follows from their definitions that the two REEs (5.3) and (5.4) lead to the REE of a disk (2.90) in this limit.

5.2 Free massive scalar field

We will calculate the EE of the cap-like region A on the cylinder for a free massive scalar field. We assume that the scalar field is conformally coupled to the background geometry in the massless limit, whose action takes the form of

$$I = \frac{1}{2}\int d^3x\,\sqrt{g}\,\left[g^{\mu\nu}\partial_\mu\phi\partial_\nu\phi + \frac{\mathcal{R}}{8}\phi^2 + m^2\phi^2\right]\,, \tag{5.5}$$

where $\mathcal{R}$ is the Ricci scalar. Applying a conformal transformation mapping the replica space to a non-singular space and regarding the theory as a relevant perturbation of a free massless scalar theory by the mass term, the entropy will be expanded in the small mass limit and the leading term of order m^2 will be evaluated. On the other hand, the large mass expansion will be carried out following [85] and the order $1/m$ term of the entropy will be fixed for a general entangling surface. Finally the results in the two limits will be confirmed by the numerical calculation that shows the REE, $\mathcal{F}_{\rm C}(\theta_0, mR)$, monotonically decreases as mR becomes large, while the other REE, $\mathcal{F}_{\rm LM}$, does not.

5.2.1 Conformal transformation to a non-singular space

Employing the replica trick, one can obtain the EE by calculating the partition function on the n-fold cover of the Euclidean space of

$$ds^2 = dt_E^2 + R^2\left(d\theta^2 + \sin^2\theta\,d\Omega_{d-2}^2\right)\,, \tag{5.6}$$

that has a surplus angle $2\pi(n-1)$ around Σ. To make it transparent, we use the coordinate transformation

$$\begin{aligned}\tanh(t_E/R) &= \frac{\sin\theta_0\,\sin\tau}{\cosh u + \cos\theta_0\,\cos\tau}\,,\\ \tan\theta &= \frac{\sin\theta_0\,\sinh u}{\cos\theta_0\,\cosh u + \cos\tau}\,,\end{aligned} \tag{5.7}$$

with $0 \le u < \infty$ and $0 \le \tau \le 2\pi$ for $n = 1$. The resulting metric becomes [58]

$$\begin{aligned}e^{2\sigma}ds^2 &= R^2\left[d\tau^2 + du^2 + \sinh^2 u\,d\Omega_{d-2}^2\right]\,,\\ e^{-2\sigma} &\equiv \frac{\sin^2\theta_0}{(\cos\tau + \cos\theta_0\,\cosh u)^2 + \sin^2\theta_0\sinh^2 u}\,.\end{aligned} \tag{5.8}$$

The n-fold cover M_n is given by the metric (5.8) with the period $\tau \sim \tau + 2\pi n$, which is conformally equivalent to $\mathbb{S}^1 \times \mathbb{H}^{d-1}$. We will denote the conformally equivalent manifold as $\mathbb{S}^1_n \times \mathbb{H}^{d-1}$. The entangling surface Σ located at $t_E = 0$ and $\theta = \theta_0$ in the original coordinates (5.6) is mapped to $u = \infty$ in the new coordinates (5.8) where the conformal factor $e^{2\sigma}$ blows up. Note that the $\mathbb{S}^1$ factor along τ is non-contractible in the resulting geometry. This $\mathbb{S}^1$ is the image of the contractible circle in the plane transverse to the entangling surface at $t_E = 0$ and $\theta = \theta_0$, which is used to perform the replica trick.

For conformal field theories, the free energies $F_n \equiv -\log Z[M_n]$ on the replica space and the conformally transformed space are the same, modulo the conformal anomaly that exists when the space-time dimension is even. The conformal anomaly part can be computed by standard methods. For general non-conformal field theories, however, the free energies on the two spaces are not equal, but they can be related if we introduce a background dilaton field, which we denote by $\tau(x)$. Let us denote the metric of the replica space by $g_{\mu\nu}(x)$. If $Z[g_{\mu\nu}(x), \tau(x)]$ is the partition function of the Euclidean theory in the presence of the background metric $g_{\mu\nu}(x)$ and dilaton field $\tau(x)$, then it satisfies the following transformation rule [123, 124, 125, 126]

$$Z[e^{2\sigma(x)} g_{\mu\nu}(x), \tau(x) + \sigma(x)] = C\, Z[g_{\mu\nu}(x), \tau(x)] \ , \tag{5.9}$$

where C is completely determined by the conformal anomaly of the ultraviolet (UV) CFT and does not depend on the mass parameters of the theory. In particular $C = 1$ in odd dimensions due to the absence of conformal anomaly. Then the free energy defined as $F = -\ln Z$ satisfies the relation:

$$F[e^{2\sigma(x)} g_{\mu\nu}, \tau(x) + \sigma(x)] = F[g_{\mu\nu}, \tau(x)] \ , \tag{5.10}$$

where we have neglected $\ln C$, because we are only interested in the part of the EE generated by the massive deformation. In odd dimensions this factor is identically zero and this equality is exact. In even dimensions this anomaly part gives rise to local terms in the dilaton effective action some of which are uniquely determined by the trace anomaly matching. These local terms in the dilaton effective action give the logarithmically divergent universal terms in the entanglement entropy which were computed by using this technique in [127, 128].

Now the equality (5.10) holds for any functional form of the dilaton field $\tau(x)$ and we can also write

$$F[e^{2\sigma(x)} g_{\mu\nu}, \sigma(x)] = F[g_{\mu\nu}, \tau(x) = 0] \ . \tag{5.11}$$

The right hand side represents the free energy on the replica space in the absence of the dilaton field, which is precisely what we want to compute, and the left hand side represents the free energy on the conformally related non-singular space but in the presence of a background dilaton field which is equal to the conformal factor $\sigma(x)$. We will use this relation to compute the EE by conformally mapping the problem to a non-singular space.

5.2.2 Small mass expansion of cap entropies

The EE is expected to have a series expansion with respect to the scalar mass in the small mass region. In order to fix the leading term of the expansion we are to calculate the

derivative of the free energy F_n on the n-fold cover $\mathcal{M}_n$ of $\mathbb{R}\times\mathbb{S}^2$

$$\frac{\partial}{\partial m^2}F_n=\frac{1}{2}\int_{\mathcal{M}_n}d^3x\,\sqrt{g}\,G_n(x,x)\ , \tag{5.12}$$

where $G_n(x,x)$ is the coincident point Green's function on $\mathcal{M}_n$.

Using the conformal transformation (5.8) and the relation between the free energies (5.11), it is equivalent to that on $\mathbb{S}^1_n\times\mathbb{H}^2$,

$$\frac{\partial}{\partial m^2}F_n=\frac{1}{2}\int_{\mathbb{S}^1_n\times\mathbb{H}^2}d^3\tilde{x}\sqrt{\tilde{g}}\ e^{-2\sigma(\tilde{x})}\tilde{G}_n(\tilde{x},\tilde{x})\ , \tag{5.13}$$

with the dilaton field

$$e^{-2\sigma(\tilde{x})}=\frac{\sin^2\theta_0}{(\cos\tau+\cos\theta_0\,\cosh u)^2+\sin^2\theta_0\sinh^2 u}\ . \tag{5.14}$$

There appears the coincident point Green's function $\tilde{G}_n(\tilde{x},\tilde{x})$ in (5.13) which is independent of the position $\tilde{x}$ due to the homogeneity of $\mathbb{S}^1_n\times\mathbb{H}^2$. This comes out of the integral and we are left with the integral of the conformal factor. There is a UV divergence in the coincident point Green's function which is canceled in the combination $F_n-n\,F_1$:

$$\frac{\partial}{\partial m^2}\left(F_n-n\,F_1\right)=\frac{V_n}{2}\left[\tilde{G}_n(\tilde{x},\tilde{x})|_{m^2=0}-n\,\tilde{G}_1(\tilde{x},\tilde{x})|_{m^2=0}\right]+O(m^2)\ , \tag{5.15}$$

where V_n is the integral of the conformal factor on $\mathbb{S}^1_n\times\mathbb{H}^2$,[2]

$$V_n=\int_{\mathbb{S}^1_n\times\mathbb{H}^2}d^3\tilde{x}\sqrt{\tilde{g}}\,e^{-2\sigma(\tilde{x})}=2n\,\pi^3\sin\theta_0\,R^3\ . \tag{5.16}$$

There remains the coincident point Green's function which can be obtained by constructing the eigenfunctions of the scalar field on $\mathbb{S}^1_n\times\mathbb{H}^2$ (see e.g. [129]). Inspecting the results in [129, 121] we find

$$\lim_{n\to1}\partial_n\left[\tilde{G}_n(\tilde{x},\tilde{x})|_{m^2=0}-n\,\tilde{G}_1(\tilde{x},\tilde{x})|_{m^2=0}\right]=-\frac{1}{32R}\ . \tag{5.17}$$

Finally, the replica trick yields the leading behavior of the EE of the cap-like region in the small mass limit:

$$S_A(\theta_0,mR)=\alpha\,\frac{2\pi R\sin\theta_0}{\epsilon}-F_{\rm scalar}-\frac{\pi^3}{32}\sin\theta_0\,(mR)^2+O\left((mR)^4\right)\ , \tag{5.18}$$

with $F_{\rm scalar}=-(\ln 2)/8+3\zeta(3)/(16\pi^2)\approx 0.0638$ [54].

It is easy to see from the above expression that the REE $\mathcal{F}_{\rm LM}(R,\theta_0)$, as defined in (5.3), is not stationary at the UV-fixed point $mR=0$ for any value of θ_0.

[2]The detail of the integral (5.16) can be found in appendix C.1.

5.2.3 Large mass expansion of cap entropies

Although the analytic calculation of entanglement entropy is intractable even for free field theories if not conformal, one can expect to find a systematic expansion (2.85) of the entropy for theories with a large mass gap m in powers of $1/m$. For a free field theory, one can systematically determine c^{Σ}_{2n+1} by the coefficient of the logarithmically divergent term of the entanglement entropy in the $(2n+4)$-dimensional massless free field theory compactified on $\mathbb{T}^{2n+1}$ [59, 85]. The compactification yields an infinite tower of massive fields in $(2+1)$ dimensions, and the entanglement entropy across the entangling surface $\Sigma_{2n+2} = \Sigma \times \mathbb{T}^{2n+1}$ should equal to the sum of the entropies for the massive fields across Σ. One finds that the sum of the entropy of the order $1/m^{2n+1}$ terms over the Kaluza-Klein modes gives rise to a logarithmic UV divergence, which should be equated with the logarithmic UV divergent term $S^{(2n+4)}_{\Sigma_{2n+2}}\big|_{\log} = s^{(2n+4)}_{\Sigma_{2n+2}} \log\epsilon$ in the higher-dimensional theory. Inspections of these coefficients lead to the following relation [85]

$$c^{\Sigma}_{2n+1} = -\frac{\pi(2\pi)^n(2n-1)!!}{\mathrm{Vol}(\mathbb{T}^{2n+1})} s^{(2n+4)}_{\Sigma_{2n+2}} \,, \tag{5.19}$$

which can be used to determine the coefficients c^{Σ}_{2n+1} from the logarithmic UV divergent term in $(2n+4)$ dimensions.

To work it out explicitly for c^{Σ}_1 (i.e., $n=0$), we start with a four-dimensional theory with an action

$$I^{(3+1)} = \frac{1}{2}\int_{\mathcal{M}\times\mathbb{S}^1} d^4x\sqrt{g}\left[(\partial\phi)^2 + \xi_3 \mathcal{R}^{(3+1)}\phi^2\right] \tag{5.20}$$

wrapped on $\mathbb{S}^1$, where $\mathcal{M} = \mathbb{R}\times\mathbb{S}^2$ is the original three-dimensional cylindrical spacetime, and consider an entangling surface $\Sigma_2 = \Sigma\times\mathbb{S}^1$ wrapped on the $\mathbb{S}^1$. Note that this action is not conformally invariant, since the coupling $\xi_3 = 1/8$ to the curvature $\mathcal{R}^{(3+1)}$ is the conformal coupling in three dimensions and is different from the one $\xi_4 = 1/6$ in four dimensions [130]. The curvature is a constant $\mathcal{R}^{(3+1)} = \mathcal{R}^{(2+1)} = \mathcal{R}(\mathbb{S}^2) = 2/R^2$ in our setup, and so we can formally regard this theory as a conformally coupled massive scalar field theory with a mass $\mu^2 = (\xi_3 - \xi_4)\mathcal{R}^{(3+1)} = -1/(12R^2)$.

The entanglement entropy has a logarithmic divergence $S^{(4)}_{\Sigma_2}\big|_{\log} = s^{(3+1)}_{\Sigma_2}\log\epsilon$ whose coefficient is composed of two terms,

$$s^{(3+1)}_{\Sigma_2} = s^{\text{Solodukhin}}_{\Sigma_2} + \delta s_{\Sigma_2} \,. \tag{5.21}$$

The first term is the conformal anomaly term known as Solodukhin's formula (2.54):

$$s^{(3+1)}_{\Sigma_2} = \frac{a}{2}\chi[\Sigma_2] + \frac{c}{2\pi}\int_{\Sigma_2}\left(\mathcal{R}_{aa} - \mathcal{R}_{abab} - \frac{\mathcal{R}}{3} + k^a_{\mu\nu}k^{\mu\nu}_a - \frac{1}{2}(k^{a\,\mu}_{\mu})^2\right) \,, \tag{5.22}$$

In the present case where Σ is topologically a circle, the entangling surface Σ_2 is topologically a torus with $\chi[\Sigma_2] = 0$, and only the second term remains. For a circular Σ parametrized by $\theta = \Theta(\phi)$, the timelike and spacelike unit normal vectors to Σ_2 are

$$n^1_\mu = (1,0,0,0) \,, \qquad n^2_\mu = \frac{R\sin\theta}{\sqrt{\sin^2\theta + (\Theta'(\phi))^2}}(0,1,-\Theta'(\phi),0) \,, \tag{5.23}$$

where the fourth components are in the $\mathbb{S}^1$ direction on which Σ_2 is wrapped. The extrinsic curvature for the timelike normal vector n^1 vanishes due to the time translation invariance. A short calculation shows that $\mathcal{R} = 2/R^2$, $\mathcal{R}_{aa} = 1/R^2$, $\mathcal{R}_{abab} = 0$, and

$$\kappa^2 \equiv k^2_{\mu\nu} k_2^{\mu\nu} - \frac{1}{2}(k^{2\,\mu}_{\mu})^2 = \frac{\left(2\cos\Theta\,\Theta'^2 + \sin\Theta(\sin\Theta\cos\Theta - \Theta'')\right)^2}{2R^2\left(\sin^2\Theta + \Theta'^2\right)^3} \,. \tag{5.24}$$

The second term

$$\delta s_{\Sigma_2} = \frac{(\xi_3 - \xi_4)\mathcal{A}_{\Sigma_2}\mathcal{R}^{(3+1)}}{24\pi} = -\frac{\mathcal{A}_{\Sigma_2}}{288\pi R^2} \,, \tag{5.25}$$

comes from the difference of the conformal coupling ξ between three and four dimensions, where $\mathcal{A}_{\Sigma_2} = \int_{\Sigma_2} 1 = \mathrm{Vol}(\mathbb{S}^1)\int_\Sigma 1$ is the area of the entangling surface $\Sigma_2 = \Sigma \times \mathbb{S}^1$. The origin of this term is explained in two ways in [130], where its relations to other studies are also discussed. One way to explain this term is the result of the mass μ^2 perturbation from the CFT's result $s(\mu^2 = 0) = s|_{\mathrm{CFT}} = s^{\mathrm{Solodukhin}}$,

$$s(\mu^2) = s(\mu^2 = 0) + \delta s + O(\mu^4), \tag{5.26}$$

where the first order term denoted as δs are calculable by replica trick as

$$\delta s = \frac{\mathcal{A}_{\Sigma_2}}{24\pi}\mu^2 \,. \tag{5.27}$$

Combining with (5.19), (5.21) and (2.54), we find

$$c_1^\Sigma = \int_\Sigma \left[-\frac{c}{2}\left(\frac{1}{3R^2} + \kappa^2\right) + \frac{1}{288R^2}\right] \,. \tag{5.28}$$

A few comments are in order:

- Our result (5.28) for the coefficient c_1^Σ reproduces that of [85] in the $R \to \infty$ and $\Theta \to 0$ limit with $R\sin\Theta$ kept fixed, under which the entangling surface becomes a curve on $\mathbb{R}^2$.
- We assumed that Σ is a single curve on a sphere so far, but this result (5.28) holds for any entangling surface which is a disjoint union of curves because the uplifted entangling surface Σ_2 in $(3+1)$ dimensions is a disjoint union of tori whose Euler characteristics vanish and the integral (5.28) over Σ is just the sum of the integrals over all disjoint curves.

In particular, a cap-like entangling region with opening angle θ_0 is defined by $\Theta(\phi) = \theta_0$, and the coefficient (5.28) takes the simple form:

$$c_1^{\mathrm{cap}} = -\frac{c\,\pi}{R}\sin\theta_0\left[\frac{1}{3} + \frac{\cot^2\theta_0}{2}\right] + \frac{\pi\sin\theta_0}{144R} \,. \tag{5.29}$$

Combined with the expansion (2.85) we find

$$S_A(\theta_0, mR) = \alpha\,\frac{2\pi R\sin\theta_0}{\epsilon} - \frac{\pi}{6}mR\sin\theta_0 + \frac{\pi}{120\,mR\sin\theta_0}\left(-\frac{1}{2} + \sin^2\theta_0\right) + O\left((mR)^{-3}\right) \,, \tag{5.30}$$

in the large mR limit.

5.2.4 The two REE's and numerical results

We numerically calculated the EE of the cap-like region A on the cylinder $\mathbb{R} \times \mathbb{S}^2$ by putting a free massive scalar field on the lattice. We closely follow the method of [51, 59] whose details are found in appendix A.2.

Firstly, we check if the expansion (5.18) derived by using the conformal decompactification is valid in the small mass limit. We calculate the derivative of $S_A(mR, \theta_0 = \pi/2)$ with respect to $(mR)^2$ to avoid the UV divergence which contaminates our numerical precision. Fig. 5.1 shows that the entropy has a linear slope

$$\frac{\partial}{\partial (mR)^2} S_A(mR, \theta_0 = \pi/2) = -0.968 + O\left((mR)^2\right) \ , \tag{5.31}$$

in the small mass region $mR \ll 1$. Integrating it by $(mR)^2$ leads that the entropy takes the form of

$$S_A(mR, \theta_0 = \pi/2) = S_A(0, \theta_0 = \pi/2) - 0.968\,(mR)^2 + O\left((mR)^4\right) \ . \tag{5.32}$$

Reassuringly, this is consistent with the analytic expression (5.18) for $\theta_0 = \pi/2$ with $-\pi^3/32 \approx -0.969$.

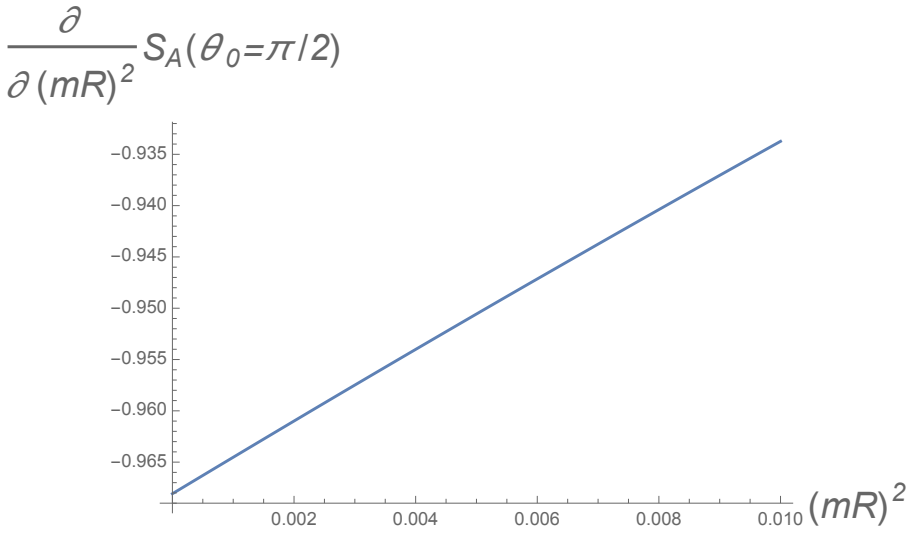

Figure 5.1: The $(mR)^2$ derivative of the bare entanglement entropy $S_A(\theta_0 = \pi/2)$ of the hemisphere A, in the small mass region $mR \ll 1$. In taking the $(mR)^2$ derivative, we calculate bare entropies $S_A(\theta_0 = \pi/2)$ increasing $(mR)^2$, and fit it as a function of $(mR)^2$. The lattice size is taken as $N = 1001$.

REE $\mathcal{F}_C$

Next we examine the REE $\mathcal{F}_C(mR, \theta_0)$ defined by (5.4) to inspect the dependences of the entropy on mR and θ_0 in the broader ranges. A detailed plot in the small mass region

is shown in Fig. 5.2 (a). The REE starts decreasing from $0.0638 \approx F_{\text{scalar}}$ at the UV fixed point $mR = 0$ for any θ_0. Furthermore, it is stationary in the sense that the first derivative with respect to $(mR)^2$ vanishes at the UV fixed point:

$$\mathcal{F}_{\text{C}}(mR, \theta_0) = F_{\text{scalar}} + O\left((mR)^4\right) \ , \tag{5.33}$$

as predicted by the small mass expansion (5.18). This is in contrast to the REE $\mathcal{F}$ of a disk [65] which is not stationary at the UV fixed point of a free massive scalar theory [121, 122] though our $\mathcal{F}_C$ is supposed to reduce to $\mathcal{F}$ in the flat space limit. This difference may stem from the existence of the IR divergence on the flat space, which is regularized by the size of the sphere in the present setup.

In the other extreme limit of the large mR region, we find $\mathcal{F}_{\text{C}}$ decays to zero monotonically as shown in Fig. 5.2 (b). Comparing with the expansion (5.30) which yields the large mass behavior of the REE

$$\mathcal{F}_{\text{C}}(mR, \theta_0) = \frac{\pi}{120\, mR \sin\theta_0} + O\left((mR)^{-3}\right) \ , \tag{5.34}$$

our numerical data are well-fitted by the curves given by (5.34) as mR becomes large.

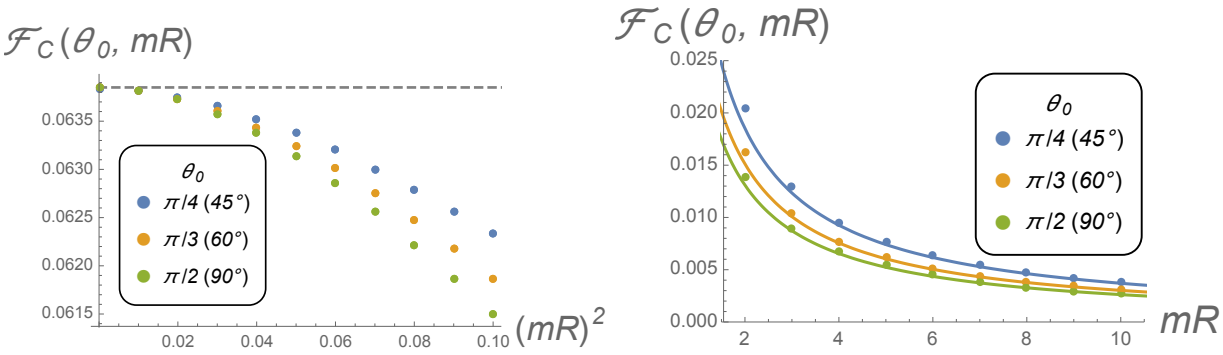

(a) (b)

Figure 5.2: The mR dependence of the REE $\mathcal{F}_{\text{C}}(mR, \theta_0)$ in the small mass region $mR \ll 1$ (a) and the large mass region $mR \gg 1$ (b), with different cap angles $\theta_0 = \pi/4$ (blue dots), $\pi/3$ (yellow dots) and $\pi/2$ (green dots). The lattice size is taken as $N = 501$. (a) The $\mathcal{F}_{\text{C}}$ starts from a value $\mathcal{F}_{\text{C}}(mR = 0) \simeq 0.06385$ (gray dotted line) at $mR = 0$ with vanishing slope with respect to $(mR)^2$. This result reproduces the expected small mass expansion (5.33) $\mathcal{F}_{\text{C}} = F_{\text{scalar}} + O\left((mR)^4\right)$ in the small mass region $mR \ll 1$, which means that $\mathcal{F}_{\text{C}}$ starts from the UV CFT value $F_{\text{scalar}} \simeq 0.06381$ at $mR = 0$ without any first order term of $(mR)^2$. (b) It asymptotes to the leading term $\pi/(120 mR \sin\theta_0)$ (solid lines) of the expected large mass expansion (5.34) $\mathcal{F}_{\text{C}} = \pi/(120 mR \sin\theta_0) + O\left(1/(mR)^3\right)$ in the large mass region $mR \gg 1$.

The whole shapes of the REEs are depicted in Fig. 5.3. Clearly, the REEs are finite and monotonically decreasing to zero as mR is increased for any θ_0. Also it is a monotonic function of θ_0 for fixed mR, implying that increasing θ_0 from 0 to $\pi/2$ can be regarded as

an RG flow. The behavior of $\mathcal{F}_{\rm C}(mR,\theta_0)$ is reminiscent of the REE of a disk on the flat space [65, 121, 122] and the proof of monotonicity might proceed along the same lines as the proof of the F-theorem in [55].

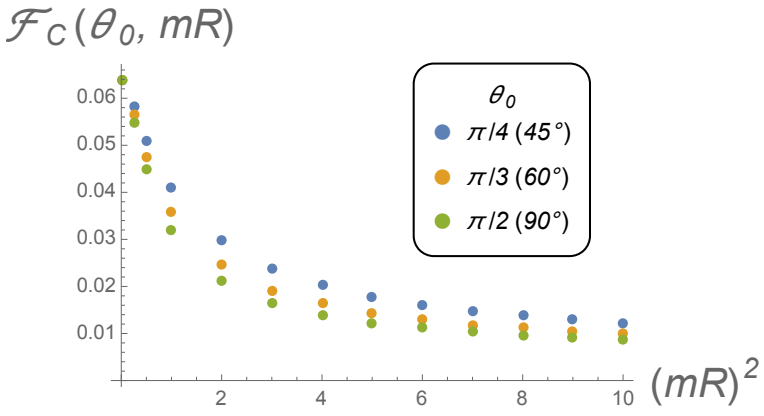

Figure 5.3: The mR dependence of the REE $\mathcal{F}_{\rm C}(mR,\theta_0)$ with different cap angles $\theta_0=\pi/4$ (blue dots), $\pi/3$ (yellow dots) and $\pi/2$ (green dots). It is monotonically decreasing for the all mR. In taking the θ_0 derivative, we calculate bare entropies $S_A(\theta_0)$ increasing θ_0, and fit it as a function of θ_0. The lattice size is taken as $N=501$.

REE $\mathcal{F}_{\rm LM}$

The small mass expansion (5.18) of the EE of a free massive scalar field of mass m leads to the small mass behavior of the Liu-Mezei type REE

$$\mathcal{F}_{\rm LM}(mR,\theta_0)=F_{\rm scalar}-\frac{\pi^3}{32}\sin\theta_0(mR)^2+O\left((mR)^4\right)\ , \tag{5.35}$$

which decreases linearly in $(mR)^2$ around the UV fixed point. It is *not* stationary in the Zamolodchikov's sense as the REE on the flat space is not [65, 121, 122] while (5.35) is not a sensible expansion on the flat space because the $O(m^2)$ term diverges in the limit $R\to\infty$ and $\theta_0\to 0$ with $R\,\theta_0$ fixed. It clearly shows that the breakdown of the perturbation theory emanates from the IR divergence, the volume of the flat space [104, 122]. The REE on the cylinder, on the other hand, regularizes both the UV and IR divergences and is suited to the perturbative expansions.

In the numerical calculation of $\mathcal{F}_{\rm LM}$, one can no longer use the same algorithm as for $\mathcal{F}_{\rm C}$ due to two obstacles. One is that the definition (5.3) includes the derivative ∂_R that requires the variation of the sphere radius R as opposed to the previous case. The other is that the discretization of the angle θ by $\delta\theta=\pi/N$ causes the linear growth of the lattice spacing $\epsilon=R\delta\theta=\pi R/N$ in R, and one cannot remove by the differential operator $(R\partial_R-1)$ the ϵ dependence of the entanglement entropy because the area law term $\alpha(2\pi R\sin\theta_0)/\epsilon=\alpha(2N\sin\theta_0)$ becomes independent of R. To circumvent these obstacles, we employ a different regularization method; we calculate entropies by increasing both mR and $N=\pi R/\epsilon$ simultaneously, that is, fixing their ratio $mR/N=m\epsilon/\pi$,

and apply the differential operator $mR\,\partial_{(mR)} - 1 = N\partial_N - 1$ on the fitted results. This prescription removes the dominant order $O(N)$ area law term successfully. We checked that $\mathcal{F}_{\rm LM}(mR, \theta_0, N)$ becomes independent of N, namely, the REE $\mathcal{F}_{\rm LM}$ takes the same value for a different ratio $mR/N = m\epsilon/\pi$ as long as mR is the same. In this way, the ϵ dependence of the entropy is removed in the numerical calculation.

The resultant $\mathcal{F}_{\rm LM}$ correctly reproduces the expected small mass expansion (5.35) in the small mass region $mR \ll 1$, as shown in Fig. 5.4. The REE $\mathcal{F}_{\rm LM}$ starts from the value $\mathcal{F}_{\rm LM}|_{(mR)^2=0} = F_{\rm scalar} \simeq 0.0638$ of the UV CFT (a free massless scalar field) like the REE $\mathcal{F}_{\rm C}$, but in a non-stationary way $\partial_{(mR)^2}\mathcal{F}_{\rm LM}|_{(mR)^2=0} \neq 0$.

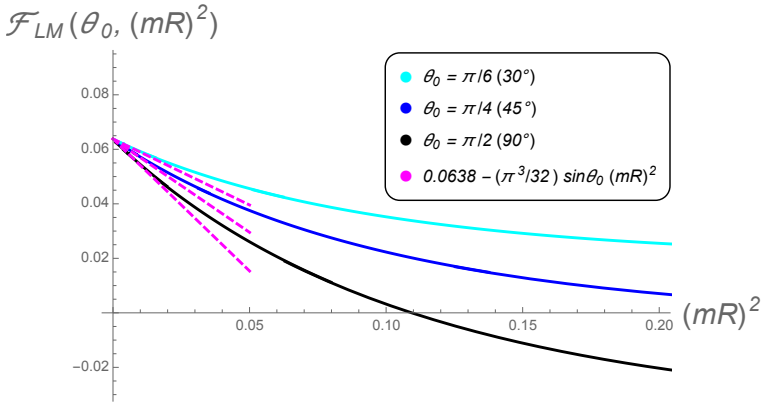

Figure 5.4: The $(mR)^2$ dependence of the REE $\mathcal{F}_{\rm LM}(mR, \theta_0)$ with different cap angles $\theta_0 = \pi/6$ (light blue curve), $\pi/4$ (blue curve) and $\pi/2$ (black curve). They correctly reproduce the small mass expansion (dotted magenta line) in the small mass region $mR \ll 1$. In taking the R derivative, we calculate bare entropies $S_A(mR, N)$ increasing both mR and N proportionally, and fit it as a function of R.

Similarly using (5.30), the leading term in the large mass expansion is given by

$$\mathcal{F}_{\rm LM}(mR, \theta_0) = \frac{\pi}{120\, mR \sin\theta_0}\left(1 - 2\sin^2\theta_0\right) + O\left((mR)^{-3}\right) \ , \tag{5.36}$$

that equals to (5.34) up to the θ_0 dependent constant. Thus for $\theta_0 > \pi/4$, it does not decrease monotonically as increasing mR for fixed θ_0. It monotonically decreases as increasing θ_0 for fixed mR, but becomes negative at $\theta_0 = \pi/4$. Both (5.34) and (5.36) precisely reduce to the flat space result in [121] as expected. This analytic result demonstrates that the Liu-Mezei type REE $\mathcal{F}_{\rm LM}$ is not a candidate of F-function.

This large mass expansion is also correctly reproduced by our numerical results. The whole mR dependence of $\mathcal{F}_{\rm LM}$ is drawn in Fig. 5.5. In the large mass region $mR \gg 1$, The plot shows $\mathcal{F}_{\rm LM}$ asymptotes to the trivial IR CFT value $\mathcal{F}_{\rm LM} = 0$, but it does not monotonically decrease with mR and is well-fitted by the curves given by (5.34) as mR becomes large.

To recapitulate, all of the numerical results correctly reproduce both the small and large mass expansions in the previous two subsections, and shows that the REE $\mathcal{F}_{\rm C}$ (5.4)

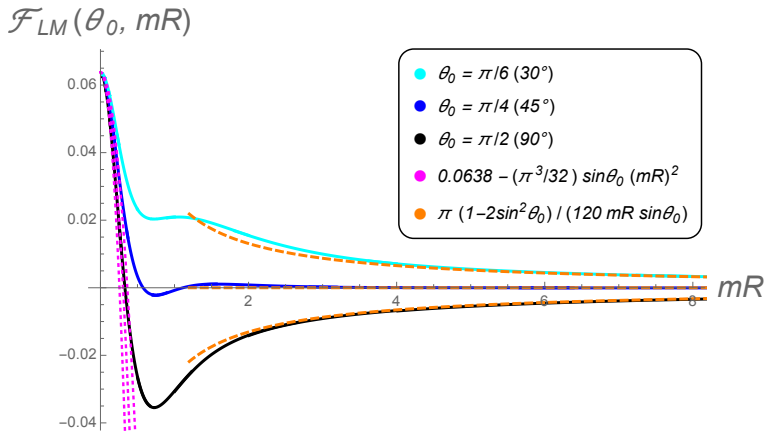

Figure 5.5: The mR dependence of the REE $\mathcal{F}_{\rm LM}(mR, \theta_0)$ with different cap angles $\theta_0 = \pi/6$ (light blue curve), $\pi/4$ (blue curve) and $\pi/2$ (black curve). They obey a large mass expansion $\mathcal{F}_{\rm LM}(mR, \theta_0) = \pi(1 - 2\sin^2\theta_0)/(120\, mR \sin\theta_0) + O((mR)^{-3})$ (orange dotted curve) of (5.36).

always decreases monotonically with both the scale mR and the cap size θ_0 increased. These numerical calculations give non-trivial checks for the calculation introducing dilaton field and the Solodukhin's formula (2.54) on a curved space because our numerical algorithm does not rely on any replica trick.

Chapter 6

Rényi Entropic Inequalities and Holography

Rényi entropy is more informative about quantum entanglement than entanglement entropy, and so the recent proposal [80][1] for its holographic formula is attracting much interest, since it may know more about how the spacetime structure is encoded as quantum information via holography. The formula is a generalization of the formula for entanglement entropy (1.2), and now the minimal surface γ_A has its own tension or mass and bends the spacetime geometry according to Einstein equation, while in the formula for entanglement entropy, the minimal surface γ_A is tensionless or massless and does not affect the background geometry. To give a consistency check of this holographic formula, we showed that the formula expectedly fulfills mathematical inequalities of Rényi entropies, under an assumption that bulk geometries are stable. By presenting a new way to interpret Rényi entropies and its inequalities in analogy to statistical mechanics, we found out a thermodynamic structure in the derivation of the formula as a byproduct.

This chapter is based on the author's work [4] with T. Nishioka.

6.1 Rényi entropic inequalities

Since many mathematical properties of entanglement entropy such as the strong-subadditivity has been holographically understood via its holographic formula, it is natural to think about how mathematical properties of the Rényi entropy are transcribed to the bulk side in a geometric language. Although it is known that the Rényi entropy is not strongly

[1] Earlier works on the holographic Rényi entropies include [131, 132, 133].

sub-additive, it satisfies inequalities involving the derivative with respect to n [134, 135][2]

$$\partial_n S_n \leq 0\,, \tag{6.1}$$

$$\partial_n \left(\frac{n-1}{n} S_n\right) \geq 0\,, \tag{6.2}$$

$$\partial_n \left((n-1)S_n\right) \geq 0\,, \tag{6.3}$$

$$\partial_n^2 \left((n-1)S_n\right) \leq 0\,. \tag{6.4}$$

These inequalities are originally proved for the classical Rényi entropy $S_n[p_i] \equiv -\frac{1}{n-1}\sum_i p_i^n$ of a probability distribution p_i, but are still true for the quantum Rényi entropy (1.4). The proof for a quantum case immediately follows by diagonalizing the density matrix ρ as $U\rho U^\dagger = \mathrm{diag}(p_1, p_2, \dots)$ with a unitary matrix U. The first inequality (6.1) implies the positivity of the Rényi entropy $S_n \geq 0$ as $S_\infty = \min_i(-\log p_i) \geq 0$.

The aim of this chapter is to prove these inequalities by the holographic formula of the Rényi entropy. Before proceeding to the proof, we rewrite the inequalities in more concise forms that manifest their meanings as the positivities of energy, entropy and heat capacity in analogy to statistical mechanics. It also clarifies that not all of (6.1)-(6.4) are independent, but the two inequalities (6.2) and (6.4) are essential. (6.2) turns out to be simple to prove as it stands for the positivity of the area of a codimension-two surface in the bulk, while the proof of (6.4) is more intricate. In view of statistical mechanics, (6.4) implies the positivity of the heat capacity and encodes the unitarity of quantum mechanical system. Our proof of (6.4) in the bulk is differential geometric in its nature and turns out to relate it to the stability of the spacetime on which the holographic formula is supposed to be applied. Therefore, our proof serves as a nontrivial consistency check for the holographic formula, and moreover reveals a direct connection between the unitarity and the stability in the boundary and bulk theories, respectively. In due course of the proof, we also obtain a holographic formula for calculating the quantum fluctuation of the modular Hamiltonian.

Our proof is heavily based on the stability of the bulk geometry. We admit that the bulk stability is a nontrivial assumption whose justification is even challenging. For instance, Euclidean gravity actions are known to be indefinite against metric perturbations [136, 137]. We are not aware of any compelling argument to support the assumption, but in view of holographic duality we believe that stable quantum states should have stable bulk duals. We will not touch on this subject anymore in this paper until section 6.5.

6.2 Analogy to statistical mechanics

As explained in chapter 2, the calculation of Rényi entropy of a ball in CFT_d can be recasted as a calculation of a thermal entropy, since the replica manifold M_n is conformally equivalent to a thermal hyperbolic space $\mathbb{S}^1 \times \mathbb{H}^{d-1}$ with an inverse temperature $\beta = 2\pi n$ [133, 58]. In that situation, the inequalities (6.2) and (6.4) reduce to the non-negativity

[2]The finite version of these inequalities, such as $S_n \geq S_m$ and $\frac{n-1}{n} S_n \geq \frac{m-1}{m} S_m$ for $n \leq m$, are true, even if the n derivatives are ill-defined because of some discontinuity.

of the thermal entropy and the heat capacity, and the others immediately follow from these two. A formal similarity between the Rényi entropy and a thermal entropy is also pointed out in [80].

In this section, inspired by these observations, we will formulate the complete analogy between the Rényi entropy and statistical mechanics valid for any quantum system. Moreover, the following discussions apply not only to reduced density matrices $\rho_A = \mathrm{Tr}_{\bar{A}}[\rho_{\mathrm{tot}}]$, but also to a general density matrix ρ.

6.2.1 Partition function Z and the escort density matrix ρ_n

In the calculation of the Rényi entropy $S_n = -\frac{1}{n-1}\log \mathrm{Tr}[\rho^n]$ (1.4), we can regard the trace $Z(n) \equiv \mathrm{Tr}[\rho^n]$ as a thermal partition function

$$Z(\beta) = \mathrm{Tr}[e^{-\beta H}]\,, \tag{6.5}$$

with[3] the inverse temperature β and the Hamiltonian H

$$\beta = n\,, \tag{6.8}$$
$$H = -\log \rho\,. \tag{6.9}$$

The latter is called the entanglement Hamiltonian or modular Hamiltonian. Its eigenvalues ϵ_i are called the entanglement spectrum, and are non-negative $\epsilon_i \geq 0$ as the eigenvalues $p_i = e^{-\epsilon_i}$ of ρ satisfies $0 \leq p_i \leq 1$. In calculating the partition function Z, we can regard the state as a density matrix given by the normalized n-th power of ρ

$$\rho_n \equiv \frac{\rho^n}{\mathrm{Tr}[\rho^n]}\,. \tag{6.10}$$

In the area of chaotic systems, the probability distribution of the classical version $P_i^{(n)} \equiv p_i^n / \sum_i p_i^n$ is called the escort distribution [135], and we will accordingly call ρ_n the escort density matrix.

Let us push forward this analogy to statistical mechanics. The free energy $F = F(n)$ and the total energy $E = E(n)$ related to the density matrix ρ are defined as

$$F \equiv -\frac{1}{n}\log \mathrm{Tr}[\rho^n]\,, \tag{6.11}$$
$$E \equiv -\frac{\partial}{\partial n}\log \mathrm{Tr}[\rho^n] = \langle H \rangle_n\,, \tag{6.12}$$

where $\langle\cdot\rangle_n$ stands for the expectation values with respect to the escort density matrix ρ_n,

$$\langle X \rangle_n \equiv \mathrm{Tr}[\rho_n X] = \frac{\mathrm{Tr}[\rho^n X]}{\mathrm{Tr}[\rho^n]}\,. \tag{6.13}$$

In what follows, we will make use of this notation when available.

[3] If you feel uneasy about the mismatch of their physical dimensions, you may define them instead as

$$\beta E_0 = n\,, \tag{6.6}$$
$$H/E_0 = -\log \rho\,, \tag{6.7}$$

with any constant E_0 of the dimension of energy. In the following discussions we take a unit $E_0 = 1$. Another choice $E_0 = 1/2\pi$ is also common in literatures.

6.2.2 Modular entropy $\tilde{S}_n$

What quantity should correspond to the thermal entropy in this analogy to statistical mechanics? The answer is not the Rényi entropy $S_n[\rho]$, but the modular entropy $\tilde{S}_n[\rho]$. In fact, the equation (2.122) or (2.123) leads to the formulae of the entropy together with (6.11) and (6.12),

$$\begin{aligned} \tilde{S} &= n(E-F)\,, \\ &= -\frac{\partial F}{\partial T}\,, \end{aligned} \tag{6.14}$$

where $T \equiv 1/n$ and we omit the subscript of $\tilde{S}_n$ to stress the correspondence to statistical mechanics. One can also show that the modular entropy is nothing but the von Neumann entropy of the escort density matrix ρ_n, that is,

$$\tilde{S}_n[\rho] = S_{\rm vN}[\rho^n/{\rm Tr}[\rho^n]]\,. \tag{6.15}$$

The modular entropy $\tilde{S}_n$ is another generalization of the von Neumann entropy $S_{\rm vN}$ as it also reduces to the entanglement entropy $\tilde{S}_1[\rho] = S_{\rm vN}[\rho]$ in the limit $n \to 1$.

An equivalent relation to (2.121)

$$(n-1)^2 \partial_n S_n = \tilde{S}_n - E\,, \tag{6.16}$$

yields a useful formula for calculating $\partial_n S_n$ in terms of F

$$\partial_n S_n = T^2 \frac{F(1) - F(T) - (1-T)\partial_T F}{(1-T)^2}\,, \tag{6.17}$$

where we used the relations $E = F + T\tilde{S}$, $\tilde{S} = -\partial_T F$ and $F(1) = 0$.

6.2.3 Capacity of entanglement $C(n)$

Now that we have defined thermodynamic state functions consisting of the first derivative of the free energy such as the total energy $E = \partial_n(nF)$ and the thermal entropy $\tilde{S} = -\partial_T F$, we proceed to implement the heat capacity $C = C(n)$ including the second derivative,

$$C \equiv \frac{\partial E}{\partial T} = T\frac{\partial \tilde{S}}{\partial T} = -T\frac{\partial^2 F}{\partial T^2}\,. \tag{6.18}$$

It was originally introduced to characterize topologically ordered states by [138] and named capacity of entanglement. The capacity of entanglement has not attracted much attention so far despite its importance and simplicity as we will see below.

One can show the non-negativity $C \geq 0$ as in the same way as statistical mechanics,

$$\begin{aligned} C(n) = n^2 \frac{\partial^2}{\partial n^2} \log Z(n) &= n^2(\langle H^2 \rangle_n - \langle H \rangle_n^2)\,, \\ &= n^2 \left\langle (H - \langle H \rangle_n)^2 \right\rangle_n\,. \end{aligned} \tag{6.19}$$

It follows that the capacity measures the quantum fluctuation of the modular Hamiltonian $H = -\log\rho$, and in particular $C(1) = \langle H^2 \rangle - \langle H \rangle^2$ gives the quantum fluctuation with respect to the original state ρ.

6.2.4 Rényi entropic inequalities from the viewpoint of the analogy

Having established the analogy to statistical mechanics, we rewrite the Rényi entropic inequalities in the thermodynamic representation. The second (6.2), third (6.3) and forth (6.4) inequalities turn out to be the non-negativity of the modular entropy $\tilde{S}$ (2.121), the total energy E (6.12) and the entanglement heat capacity C, respectively

$$\tilde{S} \geq 0\,, \tag{6.20}$$
$$E \geq 0\,, \tag{6.21}$$
$$C \geq 0\,. \tag{6.22}$$

The non-negativity of $\tilde{S}$ and $E = \langle H \rangle_n$ immediately follows from the relations $\tilde{S}_n[\rho] = \langle -\log \rho_n \rangle_n = S_{\rm vN}[\rho_n]$ and the definition $H = -\log \rho$ of the modular hamiltonian. The last inequality $C \geq 0$ has already been proved by (6.19). Note that the condition $C \geq 0$ is equivalent to

$$\partial_n \tilde{S}_n \leq 0\,, \tag{6.23}$$

because of $C = T\partial_T \tilde{S} = -n\partial_n \tilde{S}$.

The first inequality $\partial_n S_n \leq 0$ (6.1) can be derived from the forth inequality (6.4) as shown in [133]. Indeed, the forth inequality $C = -T\partial_T^2 F \geq 0$ is equivalent to the concavity of the free energy F, and (6.17) is clearly non-positive as $f(x) \leq f(a) + (x-a)f'(a)$ for any concave function $f(x)$. An alternative way to show this inequality uses the non-negativity of the relative entropy $S[\rho|\sigma] \equiv \mathrm{Tr}[\rho(\log\rho - \log\sigma)] \geq 0$ for (6.16)

$$\begin{aligned}(n-1)^2 \partial_n S_n &= \tilde{S}_n - E\,, \\ &= -\left\langle \log\rho_n - \log\rho \right\rangle_n\,, \\ &= -S[\rho_n|\rho] \leq 0\,.\end{aligned} \tag{6.24}$$

6.2.5 Holographic formula from the view point of the analogy

This analogy also gives us a thermodynamic interpretation for the derivation of the holographic formula explained in chapter 2. The free energy $F(T)$ is holographically given as the difference of the actions between n and $n = 1$

$$F = -\frac{1}{n}\log \mathrm{Tr}[\rho^n] = I - I|_{n=1}\,. \tag{6.25}$$

The second term $-I|_{n=1}$ ensures the normalization $F(1) = -\log \mathrm{Tr}[\rho] = 0$. The free energy results from the minimization with respect to the fields $\phi = \{G_{\mu\nu}(X), \psi(X), X^\mu(y)\}$

$$F(T) = \min_{\phi}\left(I[\phi]\right) - I|_{n=1}\,, \tag{6.26}$$

as the action I is on-shell. Here we introduce a temperature $T = 1/n$ and rewrite the action as

$$I = I_{\rm bulk}[\hat{B}_n] + (1-T)\,\frac{\mathcal{A}}{4G_N}\,. \tag{6.27}$$

This succinct form is convenient to derive the entropy $\tilde{S}_n$

$$\tilde{S}_n = -\frac{\partial F}{\partial T} = -\frac{\delta I[\phi]}{\delta \phi}\frac{\delta \phi}{\delta T} + \frac{\mathcal{A}}{4G_N} = \frac{\mathcal{A}}{4G_N}\,, \tag{6.28}$$

where we used the equation of motion, $\delta I/\delta\phi = 0$. Finally we derive the total energy E by the Legendre transformation

$$\begin{aligned} E &= F + T\tilde{S}_n\,, \\ &= I_{\text{bulk}}[\hat{B}_n] - I_{\text{bulk}}[B_1] + \frac{\mathcal{A}}{4G_N}\,. \end{aligned} \tag{6.29}$$

And so this derivation of the formula is exactly the same as the one in thermodynamics; $\delta E - T\delta S$ vanishes because of the minimization in the Legendre transformation $F(T) \equiv \min_S(E(S) - TS)$, yielding $\delta F = \delta(E - TS) = (\delta E - T\delta S) - S\delta T = -S\delta T$. In our derivation of the holographic formula, the minimization of the free energy leads to a first-law like relation $0 = \delta_\phi I = \delta_\phi E - T\delta_\phi \tilde{S}$. The only difference is the meaning of the variation; δ_ϕ is taken with respect to fields ϕ in our case.

6.3 Proof of the Rényi entropic inequalities

Having established the necessary tools in the preceding sections, we want to examine under what condition the holographic formula (2.124) satisfies the inequalities (6.1)-(6.4) of the Rényi entropy. Instead of dealing with the original ones, we prove the concise inequalities (6.20)-(6.22) whose physical meaning is more transparent. They imply the stability of the system in the thermodynamic language, which is translated to the stability of the gravity theory as we will see soon.

6.3.1 A holographic proof

Some of the Rényi entropic inequalities follow straightforwardly from the holographic formula $\tilde{S}_n = \mathcal{A}/4G_N$ (2.124). The second inequality $\tilde{S} \geq 0$ (6.20) is trivial as the area $\mathcal{A}$ is always non-negative. The non-negativity of the Rényi entropy $S_n = \frac{n}{n-1}F \geq 0$, which is equivalent to $F < 0$ for $n < 1$ and $F > 0$ for $n > 1$, also follows from $\partial_n F = \tilde{S}_n/n^2 \geq 0$ and $F(1) = 0$. The first inequality (6.1) descents from the forth inequality (6.22) as mentioned in section 6.2.

Let us move on to the proof of the forth inequality (6.22)

$$C = -n\frac{\partial \tilde{S}_n}{\partial n} = -\frac{n}{4G_N}\frac{\delta \mathcal{A}}{\delta n} \geq 0\,. \tag{6.30}$$

As the parameter n varies slightly by δn, the brane area $\mathcal{A}$ changes slightly by

$$\begin{aligned} \frac{\delta \mathcal{A}[G,X]}{\delta n} &= \int d^{d+1}X\,\frac{\delta \mathcal{A}}{\delta G_{\mu\nu}(X)}\frac{\delta G_{\mu\nu}(X)}{\delta n} + \int d^{d-1}y\,\frac{\delta \mathcal{A}}{\delta X^\mu(y)}\frac{\delta X^\mu(y)}{\delta n}\,, \\ &= \int d^{d+1}X\,\frac{\delta \mathcal{A}}{\delta G_{\mu\nu}(X)}\frac{\delta G_{\mu\nu}(X)}{\delta n}\,, \end{aligned} \tag{6.31}$$

where we used the minimality condition $\delta\mathcal{A}/\delta X^\mu = 0$ for the embedding in the second equality. Plugging this result into (6.30), we have

$$C = -\frac{n}{4G_N}\int d^{d+1}X\,\frac{\delta\mathcal{A}}{\delta G_{\mu\nu}(X)}\frac{\delta G_{\mu\nu}(X)}{\delta n}\,. \tag{6.32}$$

The derivatives $\delta\mathcal{A}/\delta G_{\mu\nu}$ and $\delta G_{\mu\nu}(X)/\delta n$ are not independent due to the equation of motion of the bulk metric $G_{\mu\nu}$. The variation with respect to n gives

$$\frac{\delta I_{\text{bulk}}}{\delta G_{\mu\nu}(X)}[G+\delta G,\psi+\delta\psi] + (T_n+\delta T_n)\frac{\delta\mathcal{A}}{\delta G_{\mu\nu}(X)}[G+\delta G, X+\delta X] = 0 \tag{6.33}$$

or

$$\frac{\delta I}{\delta G_{\mu\nu}(X)}[G+\delta G, X+\delta X,\psi+\delta\psi] + \frac{\delta n}{4G_N n^2}\frac{\delta\mathcal{A}}{\delta G_{\mu\nu}(X)}[G,\psi,X] = 0\,, \tag{6.34}$$

where we used $\delta T_n = \delta n/(4G_N n^2)$. In the leading order of δn, the difference from the original equation motion is

$$\int d^{d+1}X'\left[\frac{\delta^2 I}{\delta G_{\mu\nu}(X)\delta G_{\alpha\beta}(X')}\delta G_{\alpha\beta}(X') + \frac{\delta^2 I}{\delta G_{\mu\nu}(X)\delta\psi(X')}\delta\psi(X')\right] + \int d^{d-1}y\,\frac{\delta^2 I}{\delta G_{\mu\nu}(X)\delta X^\alpha(y)}\delta X^\alpha(y) + \frac{\delta n}{4G_N n^2}\frac{\delta\mathcal{A}}{\delta G_{\mu\nu}} = 0\,. \tag{6.35}$$

This gives the following relation

$$\frac{\delta\mathcal{A}}{\delta G_{\mu\nu}(X)} = -4G_N n^2\int d^{d+1}X'\frac{\delta^2 I}{\delta G_{\mu\nu}(X)\delta G_{\alpha\beta}(X')}\frac{\delta G_{\alpha\beta}(X')}{\delta n}\,, \tag{6.36}$$

where we used the equations of motion $\delta I/\delta\psi = 0$ and $\delta I/\delta X^\mu = 0$. Plugging this $\delta A/\delta G$ into (6.32), finally we obtain a symmetric formula for the capacity of entanglement [4]

$$C = n^3\int d^{d+1}X d^{d+1}X'\,\frac{\delta G_{\mu\nu}(X)}{\delta n}\frac{\delta^2 I}{\delta G_{\mu\nu}(X)\delta G_{\alpha\beta}(X')}\frac{\delta G_{\alpha\beta}(X')}{\delta n}\,. \tag{6.38}$$

To prove the non-negativity of C, it is sufficient to show that the Hessian matrix $\frac{\delta^2 I}{\delta G_{\mu\nu}(X)\delta G_{\alpha\beta}(X')}$ is non-negative definite on the on-shell bulk $G_{\mu\nu}$. This condition means that the bulk geometry is stable against any perturbation, which is the main assumption in this paper as mentioned in Introduction. We will have a few comments on this assumption in section 6.5.

[4] If we extend the domain of the integral from $\hat{B}_n$ to B_n and use the action $I_{\text{bulk}}[B_n] = nI$, then the coefficient n^3 can be absorbed as

$$C = \int_{B_n} d^{d+1}X d^{d+1}X'\,\frac{\delta G_{\mu\nu}(X)}{\delta n}\frac{\delta^2 I_{\text{bulk}}[B_n]}{\delta G_{\mu\nu}(X)\delta G_{\alpha\beta}(X')}\frac{\delta G_{\alpha\beta}(X')}{\delta n}\,. \tag{6.37}$$

This formula maybe applies to cases when the replica symmetry $\mathbb{Z}_n$ is spontaneously broken in the on-shell bulk B_n.

This proof also provides a holographic formula for calculating the capacity of entanglement C. Especially, the quantum fluctuation of the modular Hamiltonian with respect to the original state is given by

$$\begin{aligned} C(1) &= \langle H^2 \rangle - \langle H \rangle^2 \ , \\ &= \int d^{d+1}X d^{d+1}X' \ \frac{\delta G_{\mu\nu}(X)}{\delta n} \frac{\delta^2 I}{\delta G_{\mu\nu}(X) \delta G_{\alpha\beta}(X')} \frac{\delta G_{\alpha\beta}(X')}{\delta n} \bigg|_{n=1} \ . \end{aligned} \tag{6.39}$$

To prove the third inequality $E \geq 0$ (6.21), we employ the expression (6.29) and it is enough to show $I_{\rm bulk}[\hat{B}_n] \geq I_{\rm bulk}[B_1]$ as $\hat{B}_n$ and B_1 obey the same boundary condition $\partial \hat{B}_n = \partial B_1 = M_1$. It is so since the functional $I_{\rm bulk}$ is supposed to have a minimum on the on-shell solution B_1, not the off-shell bulk $\hat{B}_n$, under the assumption that the bulk is stable so that the Euclidean gravity action $I_{\rm bulk}$ is non-negative definite. Instead, we can derive the third inequality $E \geq 0$ also from the second one $\tilde{S}_n \geq 0$ and the fourth one $C \geq 0$, in the same way as [133]. When $n \geq 1$, the free energy F is non-negative because $\partial_n F = \tilde{S}_n / n^2 \geq 0$ and $F(1) = 0$, and so the energy $E = F + T\tilde{S}$ is also non-negative. The non-negativity of the capacity $dE/dT = C \geq 0$ means that the energy E does not decrease with $T = 1/n$ and is still non-negative even when $n \leq 1$.

6.3.2 Legendre transformed expression for capacity of entanglement

We derive another expression of the entanglement heat capacity (6.38) using the graviton propagator, following [139] which calculates holographic entanglement entropies with probe branes inserted in the bulk.

We rewrite $\delta G_{\mu\nu}/\delta n$ appearing in (6.32), instead of $\delta \mathcal{A}/\delta G_{\mu\nu}$. By increasing the parameter n slightly by δn, the energy-momentum tensor of the brane

$$\bar{T}_{\mu\nu} \equiv \frac{\delta I}{\delta G^{\mu\nu}} = \frac{\sqrt{G}}{2} T_{\mu\nu} = T_n \frac{\delta \mathcal{A}}{\delta G^{\mu\nu}} \, , \tag{6.40}$$

changes slightly as

$$\delta \bar{T}_{\mu\nu} = \frac{1}{4G_N} \frac{\delta n}{n^2} \frac{\delta \mathcal{A}}{\delta G^{\mu\nu}} \, . \tag{6.41}$$

Correspondingly the bulk metric $G_{\mu\nu}$ shifts by

$$\begin{aligned} \delta G_{\mu\nu}(X) &= 8\pi G_N \int d^{d+1}X' \ G_{\mu\nu\alpha\beta}(X, X') \ 2\delta \bar{T}^{\alpha\beta}(X') \, , \\ &= -4\pi \frac{\delta n}{n^2} \int d^{d+1}X' \ G_{\mu\nu\alpha\beta}(X, X') \frac{\delta \mathcal{A}}{\delta G_{\alpha\beta}(X')} \, . \end{aligned} \tag{6.42}$$

Here $G_{\mu\nu\alpha\beta}$ is the Green's function of the linearized Einstein equation on the fixed background $G_{\mu\nu}$. Plugging it into (6.32), we obtain another expression of the entanglement

heat capacity

$$
\begin{aligned}
C &= \frac{\pi}{nG_N}\int d^{d+1}X d^{d+1}X' \,\frac{\delta\mathcal{A}}{\delta G_{\mu\nu}(X)} G_{\mu\nu\alpha\beta}(X,X') \frac{\delta A}{\delta G_{\alpha\beta}(X')}\,, \\
&= \frac{1}{16nG_N^2}\int d^{d+1}X d^{d+1}X' \,\frac{\delta\mathcal{A}}{\delta G_{\mu\nu}(X)} \frac{\delta^2 \log Z[\bar{T}]}{\delta\bar{T}_{\mu\nu}(X)\bar{T}_{\alpha\beta}(X')}\bigg|_{\bar{T}=0} \frac{\delta A}{\delta G_{\alpha\beta}(X')}\,,
\end{aligned}
\tag{6.43}
$$

where $Z[\bar{T}]$ is the partition function with a source $\bar{T}_{\mu\nu}$ inserted.[5] In this form, the non-negativity of C is equivalent to the concavity of $-\log Z[\bar{T}']$, which holds for $-\log Z[\bar{T}]$ is a Legendre transformation of the bulk action $-\log Z[G_{\mu\nu}(X)] \simeq I[G_{\mu\nu}(X)]$ as

$$
-\log Z[\bar{T}] = \min_{G_{\mu\nu}}\left(I[G_{\mu\nu}] - \int d^{d+1}X\, G_{\mu\nu}(X)\bar{T}^{\mu\nu}(X)\right)\,, \tag{6.46}
$$

and in general the Legendre transformation $\mathcal{F}(J) \equiv \min_M[F(M) - JM]$ interchanges the convexity and the concavity, $\mathcal{F}'' = -1/F''$.

The explicit expression

$$
\frac{\delta\mathcal{A}}{\delta G^{\mu\nu}(X)} = -\frac{1}{2}\int d^{d-1}y\sqrt{g}\, g^{ij}\frac{\partial X^\mu}{\partial y^i}\frac{\partial X^\nu}{\partial y^j}\delta^{d+1}(X - X(y))\,, \tag{6.47}
$$

allows us to rewrite the formula with integrals on the brane

$$
C = \frac{\pi}{4G_N n}\int d^{d-1}y\, d^{d-1}y'\,\sqrt{g(y)}\sqrt{g(y')}\frac{\partial X^\mu}{\partial y^i}\frac{\partial X^\nu}{\partial y_i} G_{\mu\nu\alpha\beta}(X(y),X(y'))\frac{\partial X^\alpha}{\partial y'^j}\frac{\partial X^\beta}{\partial y'_j}\,. \tag{6.48}
$$

This representation is a consequence of the Legendre transformation between the response $G_{\mu\nu}$ and the source $\bar{T}^{\mu\nu}$. In fact, for a free energy $F(M_i)$ with general responses M_i such as magnetization or chemical potential, the dual free energy $\mathcal{F}(J^i)$

$$
\mathcal{F}(J^i) = \min_{M_i}[F(M_i) - J^i M_i]\,, \tag{6.49}
$$

with J^i the dual sources such as magnetic field or charge, satisfies

$$
\delta M_i \frac{\partial^2 F}{\partial M_i \partial M_j}\delta M_j = \delta J^i \delta M_i = -\delta J^i \frac{\partial^2 \mathcal{F}}{\partial J^i \partial J^j}\delta J^j\,, \tag{6.50}
$$

as $\delta F = J^i \delta M_i$ and $\delta\mathcal{F} = -M_i\delta J^i$. The Legendre transformation interchanges the convexity and the concavity.

---

[5] Here we assumed

$$
G_{\mu\nu\alpha\beta}(X,X') = \frac{1}{16\pi G_N}\frac{\delta^2\log Z[\bar{T}]}{\delta\bar{T}_{\mu\nu}(X)\delta\bar{T}_{\alpha\beta}(X')}\,, \tag{6.44}
$$

which could be shown by taking the variation of $\langle G_{\mu\nu}(X)\rangle_{\bar{T}} = \delta\log Z[\bar{T}]/\delta\bar{T}_{\mu\nu}(X)$, as

$$
\delta\langle G_{\mu\nu}(X)\rangle_{\bar{T}} = \int d^{d+1}X'\,\frac{\delta^2\log Z[\bar{T}]}{\delta\bar{T}_{\mu\nu}(X)\delta\bar{T}_{\alpha\beta}(X')}\delta\bar{T}_{\alpha\beta}(X')\,. \tag{6.45}
$$

The normalization is determined by the definition of the graviton propagator (6.42).

6.4 Calculations of the capacity of entanglement

Our holographic proof of the inequalities for the Rényi entropy highlights a role of the stability in the bulk as a unitarity of the dual field theory. The discussion was illuminating for the formal proof, but less concrete so far. In this section, we switch gears and move onto tangible examples of the capacity of entanglement in various systems.

6.4.1 Conformal field theory

As explained in chapter 2, in two-dimensional CFT with central charge c the Rényi entropies for an interval of length L are [49, 50]

$$S_n = \frac{c}{6}\left(1+\frac{1}{n}\right)\log(L/\epsilon)\,, \tag{6.51}$$

with the UV cutoff ϵ. It yields the capacity of entanglement straightforwardly

$$C(n) = \frac{c}{3n}\log(L/\epsilon)\,. \tag{6.52}$$

As it shows, the capacity is always positive in accord with the inequality (6.22) as the length L cannot be smaller than the UV cutoff ϵ.

It is challenging to obtain the capacity $C(n)$ for general n in higher dimensional CFT, while one can calculate $C(n)$ of a sphere in the limit $n \to 1$. This is because $C(1) = -\partial_n \tilde{S}_n|_{n=1}$ is identical to the derivative of the Rényi entropy $C(1) = -2\partial_n S_n|_{n=1}$, whose calculations were already carried out for a sphere in CFT in [140]. In this case, the capacity becomes

$$C(1) = \mathrm{Vol}(\mathbb{H}^{d-1})\,\frac{2\pi^{d/2+1}(d-1)\Gamma(d/2)}{\Gamma(d+2)}C_T\,. \tag{6.53}$$

This is proportional to the coefficient C_T of the correlation function of the energy-momentum tensor [141]

$$\langle T_{ab}(x)T_{cd}(0)\rangle = C_T\frac{I_{ab,cd}(x)}{x^{2d}}, \tag{6.54}$$

where $I_{ab,cd}(x)$ is a function given by

$$\begin{aligned} I_{ab,cd}(x) &= \frac{1}{2}\left(I_{ac}(x)I_{bd}(x)+I_{ad}(x)I_{bc}(x)\right)-\frac{1}{d}\delta_{ab}\delta_{cd}\,,\\ I_{ab}(x) &= \delta_{ab}-2\frac{x_a x_b}{x^2}\,. \end{aligned} \tag{6.55}$$

The positivity of $C(1)$ manifests itself in the form (6.53) as the volume of the hyperbolic space is positively divergent. In practice, it is convenient to introduce the regularized

volume[6]

$$\text{Vol}(\mathbb{H}^{d-1}) = \pi^{d/2-1}\Gamma\left(1-\frac{d}{2}\right) , \tag{6.56}$$

to read off the so-called universal part of the Rényi entropies. This operation corresponds to adding local counter terms with respect to the background metric to render the partition function finite. It works well for any d except even integers as the poles structure of the gamma function shows in (6.56). This signals the Weyl anomaly that cannot be removed by local counter terms. In even d dimensions, one has to replace the formula (6.56) with [58, 133]

$$\text{Vol}(\mathbb{H}^{d-1}) = \frac{2(-\pi)^{d/2-1}}{\Gamma(d/2)}\log(R/\epsilon) , \qquad (d:\text{even}) , \tag{6.57}$$

by introducing the UV cutoff ϵ and the radius R of the hyperbolic space, as explained in chapter 2. When applied to the entropy of an interval of width L in $d=2$, the radius of the hyperbolic space R should be identified with the width $L/2$ in the regularized volume (6.57) and we are able to recover the CFT_2 result (6.52) upon the relation $C_T = c/(2\pi^2)$.

6.4.2 Free fields

The capacity of entanglement is less tractable to calculate for interacting QFTs as the modular Hamiltonian is non-local in general. For free field theories, things are much simpler and one is able to compute the Rényi entropies using the partition function on $\mathbb{S}^1 \times \mathbb{H}^{d-1}$ which is conformally equivalent to the replica space of a spherical entangling surface [142, 58, 129] (see also [143, 144, 145]).

Firstly we consider a conformally coupled real massless scalar field. With the help of the map to $\mathbb{S}^1 \times \mathbb{H}^{d-1}$, the partition function on the n-fold replica manifold of a spherical entangling surface becomes [129]

$$\log Z_s(n) = -\int_0^\infty d\lambda\, \mu_s(\lambda)\, \left[\log\left(1-e^{-2\pi n\sqrt{\lambda}}\right) + \pi n\sqrt{\lambda}\right] , \tag{6.58}$$

where $\mu_s(\lambda)$ is the Plancherel measure of the scalar field on $\mathbb{H}^{d-1}$ [146, 147]

$$\mu_s(\lambda) = \frac{\text{Vol}(\mathbb{H}^{d-1})}{2^{d-1}\pi^{\frac{d+1}{2}}\Gamma\left(\frac{d-1}{2}\right)}\sinh(\pi\sqrt{\lambda})\left|\Gamma\left(\frac{d}{2}-1+i\sqrt{\lambda}\right)\right|^2 . \tag{6.59}$$

Together with (6.19), it leads to the capacity of entanglement

$$C_s(n) = \pi^2 n^2 \int_0^\infty d\lambda\, \mu_s(\lambda)\, \lambda\, \text{csch}^2\left(\pi n\sqrt{\lambda}\right) . \tag{6.60}$$

[6]To derive (6.56), one can either put a cutoff near the infinity of the hyperbolic space, or use a dimensional regularization. In the former case, one ignores the power-law divergences for the cutoff to extract the universal part, while in the latter case one analytically continues the dimension d from the range $1 < d < 2$ to an arbitrary value.

Turning into a massless Dirac fermion, the partition function is written as

$$\log Z_f(n) = \int_0^\infty d\lambda\, \mu_f(\lambda)\, \left[\log\left(1+e^{-2\pi n\lambda}\right) + \pi n\lambda\right] , \tag{6.61}$$

where the Plancherel measure of the spinor on $\mathbb{H}^{d-1}$ is [147]

$$\mu_f(\lambda) = \frac{g(d)\,\mathrm{Vol}(\mathbb{H}^{d-1})}{2^{d-2}\pi^{\frac{d+1}{2}}\Gamma\left(\frac{d-1}{2}\right)} \cosh(\pi\lambda) \left|\Gamma\left(\frac{d-1}{2}+i\lambda\right)\right|^2 , \tag{6.62}$$

and $g(d) \equiv 2^{[d/2]}$ is the dimension of Dirac spinors in d dimensions. The capacity takes a similar form to the scalar field:

$$C_f(n) = \pi^2 n^2 \int_0^\infty d\lambda\, \mu_f(\lambda)\, \lambda^2\, \mathrm{sech}^2\left(\pi n\lambda\right) . \tag{6.63}$$

Both (6.60) and (6.63) are manifestly positive in their forms.

In two dimensions $d = 2$, these capacities reproduces the CFT_2 result (6.52) with $c = 1$. They are also consistent with the general formula (6.53) of $C(1)$ for CFT where the free fields have the following values of C_T [141]

$$(C_T)_{\text{scalar}} = \frac{d\,\Gamma(d/2)^2}{4\pi^d(d-1)} , \qquad (C_T)_{\text{fermion}} = \frac{g(d)\,d\,\Gamma(d/2)^2}{8\pi^d} . \tag{6.64}$$

For massive cases and for a region A other than a ball, it is hard to obtain capacities analytically, but we can resort to lattice discretization to calculate them numerically. The partition functions $\mathrm{Tr}[\rho_A^n]$ are expressed by correlation functions of discretized fields located in the region A as follows [51, 52, 53]. For free scalars ϕ_i and its conjugates π_i with correlation functions $X_{ij} = \langle\phi_i\phi_j\rangle$ and $P_{ij} = \langle\pi_i\pi_j\rangle$, the partition function is given by

$$\log \mathrm{Tr}[\rho_A^n] = -\mathrm{Tr}\left[\log\left((D_s+1/2)^n - (D_s-1/2)^n\right)\right] = -\sum_a \left(\log(e^{n\epsilon_a}-1) - n\log(e^{\epsilon_a}-1)\right) , \tag{6.65}$$

where we set the eigenvalues of $D_s = \sqrt{XP}\,(\geq 1/2)$ as $\coth(\epsilon_a/2)/2$. The indices i, j run only the ones corresponding to the sites inside the region A. This yields a manifestly non-negative capacity

$$C_s(n) = n^2\mathrm{Tr}\left[\frac{(D_s+1/2)^n(D_s-1/2)^n}{((D_s+1/2)^n-(D_s-1/2)^n)^2}\left(\log\frac{D_s+1/2}{D_s-1/2}\right)^2\right] = \frac{n^2}{4}\sum_a \epsilon_a^2\,\mathrm{csch}^2(n\epsilon_a/2) . \tag{6.66}$$

The calculation for free fermions ψ_i is similar [138]. The partition function given by

$$\log \mathrm{Tr}[\rho_A^n] = \mathrm{Tr}\left[\log\left((1-D_f)^n + D_f^n\right)\right] = \sum_a \left(\log(e^{n\epsilon_a}+1) - n\log(e^{\epsilon_a}+1)\right) , \tag{6.67}$$

yields a manifestly non-negative capacity

$$C_f(n) = n^2\mathrm{Tr}\left[\frac{D_f^n(1-D_f)^n}{(D_f^n+(1-D_f)^n)^2}\left(\log\frac{D_f}{1-D_f}\right)^2\right] = \frac{n^2}{4}\sum_a \epsilon_a^2\,\mathrm{sech}^2(n\epsilon_a/2) , \tag{6.68}$$

where the eigenvalues of the matrix $(D_f)_{ij} = \langle\psi_i\psi_j^\dagger\rangle$ are $1/(1-e^{\epsilon_a})$.

6.4.3 Gravity duals

The Rényi entropies of a spherical entangling surface are calculated through the holography using the AdS topological black hole [133]. The metric for the bulk per replica $\hat{B}_n$ is known to be

$$ds^2_{d+1} = \frac{dr^2}{f_n(r)} + f_n(r)d\tau^2 + r^2(du^2 + \sinh^2 u\, d\Omega^2_{d-2})\,, \tag{6.69}$$

with a function

$$f_n(r) = r^2 - 1 - \frac{r_n^d - r_n^{d-2}}{r^{d-2}}\,. \tag{6.70}$$

The Euclidean time direction τ has the period $\tau \sim \tau + 2\pi$ so that this metric reduces to the non-singular flat space $d\tau^2 + du^2 + \sinh^2 u\, d\Omega^2_{d-2} \sim \sum_{i=1}^d dx_i^2$ at the conformal boundary $r \to \infty$. This geometry has a conical singularity $C_A^{(n)}$ at the horizon $r = r_n$ ($f_n(r_n) = 0$), where the Euclidean time τ circle shrinks to a point. The horizon radius r_n is determined by n as

$$\frac{2\pi}{n} = \frac{f_n'(r_h)}{2}2\pi \quad \Leftrightarrow \quad n = \frac{2}{f_n'(r_h)} = \frac{2}{dr_n - (d-2)r_n^{-1}} \tag{6.71}$$

$$\Leftrightarrow \quad r_n = \frac{1 + \sqrt{1 + n^2 d(d-2)}}{n\, d}\,, \tag{6.72}$$

such that the correct conical singularity $\tau \sim \tau + 2\pi/n$ is reproduced. r_n is monotonically decreasing with n and satisfies $r_n \geq \lim_{n\to\infty} r_n = \sqrt{(d-2)/d}$.

The cosmic brane is located on the horizon and the improved Rényi entropy is nothing but the black hole entropy

$$\tilde{S}_n = r_n^{d-1}\frac{\mathrm{Vol}(\mathbb{H}^{d-1})}{4G_N}\,. \tag{6.73}$$

Integration by n gives the free energy $F(n)$

$$F(n) = \int_1^n dn'\,\frac{\tilde{S}_{n'}}{n'^2} = \frac{\mathrm{Vol}(\mathbb{H}^{d-1})}{4G_N}\frac{2 - r_n^d - r_n^{d-2}}{2}\,, \tag{6.74}$$

where we used the relation $(d + (d-2)/r_n^2)\partial_n r_n = -2/n^2$ followed from the expression (6.71). This means that the Rényi entropy $S_n = nF/(n-1)$ is

$$S_n = \frac{n}{n-1}\frac{\mathrm{Vol}(\mathbb{H}^{d-1})}{4G_N}\frac{2 - r_n^d - r_n^{d-2}}{2}\,, \tag{6.75}$$

which is non-negative for any n and d as $r_n > 1$ for $n < 1$ and $r_n < 1$ for $n > 1$. We can also check that the first inequality (6.1) holds or equivalently $S[\rho_n|\rho] = -(n-1)^2\partial_n S_n =$

$1+(d-1)(r_n^d-r_n^{d-2})/2-r_n^{d-1} \geq 0$. The total energy (6.29) and the capacity of entanglement (6.30) given by

$$E = \frac{\mathrm{Vol}(\mathbb{H}^{d-1})}{4G_N}\frac{2+(d-1)(r_n^d-r_n^{d-2})}{2}\,, \tag{6.76}$$

$$C = \frac{\mathrm{Vol}(\mathbb{H}^{d-1})}{4G_N}(d-1)\,r_n^{d-1}\frac{d\,r_n^2-(d-2)}{d\,r_n^2+(d-2)}\,, \tag{6.77}$$

are also non-negative for any n and d as $r_n > 1$ for $n < 1$ and $r_n \geq \sqrt{(d-2)/d}$ for $n > 1$.

A more direct way to get C without knowing $\tilde{S}_n$ is to use the formula

$$C = -\frac{n}{8G_N}\int_{C_A^{(n)}} d^{d-1}y\sqrt{g}\,g^{ij}\,\frac{\partial X^\mu}{\partial y^i}\frac{\partial X^\nu}{\partial y^j}\,\frac{\delta G_{\mu\nu}(X(y))}{\delta n}\,, \tag{6.78}$$

which is equivalent to the previous ones (6.32) and (6.48).[7] When applying (6.78) to the background (6.69), we take the embedding $X^\mu(y)$ of the surface as $(X^r, X^\tau, X^i) = (1, 0, y^i)$, where y^i are the coordinates of $\mathbb{H}^{d-1}$. For $\mathbb{H}^{d-1}$ is maximally symmetric, the integration just gives its volume and the formula reads

$$C = -\frac{n\mathrm{Vol}(\mathbb{H}^{d-1})}{8G_N}r_n^{d-3}\,\frac{\delta G_{uu}}{\delta n}\bigg|_{C_A^{(n)}}\,. \tag{6.79}$$

Reassuringly it agrees with (6.77) as $\delta G_{uu}/\delta n = \delta r_n^2/\delta n = 2r_n\partial_n r_n$.

When $n = 1$, the holographic capacity of entanglement takes a particularly simple form

$$C(1) = \frac{\mathrm{Vol}(\mathbb{H}^{d-1})}{4G_N}\,. \tag{6.80}$$

It takes exactly the same form as the field theory calculation (6.53) because the holographic system has [148]

$$C_T = \frac{1}{8\pi G_N}\frac{d+1}{d-1}\frac{\Gamma(d+1)}{\pi^{d/2}\Gamma(d/2)}\,. \tag{6.81}$$

One more example we are going to show is the system with two balls A_1 and A_2 of radii R_1 and R_2 separated enough (see Fig. 6.1). The Rényi entropy of the two balls for an arbitrary n is beyond our scope, but a perturbative calculation is feasible in the leading linear order of $\delta n \equiv n-1$. Indeed, an analog of the mutual information $I^{(n)}(A_1, A_2) \equiv S_n(A_1)+S_n(A_2)-S_n(A_1\cup A_2)$ has been evaluated holographically by [80] for n close to 1. We will benefit from the result to get the capacity of entanglement $C_{A_1\cup A_2}$ for the union of the two balls A_1 and A_2 in this parameter region.

The positions of the balls are parametrized by the cross ratio $0 \leq x \equiv \frac{(x_1-x_2)(x_3-x_4)}{(x_1-x_3)(x_2-x_4)} \leq 1$. x_i are the coordinates of the points where the line connecting the two centers intersects

[7] Even when the graviton propagator $G_{\mu\nu\alpha\beta}(X, X')$ is known, the expression (6.48) is too difficult to evaluate in general and it suffers from a subtle contribution from the asymptotic boundary. We will comment on this difficulty in Appendix B.2.

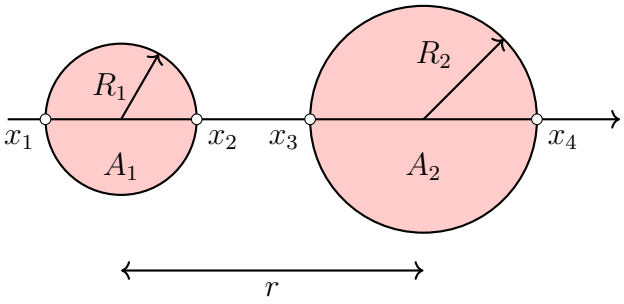

Figure 6.1: The entangling region (shown in red) consists of two balls A_1 and A_2 of radii R_1 and R_2, respectively. The four coordinates x_i are defined on the line connecting the centers of the balls. In a conformal field theory, the configuration of the balls is uniquely specified by the cross ratio $x \equiv (x_1 - x_2)(x_3 - x_4)/(x_1 - x_3)(x_2 - x_4) = 4R_1R_2/(r^2 - (R_1 - R_2)^2)$, where r is the distance between the two centers.

the balls, $x_{1,2}$ for A_1 and $x_{3,4}$ for A_2 (Fig. 6.1). There are two phases depending on the topology of the minimal surfaces in the bulk, and there is a critical point $x = x_c$ below which a disconnected surface is favored, otherwise a connected one is realized [132]. The calculation of $I^{(n)}(A_1, A_2)$ performed by [80] is in the disconnected phase ($x \leq x_c$) with the balls separated enough. To convert the result into the capacity $C(1)$, we apply a derivative $-2\partial_n|_{n=1}$ on $S_n(A_1 \cup A_2) = S_n(A_1) + S_n(A_2) - I^{(n)}(A_1, A_2)$ to get

$$C_{A_1 \cup A_2}(1) = C_{A_1}(1) + C_{A_2}(1) + 2\partial_n I^{(n)}(A_1, A_2)|_{n=1} \tag{6.82}$$

$$= \frac{\mathrm{Vol}(\mathbb{H}^{d-1})_{R_1} + \mathrm{Vol}(\mathbb{H}^{d-1})_{R_2}}{4G_N} + \frac{2^{4-d}\pi^{d+1}C_T}{d(d^2-1)\Gamma\left((d-1)/2\right)^2}\frac{2-x}{x}B\left(\left(\frac{x}{2-x}\right)^2; \frac{d+1}{2}; \frac{2-d}{2}\right), \tag{6.83}$$

where $\mathrm{Vol}(\mathbb{H}^{d-1})_R$ is the regularized volume of $\mathbb{H}^{d-1}$ of radius R given by (6.56) and (6.57).

6.4.4 Large and small n limits

Before closing this section, we examine the large and small n behaviours of the capacity $C(n)$ for a spherical entangling region in the systems we have studied. In the thermodynamic interpretation, we regard these as the low and high temperature limits for the temperature $T = 1/n$.

In the low temperature limit $n \to \infty$, the capacities of conformal theories go to zero as

$$C_s(n) \sim \mathrm{Vol}(\mathbb{H}^{d-1})\frac{\Gamma(\frac{d}{2}-1)^2}{15 \cdot 2^{d-1}\pi^{\frac{d-3}{2}}\Gamma\left(\frac{d-1}{2}\right)}\frac{1}{n^3} \quad (d \neq 2), \tag{6.84}$$

$$C_f(n) \sim \mathrm{Vol}(\mathbb{H}^{d-1})\frac{g(d))\Gamma(\frac{d-1}{2})}{3 \cdot 2^d\pi^{\frac{d-1}{2}}}\frac{1}{n}, \tag{6.85}$$

$$C_{\mathrm{AdS}}(n) \sim \frac{\mathrm{Vol}(\mathbb{H}^{d-1})}{4G_N}\frac{(d-1)(d-2)^{d/2-1}}{d^{d/2}}\frac{1}{n}, \tag{6.86}$$

for the massless scalar, massless fermion and CFT dual to the AdS spacetime, respectively. They are proportional to a power of the temperature $T = 1/n$, indicating a gapless excitation for the modular Hamiltonian. In $d = 2$, the scalar capacity also becomes proportional to $1/n$ as $C_s(n) = (c/3n)\log(L/\epsilon)$.

On the other hand, in the high temperature limit $n \to 0$, they obey the Stefan-Boltzmann's law $C(T) \propto T^{d-1}$ for thermal massless gases

$$C_s(n) \sim \mathrm{Vol}(\mathbb{H}^{d-1}) \frac{(d-1)\Gamma(d/2+1)\zeta(d)}{2^{d-2}\pi^{\frac{3}{2}d-1}} \frac{1}{n^{d-1}}, \tag{6.87}$$

$$C_f(n) \sim \mathrm{Vol}(\mathbb{H}^{d-1}) \frac{(d-1)(2^{d-1}-1)\Gamma(d/2+1)\zeta(d)g(d)}{2^{2d-3}\pi^{\frac{3}{2}d-1}} \frac{1}{n^{d-1}}, \tag{6.88}$$

$$C_{\mathrm{AdS}}(n) \sim \frac{\mathrm{Vol}(\mathbb{H}^{d-1})}{4G_N}(d-1)\left(\frac{2}{nd}\right)^{d-1}. \tag{6.89}$$

To derive these results, we used asymptotic behavior of $\mu(\lambda)$

$$\mu_s(\lambda) \sim \frac{\mathrm{Vol}(\mathbb{H}^{d-1})}{2^{d-1}\pi^{\frac{d-1}{2}}\Gamma\left(\frac{d-1}{2}\right)}\lambda^{\frac{d-3}{2}}, \qquad \mu_f(\lambda) \sim \frac{g(d)\,\mathrm{Vol}(\mathbb{H}^{d-1})}{2^{d-2}\pi^{\frac{d-1}{2}}\Gamma\left(\frac{d-1}{2}\right)}\lambda^{d-2}, \tag{6.90}$$

in the limit $\lambda \to \infty$ and mathematical relations

$$\int_0^\infty dx\ x^d \mathrm{csch}^2 x = \frac{\Gamma(d+1)\zeta(d)}{2^{d-1}}, \tag{6.91}$$

$$\int_0^\infty dx\ x^d \mathrm{sech}^2 x = \frac{(2^{d-1}-1)\Gamma(d+1)\zeta(d)}{4^{d-1}}, \tag{6.92}$$

and $\Gamma(d+1)/2^d = \Gamma(\frac{d+1}{2})\Gamma(\frac{d}{2}+1)/\sqrt{\pi}$.

6.5 Discussion

Our approach to the holographic Rényi entropy is advantageous for formal proofs and provides a clear-cut relation of the roles played by the unitarity in QFT and the stability of the gravity theory. Meanwhile, the holographic formula lacks a power of computability in a practical problems as we saw in section 6.4. The main difficulty originates from the procedure of finding the extremal surface of a cosmic brane in the backreacted geometry. One would be able to calculate the Rényi entropy perturbatively either in $n-1$ or in shape, otherwise it is generically unattainable in its nature. It is still algorithmically simple to implement in numerical calculation that would be worth more investigation.

We do not know any rigorous proof or plausible argument for the bulk stability against any perturbation that is essential in our holographic proof of the inequalities. To answer a question whether the bulk is stable or not requires the knowledge of quantum gravity which remains to be developed. It is one of the fundamental problems even in the perturbative Euclidean quantum gravity and providing the complete solution is far beyond the scope of this paper. We comment on possible attempts instead:

- The assumption we made for the bulk stability is a sufficient condition, but may not be a necessary condition, to prove the Rényi entropic inequalities in the holographic system. Namely the non-negativity of the heat capacity (6.38) could have followed from the condition for the Hessian matrix to be non-negative definite only in the subspace of the metric variation $\delta G_{\mu\nu}/\delta n$ induced by changing the replica parameter. Unfortunately we were not able to demonstrate the non-negativity of the Hessian in the subspace as the metric variation is only calculable in the neighbourhood of the cosmic brane.

- The perturbative Euclidean gravity is known to suffer from the bulk instability due to the Weyl mode.[8] There are at least two directions known in literature to fix this problem: one (ad-hoc) attempt is Gibbons-Hawking-Perry prescription which claims to change the contour of integration for the Weyl mode, called conformal rotation, in the path integral formulation of the perturbative Euclidean gravity [136, 137, 149]. (See also [150, 151] for further discussions.) For locally Euclidean AdS_3 spaces, this prescription gives the correct one-loop partition function of gravity expected from the $\mathrm{AdS}_3/\mathrm{CFT}_2$ correspondence [152], and it might well work for more general holographic theories at the one-loop level. The other is based on the canonical quantization of gravity to show the Hamiltonian is bounded from below, and then continues to Euclidean path integral with an appropriate choice of contour [153, 154]. The two approaches appear to be complimentary to each other, but a precise relation between them has not been completely explored.

As a future direction, it would also be intriguing to include quantum corrections to the holographic Rényi entropy [95]. Recent discussions [155, 156] argues a relation between the boundary modular Hamiltonian H_{bdy} and the bulk one H_{bulk}

$$H_{\mathrm{bdy}} = \frac{\hat{A}}{4G_N} + H_{\mathrm{bulk}} + \hat{S}_{\text{Wald-like}} + O(G_N)\,. \tag{6.93}$$

Here $\hat{A}$ is an operator in the bulk which is supposed to give the area of the Ryu-Takayanagi surface $\mathcal{S}$ when sandwiched by a state dual to a given state in the boundary field theory. $\hat{S}_{\text{Wald-like}}$ denotes local operators localized on $\mathcal{S}$ in the semi-classical limit. It may as well be applied to the calculation of the capacity (6.19) for $n = 1$, leading to

$$C(1)_{\mathrm{bdy}} = \frac{1}{16G_N^2}\left(\langle\hat{A}^2\rangle - \langle\hat{A}\rangle^2\right) + \frac{1}{2G_N}\left(\langle\hat{A}\,\tilde{H}_{\mathrm{bulk}}\rangle - \langle\hat{A}\rangle\langle\tilde{H}_{\mathrm{bulk}}\rangle\right) + O(1)\,, \tag{6.94}$$

where we introduced $\tilde{H}_{\mathrm{bulk}} \equiv H_{\mathrm{bulk}} + \hat{S}_{\text{Wald-like}}$ to simplify the notation. Surprisingly, the leading term is of order $1/G_N^2$, which was not observed in the examples in section 6.4. Thus we are lead to conclude that the area operator has to satisfy

$$\alpha \equiv \frac{\langle\hat{A}^2\rangle - \langle\hat{A}\rangle^2}{8G_N} = O(G_N^0)\,. \tag{6.95}$$

[8] We thank M. Headrick for drawing our attention to this subtlety.

We believe this is a defining property of the area operator that holds for any state in the semi-classical limit. A similar statement has been made in, e.g., [157] in the context of the linearity of the area operator recently. The order $1/G_N$ term is likely to contribute to the capacity, and it indeed does so for the cases considered in section 6.4. We do not know how to estimate it in practice, but the non-negativity of the capacity yields a constraint

$$\alpha + \langle \hat{A}\, \tilde{H}_{\rm bulk} \rangle - \langle \hat{A} \rangle \langle \tilde{H}_{\rm bulk} \rangle \ \geq \ 0 + O(G_N)\,. \tag{6.96}$$

Testing this inequality needs more detailed information on the area operator and the local operators on the Ryu-Takayanagi surface $\mathcal{S}$, which is far beyond the scope of the present work.

Another interesting direction is to generalize the holographic formula of the Rényi entropy to a time dependent background [78] and higher derivative gravities [81, 158]. It is not so obvious how a cosmic brane modifies the original proposals, but it is likely that the entropy is still given by variants of the area formula.

Chapter 7

Conclusions

This thesis made an attempt to have a better understanding of how quantum gravity theory encodes spacetime structure as physical degrees of freedom or quantum information, by investigating various aspects of quantum entanglements from the viewpoint of the holography. These studies turn out to include or be related to many rich physical interests as well other than quantum gravity, such as quantum information theories, the logical structure of thermodynamics, thermalization processes, ground states of gapped theories, useful conformal transformations, relevant deformations and c-functions, non-trivial classical geometries derived from string theory or M theory, cosmic branes, and black hole dynamics.

In chapter 3, we have examined entanglement entropies of an annulus or equivalently mutual informations across the annulus in three dimensions, resorting to numerical calculations. Massless and massive free scalar theories are studied by lattice discretization method, and strongly coupled theories, namely, a CFT_3 and a gapped theory holographically described by AdS_4 and CGLP background respectively, are studied by shooting method. All the resultant entropies satisfy the monotonicity and the convexity requested by the strong subadditivity. In the limits of thin or thick annuli, these entropies can be related to some analytic calculations in previous works, which expectedly agree with our numerical results. While AdS_4 has two phases for the minimal surface, one connected phase and one disconnected phase, CGLP background has four phases, three disconnected phases and one connected phase, since it is capped off somewhere in IR. In both cases, holographic mutual information characterizes the connected phase by its nonzero value. Many qualitative similarities between the results of free theories and holographic theories give concrete examples of the power of the holographic entanglement entropy formula.

Interestingly, we observed that the mutual information across the annulus exponentially decays with the mass gap times the annulus width, both in massive free scalar theory and in CGLP background. This term depends on the annulus width and thus is non-local with respect to the entangling region. From this observation, we conjectured that this exponentially decaying nonlocal behaviour is universal for mutual information in gapped theories, and because mutual information is composed of entanglement entropies, this conjecture directly means that in gapped theories, entanglement entropies also should have such exponentially decaying non-local terms, which have been neglected

in expanding entropies with respect to the inverse of the mass gap.

Moreover, the dimensionless coefficient κ of the mutual information in the thin annulus limit seems to give a measure of degrees of freedom in field theories, and more generally it would be intriguing to study whether we can use some mutual information as a c-function or not. This holds at least in our example, because our mutual information monotonically decreases with RG flow, namely decreases with the dimensionless combination of the mass, mR_2 (or mR_1), fixing the radius ratio R_2/R_1. If so, this c-function may be easy to generalize into higher dimensions.

In chapter 4, we have investigated holographic entanglement entropies in three dimensional time-dependent Janus black hole with covariant holographic entanglement entropy formula, a covariant generalization of the original holographic entanglement entropy formula. The black hole is a solution of Einstein-scalar system and one parameter γ deformation of BTZ black hole, where the parameter γ controls the scalar configuration and the strength of its time dependence. Like BTZ black hole, globally the geometry has two asymptotically AdS regions and is holographically dual to two copies of CFT's. One important difference from BTZ black hole is that the coupling constants or Hamiltonians are different between the two CFT's, while they are the same in the case of BTZ black holes.

First we studied entropies of one interval in one CFT. Luckily, the corresponding extremal surface is obtained analytically, and consequently we see a time dependence typical of thermalizing states, that is, the entropies grow linearly with time at first and become saturated at some time proportional to the interval size in the end. Some limits that simplify the results are also studied. A famous literature also constructed a holographic model of thermalization processes in a clever and mysterious way from static black holes like BTZ black hole, by taking two intervals located separately in each CFT and by taking the time direction of one CFT opposite or equivalently dividing the spacetime by $\mathbb{Z}_2$ symmetry [108]. The literature attributed the linear growth of entropies to the growth of the time slice penetrating the black hole (or the wormhole connecting the two asymptotically AdS spaces) which the corresponding surfaces rest on, but we succeeded in constructing such linearly growing holographic entanglement entropies without any growing time slices or wormholes. We speculate that the true origin of the linear growth of entropies is not the growth of some time slice but the situation that the corresponding surfaces enter into the event horizon of the black holes.

We also studied how the story of the literature, which constructed a time dependent situation using static BTZ black hole, changes if we introduce the one parameter γ deformation, that is, we also studied entropies of two intervals located separately in each CFT by taking the time direction of one CFT opposite, in the time-dependent Janus black hole as well. In the same way as BTZ black hole geometry, the surface has two phases, one connected phase and one disconnected phase. In the connected phase, which can be characterized by the nonzero mutual information between the two intervals, the surface consists of two geodesics penetrating the black holes, which gets long with increased γ. In the disconnected phase, the surface is the same as we studied before for one interval in one CFT. As a result, we found that the time for the phase transition from the connected phase to the disconnected phase to occur becomes early with increased γ, and the phase

transition does not occur with a sufficiently large γ.

We also found that the deformation γ reduces the speed of the liner growth of the entropy, and so it would be interesting to study how this slowdown occurs in dual CFT side, by calculating entropies for the proposed dual CFT state for the time-dependent Janus black hole. Such a calculation would serve a consistency check of both the proposal of the dual CFT state and our holographic calculations.

In chapter 5, on a cylindrical spacetime $\mathbb{R}\times\mathbb{S}^2$, we have defined two types of renormalized entanglement entropies (REE), $\mathcal{F}_{\rm C}$ and $\mathcal{F}_{\rm LM}$, out of cap entropies, and saw whether they are c-functions, that is, whether they decrease monotonically with RG flow like usual REE defined on the flat space. Putting the region on a sphere of radius R instead of the flat space, we can regulate possible IR divergences. In CFT's, these two REEs both correspond to the usual REE defined in the flat space, and for this reason, they are already weak c-functions in the sense that $\mathcal{F}|_{\text{UV CFT}} \geq \mathcal{F}|_{\text{IR CFT}}$. As a concrete setup, we calculate cap entropies and thus REE's by applying a mass perturbation $m^2\phi^2$ to a conformally coupled scalar ϕ, analytically in UV ($mR \ll 1$) and IR ($mR \gg 1$) regions, and numerically in the whole region of the scale mR .

UV region is studied with the assistance of a nice conformal transformation from the replica space to a non-singular space $\mathbb{S}^1 \times \mathbb{H}^2$, resulting in a spacetime dependent mass term owing to the conformal factor $e^{2\sigma(x)}$. The first order term $O((mR)^2)$ of the cap entropy is obtained by perturbing the free energy of the non-singular space with respect to the coupling m^2. It turns out that up to the first order of $(mR)^2$, both the REE's monotonically decrease with the RG flow, but $\mathcal{F}_{\rm C}$ decreases in a stationary way while $\mathcal{F}_{\rm LM}$ decreases in a non-stationary way.

On the other hand, in IR region, $O((mR)^{-1})$ term of the cap entropy is read off by uplifting the theory onto a massive scalar theory in four dimensions, since the $O((mR)^{-1})$ term is related to the logarithmic term $O(\log\epsilon)$ of entropies in four dimensions, which is known as Solodukhin's formula. Consequently we observe that up to the first order of $(mR)^{-1}$, the REE $\mathcal{F}_{\rm C}$ decreases with the RG flow while $\mathcal{F}_{\rm LM}$ does not. This example confirms that $\mathcal{F}_{\rm LM}$ is not a c-function.

Numerical calculations are performed for the whole region of the scale mR, whose results agree well with all the above analytic calculations in both UV and IR regions. The results also show that $\mathcal{F}_{\rm C}$ monotonically decreases all the way along the RG flow in our setup, and so we propose that $\mathcal{F}_{\rm C}$ is generally c-function in this cylindrical spacetime $\mathbb{R}\times\mathbb{S}^2$. As the derivative in the definition of REE, our result favors the derivative with respect to θ, the size of region, rather than with respect to R, the scaling of the spacetime; this result supports our intuition that physical degrees of freedom are encoded in entanglements of the regions. It would also be stimulating to try to prove that $\mathcal{F}_{\rm C}$ is in fact generally c-function, or to extend the notion of REE to more general curved spaces.

In chapter 6, we show that the recent proposal for the holographic formula of Rényi entropy or modular entropy expectedly satisfies four mathematical inequalities that Rényi entropies or modular entropy should fulfill, under an assumption that the bulk is stable.

In showing the Rényi entropic inequalities holographically, we found that there is an useful analogy between modular entropies and thermal entropies. Identifying the Rényi parameter n with the inverse temperature β and the modular Hamiltonian $-\log\rho$ with the

usual Hamiltonian H, namely, applying statistical mechanics to the escort density matrix $\rho_n = \rho^n/\mathrm{Tr}[\rho^n]$, the modular entropy is identified with the thermal entropy, and so-called capacity of entanglement is identified with the heat capacity. From the viewpoint of this analogy, the three of Rényi entropic inequalities are interpreted as the non-negativity of the entropy, the total energy, and the heat capacity, respectively. The remaining one inequality can be derived from the concavity of the free energy, that is, the non-negativity of the capacity. In light of this analogy, the derivation of the holographic formula of Rényi entropy gets simplified and its underling thermodynamic structure becomes clear.

Particularly, our research has revealed that capacity of entanglement is holographically related to the Hessian matrix of the action with respect to metric perturbations, and that its non-negativity, the most nontrivial inequality, is holographically related to the stability of the bulk spacetime, which is usually implicitly assumed in holographic studies. Since the inequalities are roughly just the consequences of the unitarity of quantum theories, this work suggests some connection between the unitarity and the bulk stability.

Capacities of entanglement $C(n)$ are also studied in various systems: an interval in CFT_2, a ball in CFT_d with $n = 1$, a ball for free massless scalars or fermions in d dimensions, any region on a lattice, and a ball or two separated balls in a strong coupling CFT_d holographically described by AdS_{d+1}, whose replica bulk geometry is explicitly given as AdS topological black hole. Their results are consistent with each other, and with the inequalities. We also examined the large n and small n limits of the above capacities of a ball in CFT's, the massless free scalars or fermions and the holographic theory. In the large n limit, which is interpreted as the low temperature limit in the analogy, the capacities go to zero following a power-law decay, indicating a gapless excitation of their modular Hamiltonians. On the other hand, in the small n limit, we observed Stefan-Boltzmann law for thermal massless classical gases, which is natural because the limit corresponds to the high temperature limit in the analogy to statistical mechanics.

Acknowledgements

First I want to express my special thanks to my advisor Tatsuma Nishioka. Without his warm support at all levels, I would not have complete my doctorate. I learned a lot of things from him, not only about physics but especially about how to be comfortable person to be with and how to assemble knowledge. I wish to thank Taizan Watari, who was my advisor in the master's course. I also learned plenty of things from him, particularly about how a professional should be and how to clarify things. I would like to thank Sumit Ranjan Das, who was my host during my visit to Kentucky University. I learned much from him, notably about how to be a good person living a good life, and how to discuss with people. I am forever grateful to them for all the kindness and sincere help to me. I admire them for their attitude toward life and work, and respect each of them deeply as a person. Their personalities will stay strong role models for me.

I appreciate Shamik Banerjee, Teruhiko Kawano, Noriaki Ogawa and Tomonori Ugajin very much for collaborations. The collaborations with them were invaluable times in my life. I am also thankful to all of my colleagues and friends. I enjoyed delightful days with them.

I thank my parents and my sister for supporting my decisions and for encouraging me to explore my own life. I will never forget the opportunities and experiences you gave me, which have made me who I am. Lastly, I thank my beloved Kaho so much for inspiring enthusiasm in me during the final stages of this thesis. I am happy just being with you.

This work was supported by World Premier International Research Center Initiative (WPI), MEXT, Japan, by Advanced Leading Graduate Course for Photon Science (ALPS), the University of Tokyo, and by Japan Society for the Promotion of Science (JSPS) Research Fellowship for Young Scientists.

Appendix A

Details of numerical calculations

A.1 Calculating annulus entropies

Here we summarize the numerical algorithm for calculating the entanglement entropy of the annulus for a free massive scalar field whose action is given by (3.14).

A.1.1 Radial lattice discretization

We use the polar coordinates to put the theory on the radial lattice

$$ds^2 = -dt^2 + dr^2 + r^2 d\theta^2 \ . \tag{A.1}$$

The radial coordinate r is discretized to N points with lattice spacing a. After the Fourier decomposition along the angular coordinate θ, the lattice Hamiltonian becomes

$$H = \frac{1}{2} \sum_{n=-\infty}^{\infty} \left[\sum_{i=1}^{N} \pi_{n,i}^2 + \sum_{i,j=1}^{N} \phi_{n,i} K_n^{i,j} \phi_{n,j} \right] \ , \tag{A.2}$$

where $\phi_{n,i}$ and $\pi_{n,i}$ are the discretized scalar field with angular momentum n on the i-th site and its conjugate, respectively. The matrices $K_n^{i,j}$ depend on the angular momentum and the mass m

$$K_n^{1,1} = \frac{3}{2} + n^2 + (ma)^2 \ , \qquad K_n^{i,i} = 2 + \frac{n^2}{i^2} + (ma)^2 \ , \qquad K_n^{i,i+1} = K_n^{i+1,i} = -\frac{i+1/2}{\sqrt{i(i+1)}} \ . \tag{A.3}$$

These are related to the two-point functions of the scalar fields $(X_n)_{ij} = \langle \phi_{n,i} \phi_{n,j} \rangle$ and the momenta $(P_n)_{ij} = \langle \pi_{n,i} \pi_{n,j} \rangle$ as $X_n = \frac{1}{2} K_n^{-1/2}$ and $P_n = \frac{1}{2} K_n^{1/2}$.

The outer and inner radii of the annulus are chosen to be half-integers in units of the lattice spacing, $R_1/a = r_1 + 1/2$ and $R_2/a = r_2 + 1/2$ with integers r_1, r_2. This choice corresponds to the free boundary condition in the continuum limit. In our calculation, we vary r_2 from 100 to 120 and r_1 from 5 to $r_2 - 5$. The entanglement entropy of the annulus

$S(R_1, R_2)$ is obtained by using $(r_2 - r_1) \times (r_2 - r_1)$ submatrices $(X_n^{r_1,r_2})_{ij}$ and $(P_n^{r_1,r_2})_{ij}$ of the correlation functions X_n, P_n with the ranges $r_1 + 1 \leq i, j \leq r_2$ as

$$S(R_1, R_2) = S_0 + 2\sum_{n=1}^{\infty} S_n \ , \tag{A.4}$$

where S_n is the contribution from the n-th angular mode

$$S_n = \mathrm{tr}\left[(C_n + 1/2)\log(C_n + 1/2) - (C_n - 1/2)\log(C_n - 1/2)\right] \ , \tag{A.5}$$

with $C_n \equiv \sqrt{X_n^{r_1,r_2} P_n^{r_1,r_2}}$. In the following, we describe how to perform this infinite summation over n under controlled numerical errors.

A.1.2 Finite lattice size effect

To avoid the finite lattice size effect, we repeat the calculation of S_n (A.5) by changing the lattice size N and fit the results $S_n(N)$ with the asymptotic expansion for large N

$$S_n(N) = S_n(\infty) + \sum_{k=1}^{k_{\max}} \frac{a_k}{N^k} \ . \tag{A.6}$$

We then read off the constant part $S_n(\infty)$ as the value of S_n in the large-N limit. Starting from $N = 200$, we increase the lattice size by $\Delta N = 20$ until the resultant $S_n(\infty)$ stops changing up to error $\delta = 10^{-6}$.

We choose the fitting parameter $k_{\max}$ so that the maximum lattice size N is as small as possible. Typically we find $k_{\max} = 3 \sim 10$.

The finite lattice size effect dominates only for small angular momenta n with small masses ma. In our calculation, the maximum lattice size reaches $N \sim 1000$ for $n \lesssim 10$ in the massless case, but $N = 200$ is sufficiently large for $n \gtrsim 20$ or $ma \gtrsim 0.1$. The total numerical error in (A.4) can be estimated to be $O(20\delta) \lesssim O(10^{-4})$.

A.1.3 Large angular momentum

In the large angular momentum limit $n \to \infty$, the correlation matrices X_n and P_n approach almost diagonal matrices [85]. The products of the submatrices $X_n^{r_1,r_2} P_n^{r_1,r_2}$ almost equal to $1/4$ times unit matrix up to order $1/n^8$. The nontrivial entries are at the upper-left corners

$$\begin{aligned}
(X_n^{r_1,r_2} P_n^{r_1,r_2})^{r_1+1,r_1+1} &= \frac{1}{4} + \frac{r_1^2(r_1+1)^2}{16n^4} - \frac{r_1^2(r_1+1)^2(2r_1+1)^2(m^2+2)}{32n^6} + O(1/n^8) \ , \\
(X_n^{r_1,r_2} P_n^{r_1,r_2})^{r_1+1,r_1+2} &= \frac{r_1^3(r_1+1)^{3/2}(r_1+2)^{3/2}}{64n^6} + O(1/n^8) \ , \\
(X_n^{r_1,r_2} P_n^{r_1,r_2})^{r_1+2,r_1+1} &= \frac{r_1^2(r_1+2)^{3/2}(r_1-1)^{1/2}(3(r_1+1)^2-1)}{64n^6} + O(1/n^8) \ .
\end{aligned} \tag{A.7}$$

and at the lower-right corners

$$
\begin{aligned}
(X_n^{r_1,r_2}P_n^{r_1,r_2})^{r_2,r_2} &= \frac{1}{4}+\frac{r_2^2(r_2+1)^2}{16n^4}-\frac{r_2^2(r_2+1)^2(2r_2+1)^2(m^2+2)}{32n^6}+O(1/n^8)\ ,\\
(X_n^{r_1,r_2}P_n^{r_1,r_2})^{r_2,r_2-1} &= \frac{r_2^{3/2}(r_2-1)^{3/2}(r_2+1)^3}{64n^6}+O(1/n^8)\ ,\\
(X_n^{r_1,r_2}P_n^{r_1,r_2})^{r_2-1,r_2} &= \frac{r_2^{1/2}(r_2-1)^{3/2}(r_2+1)^2(3r_2^2-1)}{64n^6}+O(1/n^8)\ .
\end{aligned}
\tag{A.8}
$$

Here we restrict the ranges of r_1, r_2 to $3 \le r_1$ and $r_1+3 < r_2$ to avoid the overlap between the upper-left and lower-right corners, which is satisfied in our set up with $5 \le r_1 \le r_2-5$.

The r_2-r_1-2 eigenvalues of the matrix $\sqrt{X_n^{r_1,r_2}P_n^{r_1,r_2}}$ are $1/2+O(1/n^8)$ and the other two are given by

$$
\frac{1}{2}+c_n^{(a)}-c_n^{(a)}\frac{(2r_a+1)^2(m^2+2)}{2n^2}\ ,\qquad c_n^{(a)}\equiv\frac{r_a^2(r_a+1)^2}{16n^4}\ ,\qquad a=1,2\ . \tag{A.9}
$$

Therefore, most of the eigenvalues do not contribute to the n-th entanglement entropy (A.5) up to order $1/n^8$ and we obtain

$$
S_n=\sum_{a=1,2}\left[c_n^{(a)}(1-\log c_n^{(a)})+\frac{(2r_a+1)^2(m^2+2)}{2n^2}c_n^{(a)}\log c_n^{(a)}\right]+O(1/n^8)\ . \tag{A.10}
$$

This asymptotic formula is much faster than the direct calculation of (A.5).

We perform the matrix trace calculation (A.5) for n less than some large angular momentum n_*, and use this asymptotic formula (A.10) for $n \ge n_*$ as long as $S_n(=O(\log n/n^4))$ is larger than the machine precision. The other higher modes are ignored.

Our n_* is determined as follows. Let the error of $O(1/n^8)$ in (A.10) be μ/n^8 with $\mu=\mu(m,r_1,r_2)$. Then the total numerical error in (A.4) is estimated to be $\sum_{n_*}^{\infty}(\mu/n^8)\sim \mu/(7n_*^7)$. We take n_* to be the angular momentum where the asymptotic formula (A.10) agrees with the matrix trace calculation (A.5) up $7\delta/n$. Then $\mu/n_*^8 \lesssim 7\delta/n_*$ holds and the total numerical error in (A.4) is bounded by $\sum_{n_*}^{\infty}(\mu/n^8)\sim\mu/(7n_*^7)\lesssim\delta$. In this way, we can handle the numerical error within $O(\delta)$.

A.2 Calculating cap entropies on cylinder

Here we summarize the numerical algorithm for calculating the entanglement entropy of the cap A on the cylinder $\mathbb{R}\times\mathbb{S}^2$ for a conformally coupled free massive scalar field.

A.2.1 Angular decomposition

The action is given by (5.5) with the Ricci scalar $\mathcal{R}=2/R^2$. We can regard this theory as a free massive scalar field theory

$$
I=-\frac{1}{2}\int_{\mathbb{R}\times\mathbb{S}^2}d^3x\sqrt{-g}\left[g^{\mu\nu}\partial_\mu\phi\partial_\nu\phi+m_{\rm eff}^2\,\phi^2\right]\ , \tag{A.11}
$$

with an effective mass $m_{\rm eff}^2 \equiv m^2 + \frac{1}{4R^2}$. The Hamiltonian is given as

$$H = \int_0^{\pi} d\theta \int_0^{2\pi} d\phi \, \frac{\sin\theta}{2} \left(R^2\pi^2 + (\partial_\theta \phi)^2 + \frac{(\partial_\phi \phi)^2}{\sin^2\theta} + m_{\rm eff}^2 \phi^2 \right) , \tag{A.12}$$

where the conjugate momentum $\pi = \partial_t \phi$ satisfies the canonical commutation relation

$$\begin{aligned} [\phi(\theta,\phi), \pi(\theta',\phi')] &= \frac{i}{\sqrt{g}} \delta(\theta-\theta')\delta(\phi-\phi') \, , \\ &= \frac{i}{R^2 \sin\theta} \delta(\theta-\theta')\delta(\phi-\phi') \, . \end{aligned} \tag{A.13}$$

The region $A = \{(\theta,\phi);\, 0 < \theta < \theta_0\}$ has the rotational symmetry in the ϕ direction, which allows us to reduce the space dimension to only the θ direction by a following angular decomposition

$$\begin{aligned} \phi(\theta,\phi) &= \frac{1}{\sqrt{\pi R \sin\theta}} \left(\frac{\phi_0(\theta)}{\sqrt{2}} + \sum_{n=1}^{\infty} \left(\phi_{-n}(\theta) \sin n\phi + \phi_n(\theta) \cos n\phi \right) \right) \, , \\ \pi(\theta,\phi) &= \frac{1}{\sqrt{\pi R^3 \sin\theta}} \left(\frac{\pi_0(\theta)}{\sqrt{2}} + \sum_{n=1}^{\infty} \left(\pi_{-n}(\theta) \sin n\phi + \pi_n(\theta) \cos n\phi \right) \right) . \end{aligned} \tag{A.14}$$

In this angular decomposition, the Hamiltonian (A.12)

$$H = \frac{1}{2R} \sum_{n=-\infty}^{\infty} \int_0^{\pi} d\theta \left[\pi_n^2(\theta) + \left((m_{\rm eff}R)^2 + \frac{n^2}{\sin^2\theta} \right) \phi_n^2(\theta) + \left(\sqrt{\sin\theta}\, \partial_\theta \left(\frac{\phi_n(\theta)}{\sqrt{\sin\theta}} \right) \right)^2 \right] , \tag{A.15}$$

and the commutation relation (A.13) becomes

$$[\phi_n(\theta), \pi_{n'}(\theta')] = i\delta_{nn'}\delta(\theta-\theta') \, . \tag{A.16}$$

A.2.2 Lattice discretization

We follow the discretization procedure [159]. The space coordinate θ is discretized as $\theta_j = j\pi/N$ $(j = 1, 2, \ldots, N-1)$ with dynamic variables

$$(\Phi_n^j,\ \Pi_n^j) \equiv \begin{cases} \left(\sqrt{\dfrac{2\pi}{N}} \phi_n(\theta_j), \quad \sqrt{\dfrac{\pi}{2N}} \pi_n(\theta_j) \right) , & (j = 1, N-1) \, , \\ \left(\sqrt{\dfrac{\pi}{N}} \phi_n(\theta_j), \quad \sqrt{\dfrac{\pi}{N}} \pi_n(\theta_j) \right) , & (j \neq 1, N-1) \, . \end{cases} \tag{A.17}$$

In this discretization procedure, the Hamiltonian (A.15)

$$H = \frac{1}{2R} \sum_{n=-\infty}^{\infty} \left(\sum_{j=1}^{N-1} (\Pi_n^j)^2 + \sum_{i,j=1}^{N-1} \Phi_n^i K_{ij}^{(n)} \Phi_n^j \right) , \tag{A.18}$$

and the commutation relation (A.16) becomes

$$[\Phi_n^j, \Pi_{n'}^{j'}] = i\delta_{nn'}\delta_{jj'}\,, \tag{A.19}$$

where $K_{ij}^{(n)}$ is an $(N-1)\times(N-1)$ real symmetric tridiagonal matrix

$$K_{jj}^{(n)} = \begin{cases} \dfrac{N^2}{\pi^2}\dfrac{\sin\theta_{3/2}}{2\sin\theta_1} + \dfrac{1}{4}\left((m_{\rm eff}R)^2 + \dfrac{n^2}{\sin^2\theta_1}\right)\,, & (j=1,N-1)\,, \\ \dfrac{N^2}{\pi^2}2\cos\dfrac{\pi}{2N} + \left((m_{\rm eff}R)^2 + \dfrac{n^2}{\sin^2\theta_j}\right)\,, & (j\neq 1,N-1)\,, \end{cases} \tag{A.20}$$

$$K_{j,j+1}^{(n)} = K_{j+1,j}^{(n)} = \begin{cases} -\dfrac{N^2}{\pi^2}\dfrac{\sin\theta_{3/2}}{\sqrt{2\sin\theta_1\sin\theta_2}}\,, & (j=1,N-2)\,, \\ -\dfrac{N^2}{\pi^2}\dfrac{\sin\theta_{j+1/2}}{\sqrt{\sin\theta_j\sin\theta_{j+1}}}\,, & (j\neq 1,N-2)\,, \end{cases} \tag{A.21}$$

$$K_{ij}^{(n)} = 0\,, \qquad (\,|i-j|>1\,)\,, \tag{A.22}$$

with a $\mathbb{Z}_2$ symmetry $K_{N-i,N-j} = K_{ij}$ corresponding the parity symmetry $\theta \to \pi - \theta$. This matrix $K^{(n)}$ is related to the correlation matrices $X_{ij}^{(n)} = \langle \Phi_n^i \Phi_n^j \rangle$ and $P_{ij}^{(n)} = \langle \Pi_n^i \Pi_n^j \rangle$ as $X^{(n)} = \frac{1}{2}(K^{(n)})^{-1/2}$ and $P = \frac{1}{2}(K^{(n)})^{1/2}$. The size θ_0 of the subsystem A is chosen to be a half-integer in units of the lattice spacing, $\theta_0 = (r+1/2)/N$ with an integer r. This choice corresponds to the free boundary condition in the continuum limit. In our calculation, we take $N = O(10^{2-3})$, which is sufficiently large for our purpose.

The entanglement entropy of the disk $S(\theta_0)$ is obtained by using $r\times r$ submatrices $X_r^{(n)} \equiv (X_{ij}^{(n)})_{1\le i,j\le r}$ and $P_r^{(n)} \equiv (P_{ij}^{(n)})_{1\le i,j\le r}$ as (A.4) with (A.5), where $C_n = \sqrt{X_r^{(n)} P_r^{(n)}}$ in this case.

A.2.3 Large angular momentum

In the large angular momentum limit $n\to\infty$, the correlation matrices $X^{(n)} = \frac{1}{2}(K^{(n)})^{-1/2}$ and $P^{(n)} = \frac{1}{2}(K^{(n)})^{1/2}$ approach almost diagonal matrices [85], for general symmetric tridiagonal matrices $K^{(n)}$ such as

$$\begin{aligned} K_{jj}^{(n)} &= k(j)n^2 + h(j)\,, \\ K_{j,j+1}^{(n)} = K_{j+1,j}^{(n)} &= t(j)\,, \\ K_{ij}^{(n)} &= 0 \qquad (\,|i-j|>2\,)\,. \end{aligned} \tag{A.23}$$

The products of the submatrices $X_r^{(n)} P_r^{(n)}$ almost equal to $1/4$ times unit matrix up to order $1/n^8$. The nontrivial entries are at the lower-right corners

$$\begin{aligned} (X_r^{(n)} P_r^{(n)})_{rr} &= \frac{1}{4} + \frac{c(r)}{n^4} - \frac{c(r)b(r)}{n^6} + O(1/n^8)\,, \\ (X_r^{(n)} P_r^{(n)})_{r,r-1} &= O(1/n^6)\,, \\ (X_r^{(n)} P_r^{(n)})_{r-1,r} &= O(1/n^6)\,, \end{aligned} \tag{A.24}$$

where

$$
\begin{aligned}
c(r) &\equiv \frac{t(r)^2}{4\sqrt{k(r)k(r+1)}\left(\sqrt{k(r)}+\sqrt{k(r+1)}\right)^2}\,, \\
&= \frac{N^4}{\pi^4}\frac{\sin^2\theta_{r+1/2}}{(1/\sin\theta_r + 1/\sin\theta_{r+1})^2}\,, \\
b(r) &\equiv \frac{\frac{h(r)}{\sqrt{k(r)}}+\frac{h(r+1)}{\sqrt{k(r+1)}}}{\sqrt{k(r)}+\sqrt{k(r+1)}} + \frac{h(r)}{2k(r)} + \frac{k(r+1)}{2k(r+1)}\,, \\
&= \frac{1}{2}\left((m_{\rm eff}R)^2 + \frac{N^2}{\pi^2}2\cos\frac{\pi}{2N}\right)(\sin\theta_r + \sin\theta_{r+1})^2\,.
\end{aligned}
\tag{A.25}
$$

The eigenvalues of the matrix $C_n = \sqrt{X_r^{(n)} P_r^{(n)}}$ are $1/2 + O(1/n^8)$, except one eigenvalue

$$
\frac{1}{2} + \frac{c(r)}{n^4} - \frac{c(r)b(r)}{n^6} + O(1/n^8)\,. \tag{A.26}
$$

Therefore, most of the eigenvalues do not contribute to the n-th entanglement entropy (A.5) up to order $1/n^8$ and we obtain

$$
S_n = \frac{c(r)}{n^4}\left(1 - \log\frac{c(r)}{n^4}\right) + \frac{c(r)b(r)}{n^6}\log\frac{c(r)}{n^4} + O(1/n^8)\ . \tag{A.27}
$$

And we perform the matrix trace calculation (A.5) in the same way as the annulus case.

Appendix B

Details of holographic calculations

B.1 γ-expansion in the Janus black hole

Here we compute the area of the extremal surface for an interval region and the phase transition time for the region of two intervals in the time-dependent Janus black hole, in the leading order of the Janus deformation parameter γ^2.

First, let us obtain the relation $y_* = y_*(t_\infty, \theta_\infty)$ in the leading order. This can be performed by expanding (4.27) in γ^2. The integrand in the left hand side can be evaluated as

$$\frac{\tilde{g}(y)^2}{\sqrt{\tilde{g}(y_*)^2 - \tilde{g}(y)^2}} = \frac{\operatorname{sech}^2 y}{\sqrt{\operatorname{sech}^2 y_* - \operatorname{sech}^2 y}} + \frac{\operatorname{sech}^2 y(2 - \operatorname{sech}^2 y + \operatorname{sech}^2 y_*)}{4\sqrt{\operatorname{sech}^2 y_* - \operatorname{sech}^2 y}}\gamma^2 + \mathcal{O}(\gamma^4)\,, \tag{B.1}$$

and thus

$$\begin{aligned}
&\int_{y_*}^{y_\infty} dy\, \frac{\tilde{g}(y)^2}{\sqrt{\tilde{g}(y_*)^2 - \tilde{g}(y)^2}} \\
&\quad = \left[\tanh^{-1}\left(\frac{\cosh y_* \sinh y}{\sqrt{\cosh^2 y_* - \cosh^2 y}}\right)\right]_{y_*}^{y_\infty} \\
&\qquad + \left[\frac{3\cosh^2 y_* + 1}{8\cosh^2 y_*}\tanh^{-1}\left(\frac{\cosh y_* \sinh y}{\sqrt{\cosh^2 y_* - \cosh^2 y}}\right) + \frac{1}{8\cosh y_*}\frac{\sqrt{\cosh^2 y - \cosh^2 y_*}}{\sinh y}\right]_{y_*}^{y_\infty}\gamma^2 + \mathcal{O}(\gamma^4) \\
&\quad = \tanh^{-1}(\operatorname{sech} y_*) + \left(\frac{3\cosh^2 y_* + 1}{8\cosh^2 y_*}\tanh^{-1}(\operatorname{sech} y_*) + \frac{1}{8\cosh y_*}\right)\gamma^2 + \mathcal{O}(\gamma^4)\,.
\end{aligned} \tag{B.2}$$

By substituting this relation into (4.27), we obtain

$$\begin{aligned}
\frac{\sinh r_0\theta}{\cosh r_0 t} &= \sinh\left[\tanh^{-1}(\operatorname{sech} y_*) + \left(\frac{3\cosh^2 y_* + 1}{8\cosh^2 y_*}\tanh^{-1}(\operatorname{sech} y_*) + \frac{1}{8\cosh y_*}\right)\gamma^2 + \mathcal{O}(\gamma^4)\right] \\
&= \frac{1}{\sinh y_*} + \left(\frac{3\cosh^2 y_* + 1}{8\cosh y_* \sinh y_*}\tanh^{-1}(\operatorname{sech} y_*) + \frac{1}{8\sinh y_*}\right)\gamma^2 + \mathcal{O}(\gamma^4)\,,
\end{aligned} \tag{B.3}$$

from which the desired relation $y_* = y_*(t_\infty, \theta_\infty)$ follows,

$$\sinh y_* = F\left[1 + \left(\frac{3F^2+4}{8\sqrt{1+F^2}} \coth^{-1}\left(\sqrt{1+F^2}\right) + \frac{1}{8}\right)\gamma^2\right] + \mathcal{O}(\gamma^4)\,, \tag{B.4}$$

where

$$F(t_\infty, \theta_\infty) = \frac{\cosh r_0 t_\infty}{\sinh r_0 \theta_\infty}\,. \tag{B.5}$$

Then the area On the other hand, from (4.28) and (4.30), γ^2-expansion gives

$$A^{(\mathrm{reg})}/L = 2\log\frac{2\cosh r_0 t}{r_0 \sinh y_*} + \left(1 + \frac{1}{2}\operatorname{sech} y_* \tanh^{-1}(\operatorname{sech} y_*)\right)\gamma^2 + \mathcal{O}(\gamma^4)\,. \tag{B.6}$$

By using (B.4) above, this results in

$$A^{(\mathrm{reg})}/L = 2\log\left(\frac{2}{r_0}\sinh r_0\theta\right) - \left(\frac{3F^2+2}{4\sqrt{1+F^2}} \coth^{-1}\left(\sqrt{1+F^2}\right) - \frac{3}{4}\right)\gamma^2 + \mathcal{O}(\gamma^4)\,. \tag{B.7}$$

On the other hand, the phase transition time t_c for a fixed value of θ can be computed by an equation

$$A^{(\mathrm{reg})}_{dc} = A^{(\mathrm{reg})}_{c}\,, \tag{B.8}$$

with the aid of (4.46), (B.7) and $A_{dc} = 2A$. This equation is solved as $t = t_c$, where

$$t_c = t_c^{(0)} + t_c^{(1)}\gamma^2 + \mathcal{O}(\gamma^4)\,, \tag{B.9}$$

$$r_0 t_c^{(0)} = \cosh^{-1}(\sinh r_0\theta)\,, \tag{B.10}$$

$$\begin{aligned} r_0 t_c^{(1)} &= -\left(\frac{1}{2} + \frac{5}{2\sqrt{2}}\coth^{-1}(\sqrt{2})\right)\frac{\sinh r_0\theta}{\sqrt{\sinh^2 r_0\theta - 1}} \\ &\simeq -2.058 \times \frac{\sinh r_0\theta}{\sqrt{\sinh^2 r_0\theta - 1}}\,. \end{aligned} \tag{B.11}$$

In the large θ limit ($\theta \gg r_0^{-1}$) in particular, we obtain

$$t_c \simeq \theta - 2.058\gamma^2 + \mathcal{O}(\gamma^4)\,. \tag{B.12}$$

B.2 On holographic calculation of $C(1)$ using graviton propagator

Here we use the expression (6.48) including the graviton propagator to calculate $C(1)$ for a spherical entangling surface. First, we reproduce the formula

$$C(n) = \frac{\pi}{4G_N n}\int d^{d-1}y\, d^{d-1}y'\, \sqrt{g(y)}\sqrt{g(y')}J(y,y')\,, \tag{B.13}$$

where

$$J(y,y') \equiv \frac{\partial X^\mu}{\partial y^i}\frac{\partial X^\nu}{\partial y_i} G_{\mu\nu\alpha\beta}(X(y),X(y'))\frac{\partial X^\alpha}{\partial y'^j}\frac{\partial X^\beta}{\partial y'_j}\,. \tag{B.14}$$

There is a difficulty related to the boundary term in this formula as commented in [139] and pointing it out is the purpose of this appendix.

The graviton propagator $G_{\mu\nu\alpha\beta}$ is not known for the backreacted metric with general n, while the metric is just AdS_{d+1} for $n=1$ whose graviton propagator $G_{\mu\nu\mu'\nu'}(X,X')$ can be represented as [160]

$$G_{\mu\nu\mu'\nu'}(X,X') = (\partial_\mu\partial_{\mu'}D\,\partial_\nu\partial_{\nu'}D + (\mu\leftrightarrow\nu))G(D) + G_{\mu\nu}(X)G_{\mu'\nu'}(X')H(D) + \cdots\,. \tag{B.15}$$

The $(\cdots)$ terms are gauge-dependent and do not matter when the bulk energy momentum tensor $T_{\mu\nu}$ vanishes at the boundary fast enough, but they would contribute in the current setup because the energy-momentum tensor of the brane does not decay at the boundary. The $(\cdots)$ term is too complicated to be taken into account, and we proceed without having them for a moment.

We are going to evaluate the $G(D)$ and $H(D)$ parts. $\partial_\mu = \partial/\partial X^\mu$ and $\partial_{\mu'} = \partial/\partial X'^{\mu'}$ are derivatives with respect to the bulk points X and X'. The two functions $G(D)$ and $H(D)$ are given by

$$G(D) = \tilde{C}_d\left(\frac{2}{D}\right)^d F(d,\frac{d+1}{2};d+1;-\frac{2}{D})\,, \tag{B.16}$$

$$H(D) = -\frac{2(D+1)^2}{d-1}G(D) + \frac{4(d-2)(D+1)}{(d-1)^2}\tilde{C}_d\left(\frac{2}{D}\right)^{d-1} F(d-1,\frac{d+1}{2};d+1;-\frac{2}{D})\,, \tag{B.17}$$

with a constant

$$\tilde{C}_d = \frac{\Gamma(\frac{d+1}{2})}{(4\pi)^{\frac{d+1}{2}}d} = \frac{1}{2^d d\,\mathrm{Vol}(\mathbb{S}^d)}\,. \tag{B.18}$$

The function $D = D(X,X')$ is the invariant distance between the two points X and X',

$$D = \frac{1}{2}\left[-(X'_{-1}-X_{-1})^2 + (X'_0-X_0)^2 + (X'_1-X_1)^2 + \cdots + (X'_d-X_d)^2\right]\,, \tag{B.19}$$

in the Euclidean AdS_{d+1} space realized as an embedding $-X_{-1}^2+X_0^2+X_1^2+\cdots+X_d^2=-1$ in $\mathbb{R}^{1,d+1}$, with the metric $ds^2 = -dX_{-1}^2 + dX_0^2 + dX_1^2 + \cdots + dX_d^2$. An expression of D in the hyperbolic coordinate

$$ds_{d+1}^2 = \frac{dr^2}{r^2-1} + (r^2-1)d\tau^2 + r^2(du^2 + \sinh^2 u\, d\Omega_{d-2}^2)\,, \tag{B.20}$$

follows from the coordinate transformation

$$\begin{aligned} X_{-1} &= r\cosh u\,, & X_i &= r\sinh u\,\Omega_{i-1} \quad (i=2,\ldots,d)\,,\\ X_0 &= \sqrt{r^2-1}\sin\tau\,, & X_1 &= \sqrt{r^2-1}\cos\tau\,. \end{aligned} \tag{B.21}$$

The minimal surface is the horizon $r = 1$ of the topological black hole at $\tau = 0$, on which the invariant distance D becomes

$$D(u', \Omega_i'; u, \Omega_i) = \cosh u \cosh u' - \sinh u \sinh u' \sum_{i=1}^{d-1} \Omega_i \Omega_i' - 1 \,. \tag{B.22}$$

The function J is calculated as[1] [2]

$$J = 2\Big((D+1)^2 + d - 2\Big) G(D) + (d-1)^2 H(D) + \cdots \,, \tag{B.25}$$

which is just a function of the invariant distance D. The symmetry of the hyperbolic space $\mathbb{H}^{d-1}$ allows us to move the two points to $(u', \Omega') = (0, 0)$ and $(u, \Omega) = (u, 0)$, and factor out the integrals over u', Ω' and Ω:

$$\begin{aligned} C(1) &= \frac{\pi}{4G_N} \int du\, du'\, d\Omega_{d-2}\, d\Omega_{d-2}' \sinh^{d-2} u \sinh^{d-2} u'\, J(D) \,, \\ &= \frac{\mathrm{Vol}(\mathbb{H}^{d-1})}{4G_N} \pi \mathrm{Vol}(\mathbb{S}^{d-2}) \int du \sinh^{d-2} u\, J(D) \,, \end{aligned} \tag{B.26}$$

where $D = D(u, 0; 0, 0) = \cosh u - 1$. The integration of $G(D)$ and $H(D)$ parts of $J(D)$ can be performed as

$$C(1) = \frac{\mathrm{Vol}(\mathbb{H}^{d-1})}{4G_N} \left(\frac{d-2}{d} + \cdots \right) . \tag{B.27}$$

Compared with the previous result (6.80), we speculate that the gauge-dependent part contributes $2/d$. It would be desirable to include the gauge-dependent contribution in order to confirm our conjecture, but we leave it to future investigations.

[1] To calculate $J = J(D)$, it is easier to work in Poincaré coordinate $ds_{d+1}^2 = (dz^2 + \sum_{i=0}^{d-1} dx_i^2)/z^2$ related by

$$X_{-1} = \frac{z}{2} + \frac{1 + \sum_{i=0}^{d-1} x_i^2}{2z}, \qquad X_i = \frac{x_i}{z} \quad (i = 0, \ldots, d-1), \qquad X_d = \frac{z}{2} + \frac{-1 + \sum_{i=0}^{d-1} x_i^2}{2z} \,, \tag{B.23}$$

because the minimal surface is mapped to just a plane $x^0 = x^1 = 0$.

[2] The $(\cdots)$ term would be represented as

$$\begin{aligned} (\cdots) = {} & 2\big(d(D+1)^2 - 1\big) X(D) + 2D(D+1)(D+2) X'(D) \\ & + 2(d+1) D(D+1)(D+2) Y(D) + 2D^2 (D+2)^2 Y'(D) \\ & + 2(d-1)^2 (D+1) Z(D) + 2(d-1) D(D+2) Z'(D) \,, \end{aligned} \tag{B.24}$$

with functions X, Y, Z given implicitly in [139].

Appendix C

Details of field theory calculations

C.1 Integration of the conformal factor

We can exactly perform the integral V_n (5.16) of the conformal factor on $\mathbb{S}^1_n \times \mathbb{H}^2$

$$\begin{aligned} V_n &= \int_0^{2n\pi} d\tau \int_0^\infty du \int_{\mathbb{S}^1} d\Omega_1 \, (R^3 \sinh u)\, e^{-2\sigma(\tau,u)} \,, \\ &= 2n\pi R^3 \int_0^{2\pi} d\tau \int_0^\infty du \, \frac{\sinh u \, \sin^2\theta_0}{(\cos\tau + \cos\theta_0 \, \cosh u)^2 + \sin^2\theta_0 \sinh^2 u} \,, \end{aligned} \tag{C.1}$$

thanks to an integration formula

$$\int_0^{2\pi} \frac{d\tau}{(\cos\tau + c)^2 + s^2} = -\frac{i\pi}{s} \left[\frac{1}{\sqrt{(c-is)^2 - 1}} - \frac{1}{\sqrt{(c+is)^2 - 1}} \right] , \tag{C.2}$$

which we will apply with $c = \cos\theta_0 \cosh u$ and $s = \sin\theta_0 \sinh u$. Because $\cos\theta_0 \cosh u \pm i \sin\theta_0 \sinh u = \cosh(u \pm i\theta_0)$, the integration formula tells us that

$$\begin{aligned} \int_0^{2\pi} \frac{d\tau}{(\cos\tau + \cos\theta_0 \cosh u)^2 + \sin^2\theta_0 \sinh^2 u} &= -\frac{i\pi}{\sin\theta_0 \sinh u} \left[\frac{1}{\sinh(u - i\theta_0)} - \frac{1}{\sinh(u + i\theta_0)} \right] , \\ &= \frac{2\pi \coth u}{\sinh^2 u + \sin^2\theta_0} \,. \end{aligned} \tag{C.3}$$

Plugging this result into the original integration (C.1), we finally obtain

$$\begin{aligned} V_n &= 4n\pi^2 \sin\theta_0^2 \, R^3 \int_0^\infty \frac{d(\sinh u)}{\sinh^2 u + \sin^2\theta_0} \,, \\ &= 2n\pi^3 \sin\theta_0 \, R^3 \,. \end{aligned} \tag{C.4}$$

C.2 Possible extension of SSA to Rényi entropies

We have given a holographic proof of the Rényi entropic inequalities, but they are not related to the strong sub-additivity of entanglement entropy (2.93). In fact, the Rényi

entropy S_n is nether strong sub-additive nor sub-additive (2.91). The modular entropy $\tilde{S}_n$ (2.121) does not satisfy them too.

To achieve the sub-additivity and strong sub-additivity of the Rényi entropy, it would be helpful to review how these inequalities for entanglement entropies are related to information theoretic measures. As explained in chapter 2, these inequalities follow from properties of the relative entropy (2.87) $S[\rho|\sigma] \equiv \mathrm{Tr}[\rho(\log\rho - \log\sigma)]$. The non-negativity of relative entropy is equivalent to the non-negativity the mutual information and thus the sub-additivity of entanglement entropy. On the other hand, its monotonicity with partial traces is equivalent to the monotonicity of the mutual information and thus the strong sub-additivity of entanglement entropy.

Now one way to generalize these inequalities to the Rényi entropy is then extending the definition of relative entropy and so mutual information to Rényi entropy. One promising proposal of such a relative Rényi entropy is [161, 162]

$$S_n[\rho|\sigma] \equiv \frac{1}{n-1}\log \mathrm{Tr}[(\sigma^{\frac{1-n}{2n}}\rho\sigma^{\frac{1-n}{2n}})^n]\,, \tag{C.5}$$

which reduces to the relative entropy $S[\rho|\sigma]$ in the limit $n \to 1$. This generalization of the relative entropy keeps the non-negativity $S_n[\rho|\sigma] \geq 0$ and monotonicity $S_n[\rho|\sigma] \geq S_n[\mathrm{Tr}_B\rho|\mathrm{Tr}_B\sigma]$ under partial traces [163]. So we assert that the Rényi generalization of the sub-additivity would be

$$I_n(A,B) \equiv S_n[\rho_{AB}|\rho_A\otimes\rho_B] \geq 0\,, \tag{C.6}$$

and the Rényi generalization of the strong sub-additivity would be

$$I_n(A, B\cup C) \geq I_n(A,C)\,. \tag{C.7}$$

For entanglement entropy with $n = 1$, these inequalities admit a holographic interpretation. For the Rényi entropy for any n, however, it is not possible to express the relative Rényi entropy $S_n[\rho|\sigma]$ or Rényi mutual information I_n as a linear combination of the Rényi entropies. So it is not clear how to interpret these Rényi-generalized inequalities holographically, even though we have the holographic Rényi entropy formula. The expression of the relative Rényi entropy (C.5) suggests that it can be calculated by the replica method [164] and it may have an interpretation and proof of these Rényi-generalized inequalities in a holographic system.

Bibliography

[1] Y. Nakaguchi and T. Nishioka, *Entanglement Entropy of Annulus in Three Dimensions*, *JHEP* **04** (2015) 072, [arXiv:1501.01293].

[2] Y. Nakaguchi, N. Ogawa, and T. Ugajin, *Holographic Entanglement and Causal Shadow in Time-Dependent Janus Black Hole*, *JHEP* **07** (2015) 080, [arXiv:1412.8600].

[3] S. Banerjee, Y. Nakaguchi, and T. Nishioka, *Renormalized Entanglement Entropy on Cylinder*, *JHEP* **03** (2016) 048, [arXiv:1508.00979].

[4] Y. Nakaguchi and T. Nishioka, *A Holographic Proof of RÉnyi Entropic Inequalities*, arXiv:1606.08443.

[5] G. 't Hooft, *Dimensional Reduction in Quantum Gravity*, in *Salamfest 1993:0284-296*, pp. 0284–296, 1993. gr-qc/9310026.

[6] L. Susskind, *The World as a Hologram*, *J. Math. Phys.* **36** (1995) 6377–6396, [hep-th/9409089].

[7] R. Bousso, *The Holographic Principle*, *Rev. Mod. Phys.* **74** (2002) 825–874, [hep-th/0203101].

[8] J. M. Maldacena, *The Large N Limit of Superconformal Field Theories and Supergravity*, *Int. J. Theor. Phys.* **38** (1999) 1113–1133, [hep-th/9711200]. [Adv. Theor. Math. Phys.2,231(1998)].

[9] A. Strominger, *Black Hole Entropy from Near Horizon Microstates*, *JHEP* **02** (1998) 009, [hep-th/9712251].

[10] E. Witten, *Anti-de Sitter Space, Thermal Phase Transition, and Confinement in Gauge Theories*, *Adv. Theor. Math. Phys.* **2** (1998) 505–532, [hep-th/9803131].

[11] J. M. Maldacena and A. Strominger, *AdS^3 Black Holes and a Stringy Exclusion Principle*, *JHEP* **12** (1998) 005, [hep-th/9804085].

[12] J. M. Maldacena, *Eternal Black Holes in Anti-de Sitter*, *JHEP* **04** (2003) 021, [hep-th/0106112].

[13] P. Kraus, H. Ooguri, and S. Shenker, *Inside the Horizon with AdS / CFT*, *Phys. Rev.* **D67** (2003) 124022, [hep-th/0212277].

[14] L. Fidkowski, V. Hubeny, M. Kleban, and S. Shenker, *The Black Hole Singularity in AdS / CFT*, *JHEP* **02** (2004) 014, [hep-th/0306170].

[15] D. Bak, M. Gutperle, and S. Hirano, *Three Dimensional Janus and Time-Dependent Black Holes*, *JHEP* **02** (2007) 068, [hep-th/0701108].

[16] D. Bak, M. Gutperle, and A. Karch, *Time Dependent Black Holes and Thermal Equilibration*, *JHEP* **12** (2007) 034, [arXiv:0708.3691].

[17] S. Bhattacharyya and S. Minwalla, *Weak Field Black Hole Formation in Asymptotically AdS Spacetimes*, *JHEP* **09** (2009) 034, [arXiv:0904.0464].

[18] V. Balasubramanian, A. Bernamonti, J. de Boer, N. Copland, B. Craps, E. Keski-Vakkuri, B. Muller, A. Schafer, M. Shigemori, and W. Staessens, *Holographic Thermalization*, *Phys. Rev.* **D84** (2011) 026010, [arXiv:1103.2683].

[19] A. Strominger and C. Vafa, *Microscopic Origin of the Bekenstein-Hawking Entropy*, *Phys. Lett.* **B379** (1996) 99–104, [hep-th/9601029].

[20] C. G. Callan and J. M. Maldacena, *D-Brane Approach to Black Hole Quantum Mechanics*, *Nucl. Phys.* **B472** (1996) 591–610, [hep-th/9602043].

[21] S. S. Gubser, I. R. Klebanov, and A. M. Polyakov, *Gauge Theory Correlators from Noncritical String Theory*, *Phys. Lett.* **B428** (1998) 105–114, [hep-th/9802109].

[22] E. Witten, *Anti-de Sitter Space and Holography*, *Adv. Theor. Math. Phys.* **2** (1998) 253–291, [hep-th/9802150].

[23] I. R. Klebanov and E. Witten, *AdS / CFT Correspondence and Symmetry Breaking*, *Nucl. Phys.* **B556** (1999) 89–114, [hep-th/9905104].

[24] O. Aharony, S. S. Gubser, J. M. Maldacena, H. Ooguri, and Y. Oz, *Large N Field Theories, String Theory and Gravity*, *Phys. Rept.* **323** (2000) 183–386, [hep-th/9905111].

[25] G. T. Horowitz and R. C. Myers, *The AdS / CFT Correspondence and a New Positive Energy Conjecture for General Relativity*, *Phys. Rev.* **D59** (1998) 026005, [hep-th/9808079].

[26] I. R. Klebanov and M. J. Strassler, *Supergravity and a Confining Gauge Theory: Duality Cascades and Chi Sb Resolution of Naked Singularities*, *JHEP* **08** (2000) 052, [hep-th/0007191].

[27] M. Cvetič, G. W. Gibbons, H. Lu, and C. N. Pope, *Ricci Flat Metrics, Harmonic Forms and Brane Resolutions*, *Commun. Math. Phys.* **232** (2003) 457–500, [hep-th/0012011].

[28] S. A. Hartnoll, C. P. Herzog, and G. T. Horowitz, *Building a Holographic Superconductor*, *Phys. Rev. Lett.* **101** (2008) 031601, [arXiv:0803.3295].

[29] S. A. Hartnoll, *Lectures on Holographic Methods for Condensed Matter Physics*, *Class. Quant. Grav.* **26** (2009) 224002, [arXiv:0903.3246].

[30] C. P. Herzog, *Lectures on Holographic Superfluidity and Superconductivity*, *J. Phys.* **A42** (2009) 343001, [arXiv:0904.1975].

[31] S. Sachdev, *Condensed Matter and AdS/CFT*, arXiv:1002.2947. [Lect. Notes Phys.828,273(2011)].

[32] S. Kachru, X. Liu, and M. Mulligan, *Gravity Duals of Lifshitz-Like Fixed Points*, *Phys. Rev.* **D78** (2008) 106005, [arXiv:0808.1725].

[33] K. Balasubramanian and J. McGreevy, *Gravity Duals for Non-Relativistic CFTs*, *Phys. Rev. Lett.* **101** (2008) 061601, [arXiv:0804.4053].

[34] D. T. Son, *Toward an AdS/Cold Atoms Correspondence: a Geometric Realization of the Schrödinger Symmetry*, *Phys. Rev.* **D78** (2008) 046003, [arXiv:0804.3972].

[35] I. R. Klebanov and A. M. Polyakov, *AdS Dual of the Critical $O(N)$ Vector Model*, *Phys. Lett.* **B550** (2002) 213–219, [hep-th/0210114].

[36] M. A. Vasiliev, *Nonlinear Equations for Symmetric Massless Higher Spin Fields in $(A)DS^D$*, *Phys. Lett.* **B567** (2003) 139–151, [hep-th/0304049].

[37] S. Giombi, *Tasi Lectures on the Higher Spin - CFT Duality*, arXiv:1607.02967.

[38] A. Strominger, *The Ds / CFT Correspondence*, *JHEP* **10** (2001) 034, [hep-th/0106113].

[39] S. W. Hawking, M. J. Perry, and A. Strominger, *Soft Hair on Black Holes*, *Phys. Rev. Lett.* **116** (2016), no. 23 231301, [arXiv:1601.00921].

[40] A. Bagchi, R. Basu, A. Kakkar, and A. Mehra, *Flat Holography: Aspects of the Dual Field Theory*, arXiv:1609.06203.

[41] S. Ryu and T. Takayanagi, *Holographic Derivation of Entanglement Entropy from AdS/CFT*, *Phys. Rev. Lett.* **96** (2006) 181602, [hep-th/0603001].

[42] S. Ryu and T. Takayanagi, *Aspects of Holographic Entanglement Entropy*, *JHEP* **08** (2006) 045, [hep-th/0605073].

[43] J. D. Bekenstein, *Black Holes and Entropy*, *Phys. Rev.* **D7** (1973) 2333–2346.

[44] S. W. Hawking, *Particle Creation by Black Holes*, in *1St Oxford Conference on Quantum Gravity Chilton, England, February 15-16, 1974*, pp. 219–267, 1975.

[45] T. Takayanagi, *Entanglement Entropy from a Holographic Viewpoint*, *Class.Quant.Grav.* **29** (2012) 153001, [arXiv:1204.2450].

[46] D. Harlow, *Jerusalem Lectures on Black Holes and Quantum Information*, *Rev. Mod. Phys.* **88** (2016) 15002, [arXiv:1409.1231]. [Rev. Mod. Phys.88,15002(2016)].

[47] T. Faulkner, M. Guica, T. Hartman, R. C. Myers, and M. Van Raamsdonk, *Gravitation from Entanglement in Holographic CFTs*, *JHEP* **03** (2014) 051, [arXiv:1312.7856].

[48] H. Li and F. D. M. Haldane, *Entanglement spectrum as a generalization of entanglement entropy: Identification of topological order in non-abelian fractional quantum hall effect states*, *Phys. Rev. Lett.* **101** (Jul, 2008) 010504.

[49] C. Holzhey, F. Larsen, and F. Wilczek, *Geometric and Renormalized Entropy in Conformal Field Theory*, *Nucl.Phys.* **B424** (1994) 443–467, [hep-th/9403108].

[50] P. Calabrese and J. L. Cardy, *Entanglement Entropy and Quantum Field Theory*, *J. Stat. Mech.* **0406** (2004) P06002, [hep-th/0405152].

[51] M. Srednicki, *Entropy and Area*, *Phys. Rev. Lett.* **71** (1993) 666–669, [hep-th/9303048].

[52] I. Peschel, *Calculation of reduced density matrices from correlation functions*, *Journal of Physics A: Mathematical and General* **36** (2003), no. 14 L205.

[53] H. Casini and M. Huerta, *Entanglement Entropy in Free Quantum Field Theory*, *J. Phys.* **A42** (2009) 504007, [arXiv:0905.2562].

[54] I. R. Klebanov, S. S. Pufu, and B. R. Safdi, *F-Theorem without Supersymmetry*, *JHEP* **10** (2011) 038, [arXiv:1105.4598].

[55] H. Casini and M. Huerta, *On the RG Running of the Entanglement Entropy of a Circle*, *Phys. Rev.* **D85** (2012) 125016, [arXiv:1202.5650].

[56] S. N. Solodukhin, *Entanglement Entropy, Conformal Invariance and Extrinsic Geometry*, *Phys. Lett.* **B665** (2008) 305–309, [arXiv:0802.3117].

[57] D. V. Fursaev, A. Patrushev, and S. N. Solodukhin, *Distributional Geometry of Squashed Cones*, *Phys. Rev.* **D88** (2013), no. 4 044054, [arXiv:1306.4000].

[58] H. Casini, M. Huerta, and R. C. Myers, *Towards a Derivation of Holographic Entanglement Entropy*, *JHEP* **05** (2011) 036, [arXiv:1102.0440].

[59] M. Huerta, *Numerical Determination of the Entanglement Entropy for Free Fields in the Cylinder*, *Phys. Lett.* **B710** (2012) 691–696, [arXiv:1112.1277].

[60] T. Grover, A. M. Turner, and A. Vishwanath, *Entanglement Entropy of Gapped Phases and Topological Order in Three Dimensions*, *Phys. Rev.* **B84** (2011) 195120, [arXiv:1108.4038].

[61] A. Kitaev and J. Preskill, *Topological Entanglement Entropy*, *Phys. Rev. Lett.* **96** (2006) 110404, [hep-th/0510092].

[62] M. Levin and X.-G. Wen, *Detecting Topological Order in a Ground State Wave Function*, *Phys. Rev. Lett.* **96** (2006) 110405.

[63] M. P. Hertzberg and F. Wilczek, *Some Calculable Contributions to Entanglement Entropy*, *Phys. Rev. Lett.* **106** (2011) 050404, [arXiv:1007.0993].

[64] A. Lewkowycz, R. C. Myers, and M. Smolkin, *Observations on Entanglement Entropy in Massive Qft's*, *JHEP* **04** (2013) 017, [arXiv:1210.6858].

[65] H. Liu and M. Mezei, *A Refinement of Entanglement Entropy and the Number of Degrees of Freedom*, *JHEP* **04** (2013) 162, [arXiv:1202.2070].

[66] D. L. Jafferis, I. R. Klebanov, S. S. Pufu, and B. R. Safdi, *Towards the F-Theorem: $\mathcal{N} = 2$ Field Theories on the Three-Sphere*, *JHEP* **06** (2011) 102, [arXiv:1103.1181].

[67] R. C. Myers and A. Sinha, *Seeing a C-Theorem with Holography*, *Phys. Rev.* **D82** (2010) 046006, [arXiv:1006.1263].

[68] R. C. Myers and A. Sinha, *Holographic C-Theorems in Arbitrary Dimensions*, *JHEP* **01** (2011) 125, [arXiv:1011.5819].

[69] A. B. Zamolodchikov, *Irreversibility of the Flux of the Renormalization Group in a 2D Field Theory*, *JETP Lett.* **43** (1986) 730–732. [Pisma Zh. Eksp. Teor. Fiz.43,565(1986)].

[70] E. Lieb and M. Ruskai, *Proof of the Strong Subadditivity of Quantum-Mechanical Entropy*, *J.Math.Phys.* **14** (1973) 1938–1941.

[71] H. Casini and M. Huerta, *A C-Theorem for the Entanglement Entropy*, *J. Phys.* **A40** (2007) 7031–7036, [cond-mat/0610375].

[72] M. Headrick and T. Takayanagi, *A Holographic Proof of the Strong Subadditivity of Entanglement Entropy*, *Phys. Rev.* **D76** (2007) 106013, [arXiv:0704.3719].

[73] A. C. Wall, *Maximin Surfaces, and the Strong Subadditivity of the Covariant Holographic Entanglement Entropy*, *Class.Quant.Grav.* **31** (2014), no. 22 225007, [arXiv:1211.3494].

[74] M. Headrick, *General Properties of Holographic Entanglement Entropy*, *JHEP* **1403** (2014) 085, [arXiv:1312.6717].

[75] P. Hayden, M. Headrick, and A. Maloney, *Holographic Mutual Information is Monogamous*, *Phys.Rev.* **D87** (2013), no. 4 046003, [arXiv:1107.2940].

[76] N. Bao, S. Nezami, H. Ooguri, B. Stoica, J. Sully, and M. Walter, *The Holographic Entropy Cone*, *JHEP* **09** (2015) 130, [arXiv:1505.07839].

[77] A. Lewkowycz and J. Maldacena, *Generalized Gravitational Entropy*, *JHEP* **08** (2013) 090, [arXiv:1304.4926].

[78] V. E. Hubeny, M. Rangamani, and T. Takayanagi, *A Covariant Holographic Entanglement Entropy Proposal*, *JHEP* **07** (2007) 062, [arXiv:0705.0016].

[79] X. Dong, A. Lewkowycz, and M. Rangamani, *Deriving Covariant Holographic Entanglement*, *JHEP* **11** (2016) 028, [arXiv:1607.07506].

[80] X. Dong, *An Area-Law Prescription for Holographic Renyi Entropies*, arXiv:1601.06788.

[81] X. Dong, *Holographic Entanglement Entropy for General Higher Derivative Gravity*, *JHEP* **01** (2014) 044, [arXiv:1310.5713].

[82] J. Camps and W. R. Kelly, *Generalized Gravitational Entropy without Replica Symmetry*, *JHEP* **03** (2015) 061, [arXiv:1412.4093].

[83] D. V. Fursaev and S. N. Solodukhin, *On the Description of the Riemannian Geometry in the Presence of Conical Defects*, *Phys. Rev.* **D52** (1995) 2133–2143, [hep-th/9501127].

[84] J. D. Brown and M. Henneaux, *Central Charges in the Canonical Realization of Asymptotic Symmetries: an Example from Three-Dimensional Gravity*, *Commun. Math. Phys.* **104** (1986) 207–226.

[85] I. R. Klebanov, T. Nishioka, S. S. Pufu, and B. R. Safdi, *On Shape Dependence and RG Flow of Entanglement Entropy*, *JHEP* **07** (2012) 001, [arXiv:1204.4160].

[86] B. R. Safdi, *Exact and Numerical Results on Entanglement Entropy in (5+1)-Dimensional CFT*, *JHEP* **12** (2012) 005, [arXiv:1206.5025].

[87] T. Hirata and T. Takayanagi, *AdS/CFT and Strong Subadditivity of Entanglement Entropy*, *JHEP* **02** (2007) 042, [hep-th/0608213].

[88] H. Casini and M. Huerta, *Entanglement and Alpha Entropies for a Massive Scalar Field in Two Dimensions*, *J. Stat. Mech.* **0512** (2005) P12012, [cond-mat/0511014].

[89] J. Cardy, *Some Results on the Mutual Information of Disjoint Regions in Higher Dimensions*, *J. Phys.* **A46** (2013) 285402, [arXiv:1304.7985].

[90] N. Shiba, *Entanglement Entropy of Two Black Holes and Entanglement Entropic Force*, *Phys. Rev.* **D83** (2011) 065002, [arXiv:1011.3760].

[91] N. Shiba, *Entanglement Entropy of Two Spheres*, *JHEP* **07** (2012) 100, [arXiv:1201.4865].

[92] N. Drukker and B. Fiol, *On the Integrability of Wilson Loops in* $\mathrm{AdS}_5 \times S^5$*: Some Periodic Ansatze*, *JHEP* **01** (2006) 056, [hep-th/0506058].

[93] A. Dekel and T. Klose, *Correlation Function of Circular Wilson Loops at Strong Coupling*, *JHEP* **11** (2013) 117, [arXiv:1309.3203].

[94] P. Fonda, L. Giomi, A. Salvio, and E. Tonni, *On Shape Dependence of Holographic Mutual Information in* AdS_4, *JHEP* **02** (2015) 005, [arXiv:1411.3608].

[95] T. Faulkner, A. Lewkowycz, and J. Maldacena, *Quantum Corrections to Holographic Entanglement Entropy*, *JHEP* **11** (2013) 074, [arXiv:1307.2892].

[96] N. Engelhardt and A. C. Wall, *Quantum Extremal Surfaces: Holographic Entanglement Entropy Beyond the Classical Regime*, *JHEP* **01** (2015) 073, [arXiv:1408.3203].

[97] I. R. Klebanov and S. S. Pufu, *M-Branes and Metastable States*, *JHEP* **08** (2011) 035, [arXiv:1006.3587].

[98] T. Nishioka and T. Takayanagi, *AdS Bubbles, Entropy and Closed String Tachyons*, *JHEP* **01** (2007) 090, [hep-th/0611035].

[99] I. R. Klebanov, D. Kutasov, and A. Murugan, *Entanglement as a Probe of Confinement*, *Nucl. Phys.* **B796** (2008) 274–293, [arXiv:0709.2140].

[100] C. A. Agon and H. J. Schnitzer, *Holographic Mutual Information at Small Separations*, arXiv:1501.03775.

[101] L. Girardello, M. Petrini, M. Porrati, and A. Zaffaroni, *Novel Local CFT and Exact Results on Perturbations of* $\mathcal{N} = 4$ *Superyang Mills from AdS Dynamics*, *JHEP* **12** (1998) 022, [hep-th/9810126].

[102] D. Z. Freedman, S. S. Gubser, K. Pilch, and N. P. Warner, *Renormalization Group Flows from Holography Supersymmetry and a c-Theorem*, *Adv. Theor. Math. Phys.* **3** (1999) 363–417, [hep-th/9904017].

[103] C. P. Herzog and M. Spillane, *Tracing Through Scalar Entanglement*, *Phys. Rev.* **D87** (2013), no. 2 025012, [arXiv:1209.6368].

[104] C. P. Herzog and T. Nishioka, *Entanglement Entropy of a Massive Fermion on a Torus*, *JHEP* **03** (2013) 077, [arXiv:1301.0336].

[105] J. Cardy and C. P. Herzog, *Universal Thermal Corrections to Single Interval Entanglement Entropy for Two Dimensional Conformal Field Theories*, *Phys. Rev. Lett.* **112** (2014), no. 17 171603, [arXiv:1403.0578].

[106] C. P. Herzog, *Universal Thermal Corrections to Entanglement Entropy for Conformal Field Theories on Spheres*, *JHEP* **10** (2014) 28, [arXiv:1407.1358].

[107] C. P. Herzog and J. Nian, *Thermal Corrections to Rnyi Entropies for Conformal Field Theories*, *JHEP* **06** (2015) 009, [arXiv:1411.6505].

[108] T. Hartman and J. Maldacena, *Time Evolution of Entanglement Entropy from Black Hole Interiors*, *JHEP* **05** (2013) 014, [arXiv:1303.1080].

[109] P. Calabrese and J. L. Cardy, *Evolution of Entanglement Entropy in One-Dimensional Systems*, *J. Stat. Mech.* **0504** (2005) P04010, [cond-mat/0503393].

[110] D. Bak, M. Gutperle, and R. A. Janik, *Janus Black Holes*, *JHEP* **10** (2011) 056, [arXiv:1109.2736].

[111] M. Headrick, V. E. Hubeny, A. Lawrence, and M. Rangamani, *Causality & Holographic Entanglement Entropy*, *JHEP* **12** (2014) 162, [arXiv:1408.6300].

[112] S. Fischetti, D. Marolf, and A. C. Wall, *A Paucity of Bulk Entangling Surfaces: AdS Wormholes with De Sitter Interiors*, *Class. Quant. Grav.* **32** (2015) 065011, [arXiv:1409.6754].

[113] V. Balasubramanian, P. Kraus, A. E. Lawrence, and S. P. Trivedi, *Holographic Probes of Anti-de Sitter Space-Times*, *Phys. Rev.* **D59** (1999) 104021, [hep-th/9808017].

[114] I. Affleck and A. W. W. Ludwig, *Universal Noninteger 'Ground State Degeneracy' in Critical Quantum Systems*, *Phys. Rev. Lett.* **67** (1991) 161–164.

[115] T. Azeyanagi, A. Karch, T. Takayanagi, and E. G. Thompson, *Holographic Calculation of Boundary Entropy*, *JHEP* **03** (2008) 054–054, [arXiv:0712.1850].

[116] S. H. Shenker and D. Stanford, *Black Holes and the Butterfly Effect*, *JHEP* **03** (2014) 067, [arXiv:1306.0622].

[117] I. A. Morrison and M. M. Roberts, *Mutual Information Between Thermo-Field Doubles and Disconnected Holographic Boundaries*, *JHEP* **07** (2013) 081, [arXiv:1211.2887].

[118] T. Azeyanagi, T. Nishioka, and T. Takayanagi, *Near Extremal Black Hole Entropy as Entanglement Entropy via AdS^2/CFT(1)*, *Phys. Rev.* **D77** (2008) 064005, [arXiv:0710.2956].

[119] N. Engelhardt and A. C. Wall, *Extremal Surface Barriers*, *JHEP* **03** (2014) 068, [arXiv:1312.3699].

[120] N. D. Birrell and P. C. W. Davies, *Quantum Fields in Curved Space*. Cambridge Monographs on Mathematical Physics. Cambridge Univ. Press, Cambridge, UK, 1984.

[121] I. R. Klebanov, T. Nishioka, S. S. Pufu, and B. R. Safdi, *Is Renormalized Entanglement Entropy Stationary at RG Fixed Points?*, *JHEP* **10** (2012) 058, [arXiv:1207.3360].

[122] T. Nishioka, *Relevant Perturbation of Entanglement Entropy and Stationarity*, *Phys. Rev.* **D90** (2014), no. 4 045006, [arXiv:1405.3650].

[123] Z. Komargodski and A. Schwimmer, *On Renormalization Group Flows in Four Dimensions*, *JHEP* **12** (2011) 099, [arXiv:1107.3987].

[124] Z. Komargodski, *The Constraints of Conformal Symmetry on RG Flows*, *JHEP* **07** (2012) 069, [arXiv:1112.4538].

[125] M. A. Luty, J. Polchinski, and R. Rattazzi, *The a-theorem and the Asymptotics of 4D Quantum Field Theory*, *JHEP* **01** (2013) 152, [arXiv:1204.5221].

[126] F. Baume, B. Keren-Zur, R. Rattazzi, and L. Vitale, *The Local Callan-Symanzik Equation: Structure and Applications*, *JHEP* **08** (2014) 152, [arXiv:1401.5983].

[127] S. Banerjee, *Trace Anomaly Matching and Exact Results for Entanglement Entropy*, arXiv:1405.4876.

[128] S. Banerjee, *Note on the Dilaton Effective Action and Entanglement Entropy*, arXiv:1406.3038.

[129] I. R. Klebanov, S. S. Pufu, S. Sachdev, and B. R. Safdi, *Renyi Entropies for Free Field Theories*, *JHEP* **1204** (2012) 074, [arXiv:1111.6290].

[130] C. P. Herzog and T. Nishioka, *The Edge of Entanglement: Getting the Boundary Right for Non-Minimally Coupled Scalar Fields*, arXiv:1610.02261.

[131] D. V. Fursaev, *Proof of the Holographic Formula for Entanglement Entropy*, *JHEP* **0609** (2006) 018, [hep-th/0606184].

[132] M. Headrick, *Entanglement Renyi Entropies in Holographic Theories*, *Phys.Rev.* **D82** (2010) 126010, [arXiv:1006.0047].

[133] L.-Y. Hung, R. C. Myers, M. Smolkin, and A. Yale, *Holographic Calculations of Renyi Entropy*, *JHEP* **12** (2011) 047, [arXiv:1110.1084].

[134] K. Życzkowski, *Rényi extrapolation of shannon entropy*, *Open Systems & Information Dynamics* **10** (2003), no. 03 297–310.

[135] C. Beck and F. Schögl, *Thermodynamics of Chaotic Systems*. Cambridge University Press, 1993.

[136] G. W. Gibbons, S. W. Hawking, and M. J. Perry, *Path Integrals and the Indefiniteness of the Gravitational Action*, *Nucl. Phys.* **B138** (1978) 141–150.

[137] S. M. Christensen and M. J. Duff, *Quantizing Gravity with a Cosmological Constant*, *Nucl. Phys.* **B170** (1980) 480–506.

[138] H. Yao and X.-L. Qi, *Entanglement entropy and entanglement spectrum of the kitaev model*, *Phys. Rev. Lett.* **105** (Aug, 2010) 080501.

[139] H.-C. Chang and A. Karch, *Entanglement Entropy for Probe Branes*, *JHEP* **01** (2014) 180, [arXiv:1307.5325].

[140] E. Perlmutter, *A universal feature of CFT Rényi entropy*, *JHEP* **03** (2014) 117, [arXiv:1308.1083].

[141] H. Osborn and A. Petkou, *Implications of Conformal Invariance in Field Theories for General Dimensions*, *Annals Phys.* **231** (1994) 311–362, [hep-th/9307010].

[142] H. Casini and M. Huerta, *Entanglement Entropy for the N-Sphere*, *Phys.Lett.* **B694** (2010) 167–171, [arXiv:1007.1813].

[143] J. S. Dowker, *Entanglement Entropy for Even Spheres*, arXiv:1009.3854.

[144] J. S. Dowker, *Entanglement Entropy for Odd Spheres*, arXiv:1012.1548.

[145] S. N. Solodukhin, *Entanglement Entropy of Round Spheres*, *Phys. Lett.* **B693** (2010) 605–608, [arXiv:1008.4314].

[146] R. Camporesi, *Harmonic Analysis and Propagators on Homogeneous Spaces*, *Phys.Rept.* **196** (1990) 1–134.

[147] A. A. Bytsenko, G. Cognola, L. Vanzo, and S. Zerbini, *Quantum Fields and Extended Objects in Space-Times with Constant Curvature Spatial Section*, *Phys. Rept.* **266** (1996) 1–126, [hep-th/9505061].

[148] A. Buchel, J. Escobedo, R. C. Myers, M. F. Paulos, A. Sinha, and M. Smolkin, *Holographic Gb Gravity in Arbitrary Dimensions*, *JHEP* **03** (2010) 111, [arXiv:0911.4257].

[149] S. W. Hawking, *The Path Integral Approach to Quantum Gravity*, in *General Relativity: An Einstein Centenary Survey*, pp. 746–789. 1980.

[150] P. O. Mazur and E. Mottola, *The Gravitational Measure, Solution of the Conformal Factor Problem and Stability of the Ground State of Quantum Gravity*, *Nucl. Phys.* **B341** (1990) 187–212.

[151] E. Mottola, *Functional Integration over Geometries*, *J. Math. Phys.* **36** (1995) 2470–2511, [hep-th/9502109].

[152] S. Giombi, A. Maloney, and X. Yin, *One-Loop Partition Functions of 3D Gravity*, *JHEP* **08** (2008) 007, [arXiv:0804.1773].

[153] H. Arisue, T. Fujiwara, M. Kato, and K. Ogawa, *Path Integral and Operator Formalism in Quantum Gravity*, *Phys. Rev.* **D35** (1987) 2309.

[154] K. SCHLeich, *Conformal Rotation in Perturbative Gravity*, *Phys. Rev.* **D36** (1987) 2342–2363.

[155] D. L. Jafferis and S. J. Suh, *The Gravity Duals of Modular Hamiltonians*, arXiv:1412.8465.

[156] D. L. Jafferis, A. Lewkowycz, J. Maldacena, and S. J. Suh, *Relative Entropy Equals Bulk Relative Entropy*, arXiv:1512.06431.

[157] A. Almheiri, X. Dong, and B. Swingle, *Linearity of Holographic Entanglement Entropy*, arXiv:1606.04537.

[158] J. Camps, *Generalized Entropy and Higher Derivative Gravity*, *JHEP* **1403** (2014) 070, [arXiv:1310.6659].

[159] P. Sabella-Garnier, *Mutual Information on the Fuzzy Sphere*, *JHEP* **02** (2015) 063, [arXiv:1409.7069].

[160] E. D'Hoker, D. Z. Freedman, S. D. Mathur, A. Matusis, and L. Rastelli, *Graviton and Gauge Boson Propagators in AdS(D+1)*, *Nucl. Phys.* **B562** (1999) 330–352, [hep-th/9902042].

[161] M. M. Wilde, A. Winter, and D. Yang, *Strong Converse for the Classical Capacity of Entanglement-Breaking and Hadamard Channels via a Sandwiched Renyi Relative Entropy*, *Commun. Math. Phys.* **331** (2014), no. 2 593–622.

[162] M. Müller-Lennert, F. Dupuis, O. Szehr, S. Fehr, and M. Tomamichel, *On quantum rényi entropies: A new generalization and some properties*, *Journal of Mathematical Physics* **54** (2013), no. 12 122203.

[163] R. L. Frank and E. H. Lieb, *Monotonicity of a relative rényi entropy*, *Journal of Mathematical Physics* **54** (2013), no. 12 122201.

[164] N. Lashkari, *Relative Entropies in Conformal Field Theory*, *Phys. Rev. Lett.* **113** (2014) 051602, [arXiv:1404.3216].